Synthesis of Ce(IV) and Ti(IV) alkoxides for use as precursors for MOCVD and ALD.

Thesis submitted in accordance with the requirements of the University of Liverpool for the degree of Doctor in Philosophy by Jacqueline Wrench

September 2011

Acknowledgements

I would first like to thank my supervisor Helen for her endless encouragement and support during my PhD. I would also like to thank Hywel Davies and everyone at SAFC Hitech for use of their facilities, advice and knowledge. Thanks to Paul Chalker and the department of Engineering Centre for Materials and Structures for their help and enduring my endless questions. Special thanks goes to Sobia Ashraf, Kate Black, Pete King, Paul Marshall and Matt Werner for the deposition studies and working on my precursors with as little complaint as possible.

It is important to acknowledge the help I received from the technical staff of this department. I am especially grateful to Tony Ellis in NMR spectroscopy, John Bacsa in X-ray crystallography and Steve Apter for elemental analysis as well as Stephen Boyer of the London Metropolitan University for elemental analysis on my air-sensitive materials. Also thanks goes to the EPSRC mass spectrometry service and John Roberts of SAFC Hitech for TGA analysis.

A great thank you to all my companions met during my PhD. I would especially like to thank Emma, Tom, Oliver, Ev, Alan, Matt and Lyndsey for their support in the local drinking establishment. Special thanks to Dave for his confidence in me and extra special thanks to Christina for listening to my woes regardless of understanding what I was talking about.

Thank you to my parents for their life-long support in all my endeavours and a special mention to my brother Brian to whom this thesis is dedicated. Thank you for always believing in me and for teaching me that no matter how difficult life gets, a cheeky grin will still get you a long way.

Abstract

A synthetic route for the general synthesis of Ce(IV) alkoxides is described utilising a reaction with ceric ammonium nitrate and *tert*-butoxide to create the *in situ* intermediate $[Ce(OBu^t)_4]$ by means of salt metathesis. A further alkoxy-exchange reaction with the desired alkoxide resulted in the formation of alkoxide complexes $[Ce(L)_4]$ (L = mmp, dmae, dmap, dmop, dmomp). The compounds $[Ce(mmp)_4]$, $[Ce(dmap)_4]$ and $[Ce(dmop)_4]$ were characterised crystallographically. $[Ce(dmae)_4]$ was shown to decompose over time and gave a crystal structure of the cluster $[Ce_{14}(dmae)_{22}(NO_3)_2O_{14}(OH)_4]$. DmomH was found to be an unsuitable ligand for the formation of a homoleptic complex.

A range of heteroleptic complexes were also synthesised by reaction of 2 equivalents of an alkoxide (dmop, dmom, dmomp) or β-diketonate ligand (thd, dbm) with the complexes $[Ce(mmp)_4]$ and $[Ce(dmap)_4]$. The thd ligand was found to be too strong a donor to make a heteroleptic complex resulting exclusively in the formation of $[Ce(thd)_4]$. These reactions yielded the complexes $[Ce(mmp)_2(L)_2]$ (L=dbm, dmom, dmomp) and $[Ce(dmap)_2(dbm)_2]$. The reaction between $[Ce(mmp)_4]$ and 2 equivalents of dmop gave the dimer $[Ce_2(mmp)_2(dmop)_4O]$ which was characterised crystallographically.

$[Ce(mmp)_4]$ and $[Ce(dmap)_4]$ were tested for use as precursors for the liquid-injection MOCVD and ALD of CeO_2 thin films on a Si(100) substrate. The results were compared with the known precursors $[Ce(thd)_4]$ and $[Ce(OC(CH_3)_2Pr^i)_4]$, $[Ce(thd)_4]$ being the most commonly used precursor for CeO_2 thin film growth. Both new precursors were found to be more volatile and have a temperature window of 200-600 °C for MOCVD. $[Ce(dmap)_4]$ showed growth at temperatures as low as 100 °C in ALD though was susceptible to decomposition via CVD processes at 250 °C. $[Ce(mmp)_4]$ was self-limiting over the temperature range of 150-350 °C.

A range of heteroleptic Ti(IV) alkoxide complexes were also synthesised by reaction of either $[Ti(OBu^t)_4]$ or $[Ti(OPr^i)_4]$ with 2 equivalents of the desired alkoxide in an alkoxy exchange reaction to give complexes with the formula $[Ti(OR)_2(L)_2]$ (R = Bu^t, Pr^i, L = dmae, mmp, dmop, dmom). $[Ti(OPr^i)_2(dmop)_2]$ and $[Ti(OBu^t)_2(dmop)_2]$ were characterised crystallographically.

These compounds were used as precursors for the MOCVD of anatase TiO_2 nanostructures on Si(100) and F-doped SnO_2 substrates. $[Ti(OPr^i)_2(dmae)_2]$ provided the optimum conditions of growth on both substrates at 450 °C for 180 minutes giving full coverage and uniform nanostructures. The precursor also interestingly grew nanorods at 600 °C on Si(100).

Abbreviations

Abbreviation	Definition
ALD	Atomic Layer Deposition
dbmH	1,3-diphenylpropane-1,3-dione
dmaeH	N,N,-dimethylaminoethanol
dmapH	1-(dimethylamino)propan-2-ol
dmomH	(4,4-dimethyl-4,5-dihydrooxazol-2-yl)methanol
dmompH	2-(4,4-dimethyl-4,5-dihydrooxazol-2-yl)-6-methylphenol
dmopH	2-(4,4-dimethyl-4,5-dihydrooxazol-2-yl)propan-2-ol
mmpH	1-methoxy-2-methylpropan-2-ol
MOCVD	Metal-Organic Chemical Vapour Deposition
NMR	Nuclear Magnetic Resonance
OBu^t	*Tert*-butoxide
OPr^i	2-propoxide
TGA	Thermogravimetric Analysis
thdH	2,2,6,6-tetramethylheptane-3,5-dione
THF	Tetrahydrofuran

Contents

Chapter 1. Introduction.

1.1 Background.

1.1.1. Moore's Law.

According to Moore's law the number of transistors that can be placed on an integrated circuit will increase exponentially, doubling approximately every 2 years leading to better chip performance.[1] Because of this the continual scaling of circuit elements has made great progress over the past few decades. This ever increasing trend for the shrinkage of capacitors used for information storage in dynamic random-access memories (DRAMs), and the complementary metal-oxide-semiconductor field-effect transistors (MOSFETS) has led to a decrease in both the channel length and the SiO_2 gate dielectric thickness (figure 1.1).

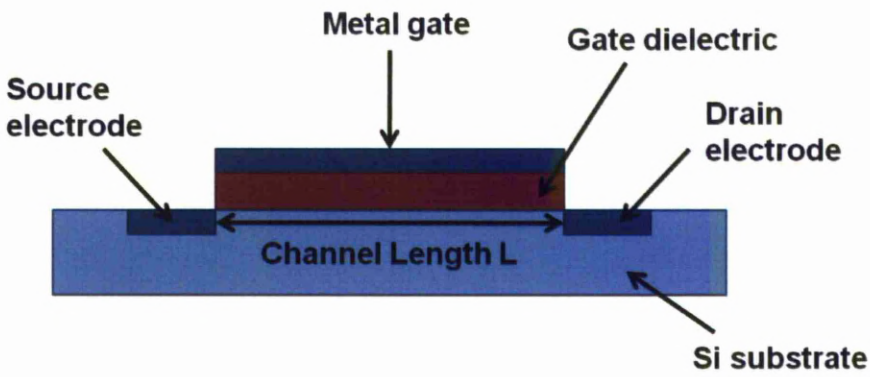

Figure 1. 1. Schematic of a MOSFET.

Unfortunately, as the gate thickness approaches 2 nm the SiO_2 insulating layer begins to break down causing high gate leakage currents, reduced drive current and poor impurity diffusion resistance causing poor device reliability. Hence, this problem can be solved by the replacement of SiO_2 by an alternative higher-*k* gate dielectric material. This would allow the use of physically thicker films reducing electron tunnelling and maintaining gate capacitance to give a more reliable device.[1,2]

1.1.2. Dielectric Materials.

Dielectrics are insulating materials that have the ability to increase the amount of charge a capacitor can store. An applied field will cause a displacement of opposable bound charges instead of an actual flow of charge. High-*k* dielectrics with high permittivity are currently of particular interest in information technology being used to enhance the properties of DRAM devices, CMOS circuits and gate dielectrics for field-effect transistors in MOSFETS.

As well as needing a higher *k* value, a dielectric material's band gap energy and conduction and valence band offsets are also important considerations when replacing SiO_2. In order to achieve an acceptable leakage current the band gap of a material should be >3.1 eV since a 1 eV barrier at the valence and the conduction band is needed apart from the silicon band-gap energy of 1.1 eV.

Structurally, a high-*k* material must be stable enough to endure the high temperatures required of a processor. These materials are therefore preferably epitaxial or amorphous. Polycrystalline layers can have grain boundaries that can

increase leakage effects and so are considered problematic. Most research focuses on the creation of amorphous materials.

1.1.3. Alternative Dielectric Materials.

In order for a dielectric material to be useful its dielectric constant must be much greater than that of SiO_2 (k = 3.9). Table 1.1 lists a few oxides and their dielectric constants.

Table 1. 1: Dielectric constants of some known oxides.

Oxide	*k*-value
SiO_2	3.9
Al_2O_3	9-11.5
CeO_2	18-26
HfO_2	20-22
La_2O_3	25-30
TiO_2	80-95
ZrO_2	22-25
$HfO_2.SiO_2$	10-13
$HfO_2.ZrO_2$	20-25
$SrTiO_3$	< 250
(Ba, Sr)TiO_3	< 400

HfO_2 and ZrO_2 have shown very promising results as alternate gate dielectrics and recently there has been a great interest in the development of their deposition.[3,4] The deposition of lanthanide oxides has also been an advancing area.[4]

1.2. Deposition Techniques.

1.2.1. Types of Deposition.

There are several techniques that can be used for the deposition of oxide thin films. These can be divided in to three different categories: physical vapour deposition (PVD), solution deposition and chemical vapour deposition. PVD involves a range of processes like ion beam sputtering and laser ablation.[5-7] These techniques use solid materials as precursors and form coatings under high vacuum conditions making them potentially expensive processes. They are also "line of sight" processes only giving non-conformal coverage. Aside from these issues, PVD does allow the formation of very complex formulas and always produces high purity films.

Chemical vapour deposition includes metal organic chemical vapour deposition and atomic layer deposition. These two processes are favourable for the growth of oxide films used in electroceramics and dielectric and microelectronic materials as they have numerous advantages over other techniques.

1.2.2. Metal Organic Chemical Vapour Deposition (MOCVD).

MOCVD involves the formation of metal oxide layers by the thermal decomposition of a chemical precursor at a substrate surface in the presence of oxygen. The process can be described in three steps (figure 1.2):

a) The precursor is transported to the heated substrate via inert gas.

b) The precursor enters a boundary layer where it slowly diffuses across the surface. Here it undergoes thermal decomposition in the presence of oxygen to form a metal oxide thin film on the substrate.

c) Reaction products are removed from the system using the transport gas stream.

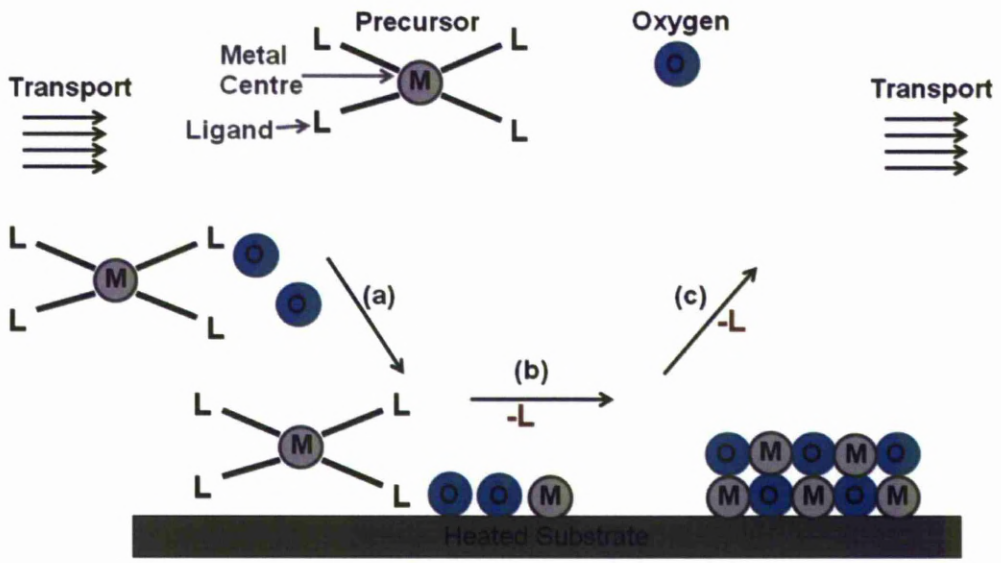

Figure 1. 2: Metal-Organic Chemical Vapour Deposition

The organic ligands surrounding the metal centre of the precursor enable the precursor to exist stably in the gas phase without decomposing with sufficient vapour pressure to allow mass transport to the substrate. Thermal decomposition of the precursor then forms a metal oxide film. The oxygen source for this process can either be from oxygen gas (dual source process) or from the oxygen contained within the metal-organic molecule which is liberated during decomposition (single source process).

MOCVD gives relatively high growth rates for semiconductor applications, good film uniformity over large areas and high quality films at temperatures >350 °C. These high growth rates can lead to lack of growth control of thin films at the atomic level and so films are often post-annealed to achieve proper stoichiometry and morphology.

High quality films require precursor decomposition to occur without the incorporation of carbon or contaminants that would reduce the film's properties. Tailoring precursors for successful film growth is therefore a big research area. There are many other factors that will affect film quality aside from the precursor, for example temperature, pressure, gas phase reactions and surface effects.

Liquid-injection MOCVD has been developed to allow the use of less volatile or temperature sensitive precursors. The precursor is dissolved in a suitable volatile solvent and this is injected in to the reactor with transport via the inert carrier gas. The ability to pulse liquid injection allows for controlling the film composition (figure 1.3).

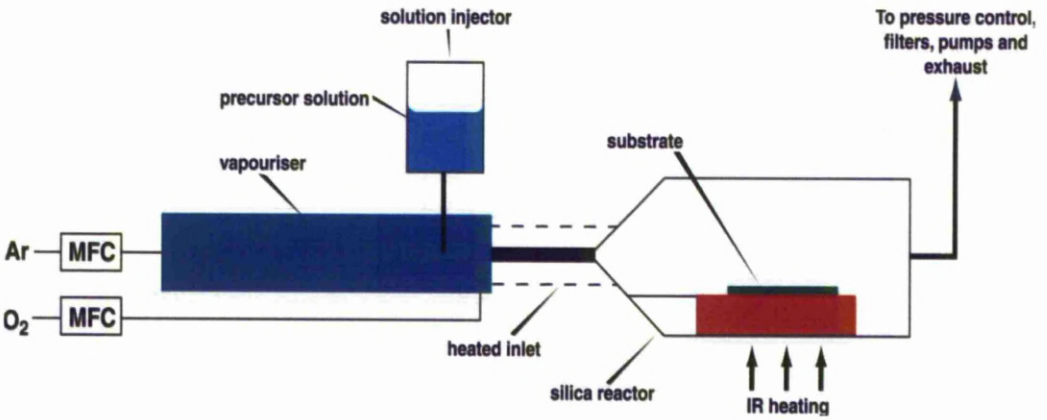

Figure 1. 3: Schematic diagram of a liquid-injection MOCVD reactor.[8]

An MOCVD study is usually plotted as a growth curve with the substrate temperature plotted against the growth rate. This curve can be characterised by three different regions (figure 1.4):

(A) The kinetic growth region. This area is controlled by the thermal decomposition of the precursor. The growth rate increases with increasing substrate temperature up to a maximum where the precursor is being decomposed most efficiently.

(B) The diffusion-controlled growth region. This area is usually quite narrow. Growth is continued for the fully decomposed precursor.

(C) Depletion region. The precursor is now found more on the reactor walls than in the gas-phase causing the growth rate to decrease.

The activation energy of deposition can be calculated from an Arrhenius plot of the kinetic region of the growth curve.

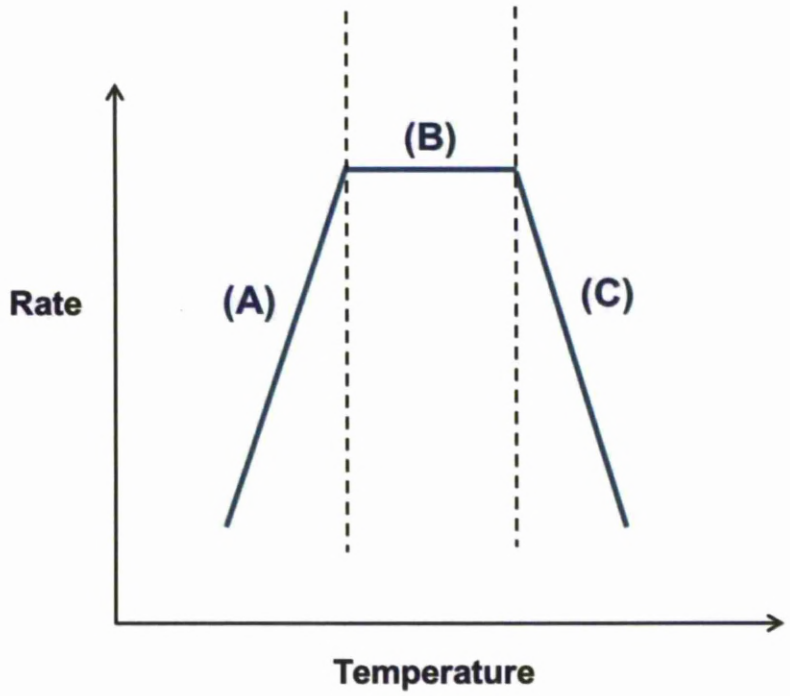

Figure 1. 4: Schematic showing different regions involved in MOCVD.

1.2.3. Atomic Layer Deposition (ALD).

Atomic layer deposition (ALD) is similar to MOCVD in that it occurs at low pressure, allowing for growth of thin films with precise thickness and film uniformity. Instead of depositing the oxygenated precursor in one run the process utilises cyclic chemical reactions between the precursor and surface bonded hydroxyl groups. The cycle can be described in four steps (figure 1.5):

a) The precursor is transported to the heated surface where hydroxyl groups are present via an inert carrier gas.

b) The precursor ligand groups (L) react with the surface hydroxyls binding the ligand to the surface with a loss of HL. The metal centre now has two O bridges bonding it to the substrate and two outward facing ligand groups.

c) Water vapour is pulsed through the system

d) Reaction of the water with the L groups liberates HL to leave hydroxyls bonded to the metal.

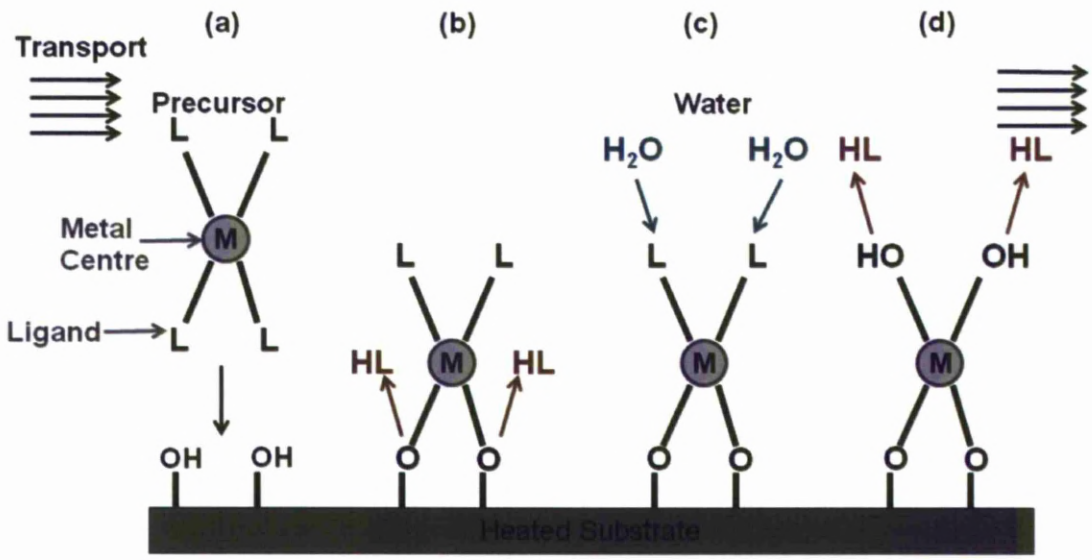

Figure 1. 5: Atomic Layer Deposition.

Ideally the process is self-limiting only allowing for one layer to form per each cycle. The film thickness can be controlled by the number of cycles repeated. This ensures that all surface sites are occupied and so film coverage can be achieved on irregular shaped surfaces even vertical surfaces. ALD typically runs at temperatures between 150-300 °C.

1.3. Precursors for CVD and ALD.

In order for liquid-injection MOCVD to be successful there are several desirable decomposition characteristics and physical properties that a precursor should possess. They are as following:

- Good volatility for efficient vapour phase transport.
- A large temperature window between evaporation and decomposition.
- Clean decomposition without the incorporation of impurities.
- Compatibility with co-precursors during the growth of complex oxides.
- Solution stability for liquid-injection and long shelf-life.
- Low hazards.
- Synthesis in high yield at low cost.

An ALD precursor should have similar characteristics to liquid-injection MOCVD with regards to the volatility and temperature window of the precursor but ALD precursors require a relatively high thermal stability so that surface exchange reactions will predominate over thermal decomposition. This helps the precursor become self-limiting. The precursor must also be highly reactive to nucleophiles like [$^-$OH] or the ALD growth rates will be greatly inhibited.

1.3.1. Precursor Volatility.

The volatility of precursors can be improved by reducing the intermolecular forces. Ideally, monomeric precursors are used where the ligands will completely fill the coordination sphere of the metal preventing the formation of oligomers or polymers. This is easily achieved for small metals but can be very difficult for larger metals with a lower charge. Increasing the steric demand of a ligand can help fill the coordination sphere of a metal. This can be done by increasing the number of donor atoms of a ligand or increasing the bulk of the substituents on a donor atom.

A common method for increasing the volatility is the introduction of fluorine groups. Flourination effects volatility in two ways: firstly, replacing H atoms with less polarisable F atoms decreases intermolecular attractions and, secondly, the increased number of lone pairs on the periphery of the complex results in increased intermolecular repulsion. Unfortunately, fluorinated complexes lead to contamination of the resulting oxide films with flourine. This can be reduced by the addition of H_2O during film growth.[4,5,9]

1.3.2. β-diketonates.

β-diketonate complexes can be desirably changed by altering the structure of the ligand (table 1.2). For instance, an increase in the steric bulk of the R group or fluorine substitution can increase the volatility of the precursor.[10]

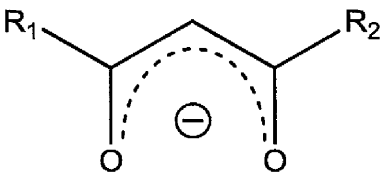

Table 1. 2: Some β-diketonate ligands used in metal oxide MOCVD precursor complexes

R_1	R_2	Name	Abbrevi-ation
CH_3	CH_3	Pentane-2,4-dionate	acacH
CH_3	CF_3	1,1,1-Trifluoropentane-2,4-dionate	tfacH
CF_3	CF_3	1,1,1,5,5,5-Hexafluoropentane-2,4-dionate	hfacH
$C(CH_3)_3$	$C(CH_3)_3$	2,2,6,6-Tetramethylheptane-3,5-dionate	thdH
$C(CH_3)_3$	$CH_2CH(CH_3)_2$	2,2,7,-Trimethyloctane-3,5-dionate	tmodH
$(CH_3)_3C$	$CF_2CF_2CF_3$	6,6,7,7,8,8,8 Heptafluoro-2,2-dimethyloctane-3-5-dionate	fodH
Ph	Ph	1,3-Diphenylpropane-1,3- dionate	dbmH

These bulkier ligands shield the positive metal nucleus causing a decrease in solid state intermolecular oxygen-metal interactions. Increasing the coordination number of the metal by the introduction of neutral donor ligands, like tetraglyme ($CH_3O(CH_2CH_2O)_4CH_3$)[11] and other polyether ligands[12] can also lead to the formation of monomeric complexes.

1.3.3. Alkoxides.

Since an alkoxide ligand can act as a terminal, doubly or triply bridging ligand, oligomerisation to form $[M(OR)_x]_n$ clusters can occur relatively easily (figure 1.6) to achieve coordination saturation of the metal. The degree of n has a major effect on the volatility of the complex which depends on the metal radius and steric demands of R groups.

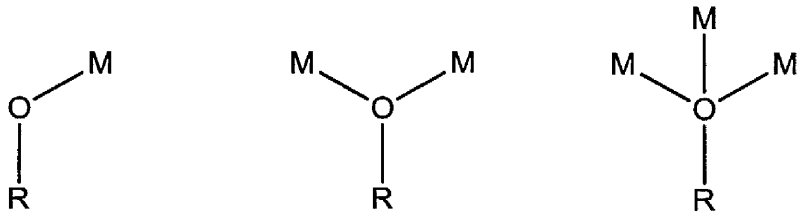

Figure 1. 6: Coordination modes of an alkoxide ligand.

An increase in the bulkiness of the alkoxide can prevent oligomerisation from occurring. This can also be achieved by using ligands with more than one donor atom.[4,13,14] Substitution of alkyl groups on the α-position in a donor-functionalised ligand favours chelation over bridging modes. Hence, mmpH ($HOC(CH_3)_2CH_2OCH_3$) has been an important ligand in the synthesis of MOCVD and ALD precursors, for example $[Hf(mmp)_4]$ and $[Zr(mmp)_4]$.[14]

Amino-functionalised alkoxides have been somewhat less studied though homoleptic and heteroleptic complexes of Hf and Zr with dmae ($HOCH_2CH_2N(CH_3)_2$) and dmap ($HOCH(CH_3)CH_2N(CH_3)_2$) have been used in MOCVD and ALD.[15] The lack of alkyl substituents on the α-carbon results in complexes like $[Zr(OBu^t)_2(dmae)_2]_2$ [16] and $[Zr(OPr^i)_3(dmap)]_2$[15] which are asymmetric dimers with relatively low volatilities.

Heterometallic alkoxides are also available due to the Lewis acidity of simple metal alkoxides and the tendency of the alkoxide O donor to act as a bridging ligand. These complexes are generally volatile enough to be useful precursors for MOCVD and ALD. Ideally, a heterometallic alkoxide has the metals in the correct ratio to deposit a film of the desired stoichiometry, for example, $[LaAl(OPr^i)_6(Pr^iOH)]$ has been used as a single source precursor for the MOCVD of $LaAlO_3$.[17]

Metal alkoxides have a significantly lower thermal stability than the β-diketonates and so oxide films can be grown at lower temperatures in MOCVD. The thermal stability of a metal alkoxide is greatly determined by the presence of a β - hydrogen. This β-hydrogen can often be eliminated to liberate an alkene and an M-OH group.

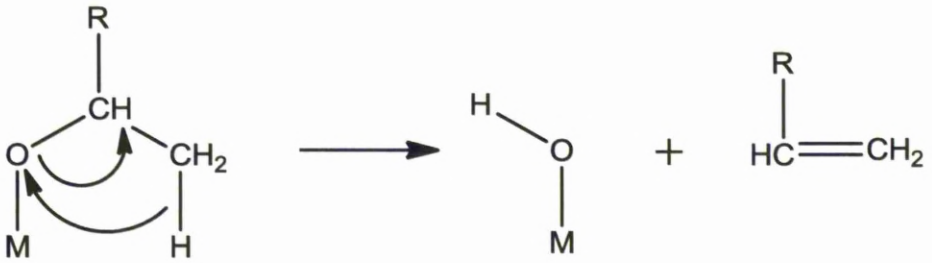

Figure 1. 7: β-hydrogen elimination from an alkoxide ligand.

There are three factors that have been identified as important in controlling ALD growth from metal alkoxides:

1, ease of β-hydride elimination to form reactive M-OH sites, important at lower deposition temperatures (< 300 °C)

2, steric shielding of the metal centre by the ligands

3, the thermal stability of the M-OH bonds, important at higher deposition temperatures (>350 °C)

Even though the volatility of a precursor is improved by the use of sterically demanding ligands, this steric hindrance around the metal centre may hinder the access of H_2O to the metal causing a reduction in ALD growth rates. Also, the

presence of β-hydrogens in the ligand may result in low thermal stability, preventing self-limiting growth.

1.3.4. Alkylamides and Amidinates.

Volatile, monomeric alkylamide structures are more readily available than their alkoxide counterparts since they are naturally more stable given their greater steric bulk. There are several examples of volatile transition metal dialkylamides $[M(NR_2)_x]$ and these are widely used for the MOCVD of metal nitrides like TiN.[18] For oxide thin films $[Hf(NEt_2)_4]$ has been used successfully for the MOCVD of HfO_2.[19] The alkylamide ligand can easily be displaced in the presence of excess oxygen allowing for the growth of high purity oxide films at lower substrate temperatures. The only monomeric lanthanide alkylamides known have very poor thermal stability and cannot be sublimed and so have not been used for rare earth oxide deposition.

Amidinates are bidentate N-donor ligands which allow for steric tuning by changing the R substituents of the ligands (figure 1.8). $[M(amidinate)_n]$ can adopt many different structures depending on the oxidation state of the metal and the steric bulk of the ligand. Amidinate complexes generally have higher thermal stability than the dialkylamides partly due to the chelate effect. These complexes are therefore attractive for use as ALD precursors and have been used for the ALD of transition metals, Y_2O_3[20] and rare earth aluminates.[21]

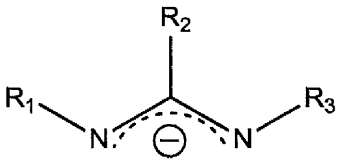

Figure 1. 8: Schematic of a general amidinate ligand (R_1, R_2, R_3 = alkyl groups).

1.4. Ligands of Interest.

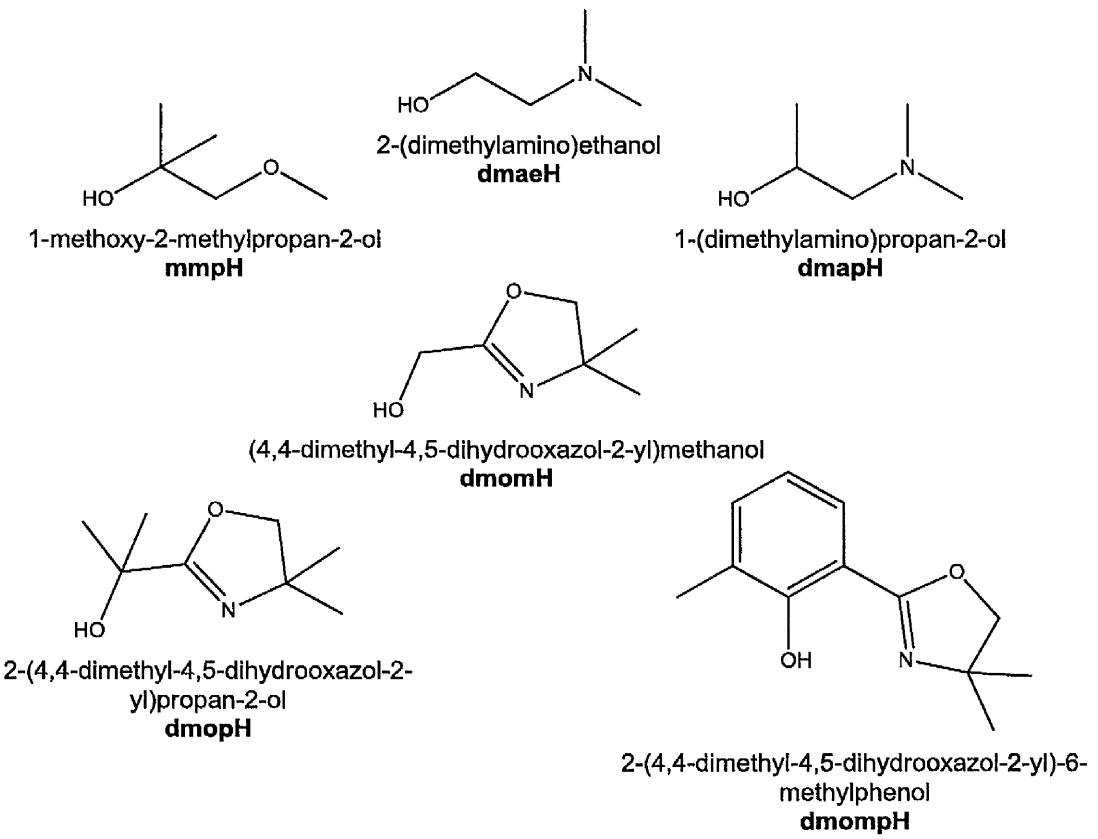

Figure 1. 9: Structures of alcohols used to synthesise metal alkoxide complexes.

The alcohols in figure 1.9 were chosen to study the synthesis of metal alkoxide complexes. All of the alcohols are donor-functionalised with one alkoxide donor

[RO^-] and a second neutral donor. The [RO^-] group in general is a stronger donor than neutral functional groups. Hence, in mmpH, dmaeH and dmapH the methoxy and amino donor moieties should be less stronger donors. There is also a comparison between the substituents on the α-carbon next to the [RO^-] group. Sterically speaking monomeric stable complexes would be more feasible in the order mmpH > dmapH > dmaeH given the presence of methyl groups in this position.

DmopH, dmomH and dmompH belong to a group of oxazolinyl-alcohols. The imine nitrogen on the oxazoline ring is expected to be a stronger donor than the OMe of mmpH. Together with the added bulk of the methyl substituents on the oxazoline ring this should favour the formation of monomeric complexes. The dmompH oxazolinylphenol is an interesting ligand as the lack of β-hydrogens block an easy decomposition route (figure 1.7). This gives the ligand an enhanced thermal stability which is important for ALD.

Chapter 2. Ce(IV) Alkoxide Complexes.

2.1. Introduction.

2.1.1. General Lanthanide Chemistry.

The lanthanides consist of 14 elements starting with lanthanum (electronic configuration ($[Xe]5d^16s^2$) and ending with lutetium ($[Xe]4f^{14}5d^16s^1$). The 4f electrons in the lanthanide series are almost completely shielded from external ligand or crystal fields by the outermost 5s and 5p electrons. The 5s and 5p orbitals however penetrate the 4f subshell and are not shielded from the increasing nuclear charge. Because of this there is a decrease in atomic and ionic size with increasing atomic number. This is known as the lanthanide contraction.

Generally speaking the preferred oxidation state of the lanthanides in solution and in solids is +3 with electrons being removed from the 6s and 5d orbitals to form the Ln^{3+} ions. Under certain conditions Ce, Tb and Pr can give a +4 ion and Sm, Eu and Yb can exist in a 2+ state. This is due to the formation of stable electron configurations of the empty $4f^0$ (Ce^{4+}), half-filled $4f^7$ (Eu^{2+}, Tb^{4+}) and filled $4f^{14}$ (Yb^{4+}) subshells.

Given their large ionic radii and the electrostatic nature of their metal-ligand bonding lanthanide complexes can exhibit larger coordination numbers than many other metal ions ranging from 3 to 14. More commonly they exist as 8 or 9 coordinate. The more electrostatic bonding exists due to the shielding effect of the 4f orbitals by the outermost 5s and 5p electrons. The lack of crystal field effects allows the lanthanide complexes their increase in coordination spheres. The lanthanides are

hard Lewis acids and so prefer to form compounds with hard bases like oxygen, nitrogen and fluorine.

2.1.2. Ce^{3+} and Ce^{4+}

The ability of cerium to exist in a +3 and +4 oxidation state has led to some interesting chemistry. $CeCl_3$ is useful not only as a starting material for other Ce^{3+} complexes but also itself as a Lewis acid in organic reactions such as Friedel-Crafts alkylations[22] and the alkylation of ketones.[23]

Aside from making other Ce^{3+} complexes $CeCl_3$ is also a useful starting material for making Ce^{4+} complexes. A compound can be initially made as Ce^{3+} and then be oxidised up to Ce^{4+} as in making homoleptic Ce(IV) amides by reaction of $CeCl_3$ with $LiNCy_2$ followed by oxidation up to Ce^{4+} using O_2 gas to give $[Ce(NCy_2)_4]$.[24] In another example Ce(IV) metallocene type complexes were made using $CeCl_3$ as starting material and oxidising after reaction using $PhICl_2$.[25]

Ce(IV) is one of the most powerful one-electron oxidising agents ($E^o(Ce^{4+}/Ce^{3+})$ = 1.72 V in acid solution) and is used in a variety of reactions typically as ceric ammonium nitrate ($[NH_4]_2[Ce(NO_3)_6]$, CAN) or ceric ammonium sulphate ($[NH_4]_4[Ce(SO_4)_4]$, CAS) . These reagents are stable in acidic aqueous solution for reasonably long periods of time and are used in transformations like oxidation of alcohols to aldehydes and as a catalyst for other oxidations. [26,27]

Ce^{3+} has a larger ionic radius than Ce^{4+} since the extra positive charge in Ce^{4+} pulls in the electrons in its outer shell. Because of this, Ce^{3+} exhibits a larger surface area giving it a larger coordination sphere. This makes Ce^{3+} complexes more

susceptible to oligomerisation than those of Ce^{4+} since fewer charged ligands can fit around the sphere. To counteract this, neutral donor ligands like diglyme have been used to increase the Ce^{3+} coordination sphere.[28]

2.1.3. Ce(IV) alkoxide complexes.

2.1.3.1. Homoleptic Ce(IV) alkoxides.

There are few known Ce(IV) alkoxide complexes. Bradley *et al* began work on $[Ce(OBu^t)_4]$ chemistry and its stability in 1956 where a range of Ce(IV) alkoxides with different monodentate alcohols were synthesised.[29] Further investigation by the reaction of CAN with different ratios of sodium *tert*-butoxide in THF and *tert*-butyl alcohol led to the isolation of a series of complexes involving one cerium atom with different numbers of OBu^t, NO_3, Na and solvent molecules in coordination along with the formation of the trimer $[Ce_3(OBu^t)_{10}O]$[30] whose structure is analogous to $[U_3(OBu^t)_{10}O]$[31] (figure 2.1).

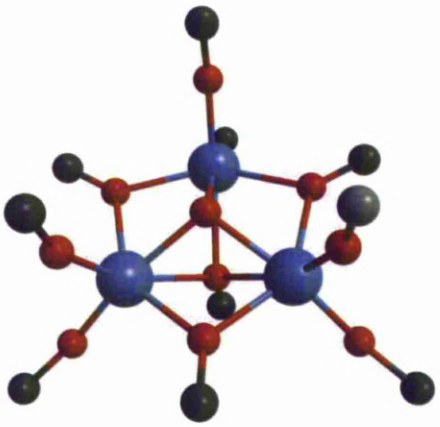

Figure 2. 1: Crystal structure of $[U_3(OBu^t)_{10}O]$ to demonstrate the structure of $[Ce_3(OBu^t)_{10}O]$.[31]

Most importantly this paper highlighted the difficulty of stabilising Ce^{4+} with a monodentate ligand like *tert*-butoxide and subsequent trials have led to similar discoveries.[30,32] Figure 2.2 shows examples of trimetallic cerium *tert*-butoxide clusters found after these reactions. Clusters **A** and **B** contain both Ce^{3+} and Ce^{4+} whereas **C** and **D** are exclusively Ce^{3+} and Ce^{4+} respectively.

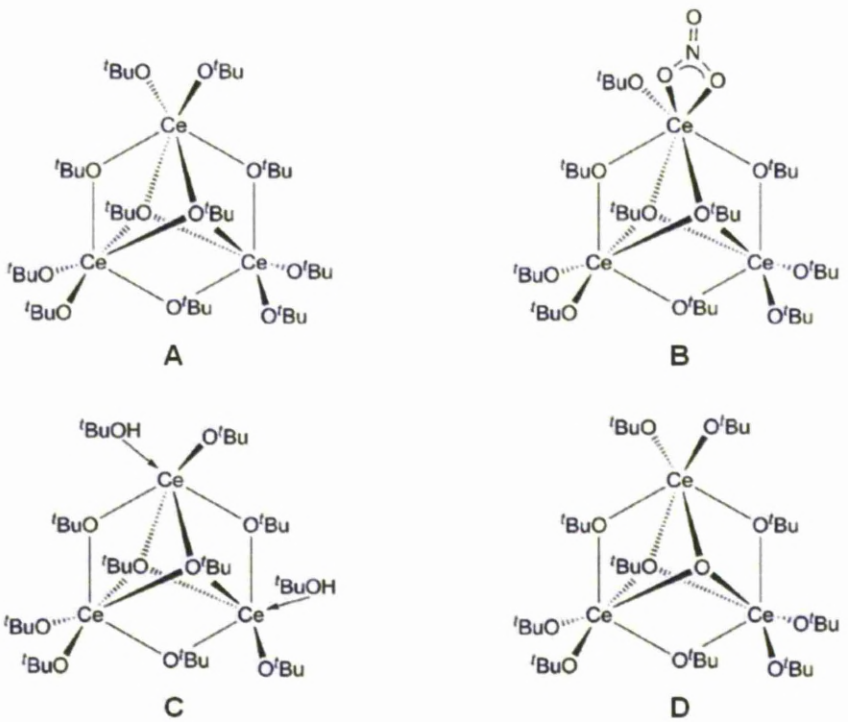

Figure 2. 2: Examples of trimetallic clusters of Ce^{3+} and Ce^{4+} possible from reactions with $[Ce(OBu^t)_4]$.[32]

The reaction of sodium isopropoxide with ceric ammonium nitrate in DME and isopropanol has been used to isolate $[Ce(OPr^i)_4]$.[33] This led to the synthesis of the dimer $[Ce_2(OPr^i)_8(HOPr^i)_2]$. It was later shown that this complex exists as the dimer where each Ce atom is 6-coordinate, bonded to 4 isopropoxides, sharing

bonding from another 2 isopropoxide ligands. The complex is also stabilised by intermolecular hydrogen bonding from the isopropanol.[34]

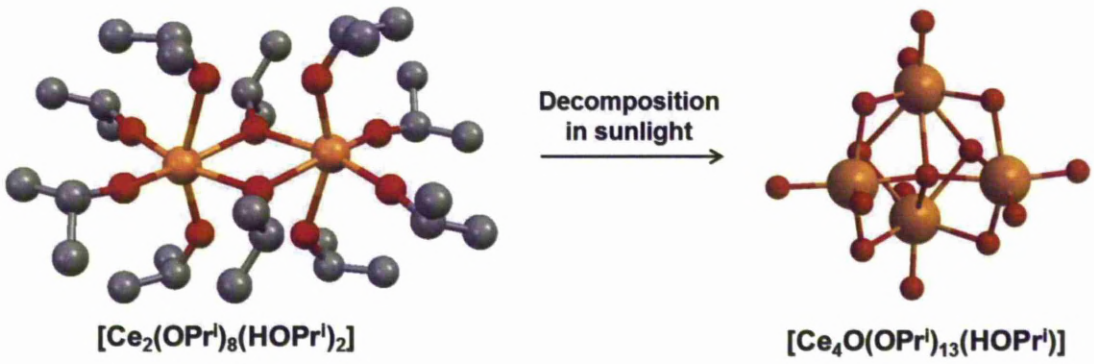

Figure 2. 3: Crystal structure of $[Ce_2(OPr^i)_8(HOPr^i)_2]$ and its decomposition to $[Ce_4O(OPr^i)_{13}(HOPr^i)]$ in sunlight (50 hours in solution, 15 hours in the solid state).[35]

The dimer was found to be photosensitive in solution and in the solid state. When left in isopropanol in sunlight for 50 hours a colour change from yellow to green to orange/brown was observed whereas in the solid-state conversion only took 15 hours.[35] This material was found to be the tetramer $[Ce_4O(OPr^i)_{13}(HOPr^i)]$. Thermal desolvation of the dimer gives the Ce^{4+} oxo-cluster $[Ce_4O(OPr^i)_{14}]$ after heating in the solid state for 15 minutes at 70 °C (figure 2.3).

The precursor $[Ce(OC(CH_3)_2Pr^i)_4]$ has been used previously for CVD being made in the similar manner as the other Ce(IV) alkoxides via reaction of the sodium salt of the alcohol with ceric ammonium nitrate.[36] Although this precursor showed promising growth rates at lower temperatures they only occurred during a small temperature window of around 50 °C. This gives less practical use of the compound.

To increase the stability and volatility of the alkoxide complexes donor functionalised alcohols are the main focus in this study. By synthesising monomeric structures with bulkier groups the volatility of the complexes should increase.

2.1.3.2. Heteroleptic Ce (IV) alkoxide Complexes

Heteroleptic complexes of Ce(IV) are quite rare. Complexes with amides are known such as $[Ce(N(SiMe_3)_2)_3X]$ (X = Cl or Br)[37] and $[CeI\{N(SiMe_2Bu^t)CH_2CH_2\}_3N]$[38] which were synthesised via oxidation with an appropriate oxidising agent. Larger tripodal Schiff-base ligands have also been studied making Ce complexes containing the ligand and a nitrate or chlorine group (figure 2.4). [39]

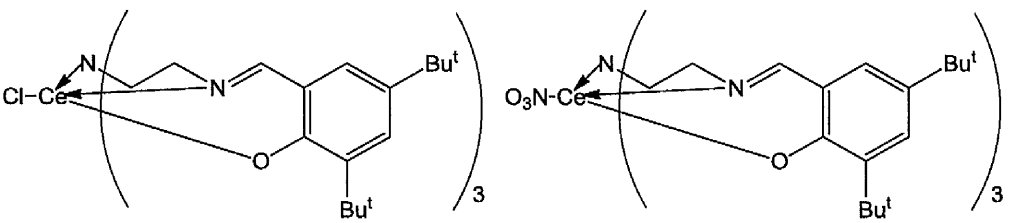

Figure 2.4: Ce(IV) heteroleptic complexes made using Schiff-base ligands.

Aside from these structures simpler Ce(IV) heteroleptics with alkoxides and β-diketonates are not so well known. Modification of $[Ce_2(OPr^i)_8(HOPr^i)_2]$ with the β-diketonate acetylacetonate ligand gives complexes of the formula $[Ce_2(OPr^i)_7(acac).(HOPr^i)]$ and $[Ce_2(OPr^i)_6(acac)_2.(2HOPr^i)]$ stabilised in isopropanol (figure 2.5).[40] Combining alkoxides and β-diketonates in one complex

could make a complex volatile and reactive enough to be a useful CeO_2 precursor given the usefulness of $[Ce(thd)_4]$ as a precursor.[41,42]

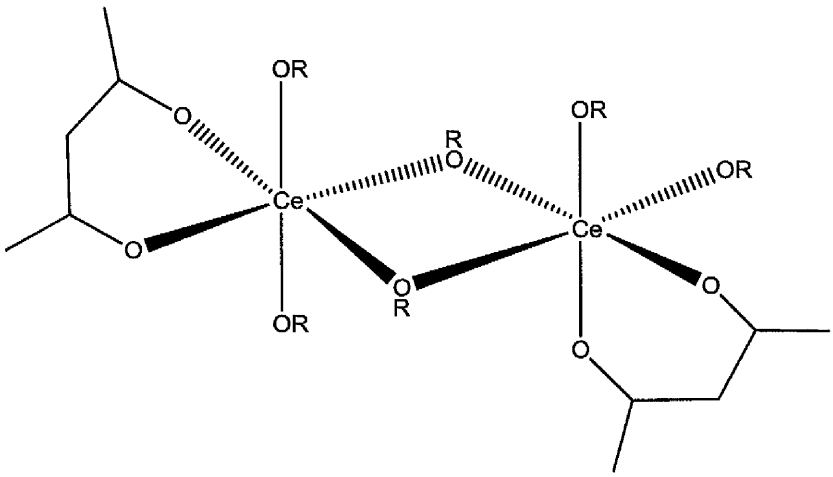

Figure 2.5: Schematic representation of proposed dimer structure of $[Ce(OPr^i)_3(acac)]$ stabilised in isopropyl alcohol $[Ce_2(OPr^i)_6(acac)_2(2HOPr^i)]$.

2.1.4. Ligands of Interest.

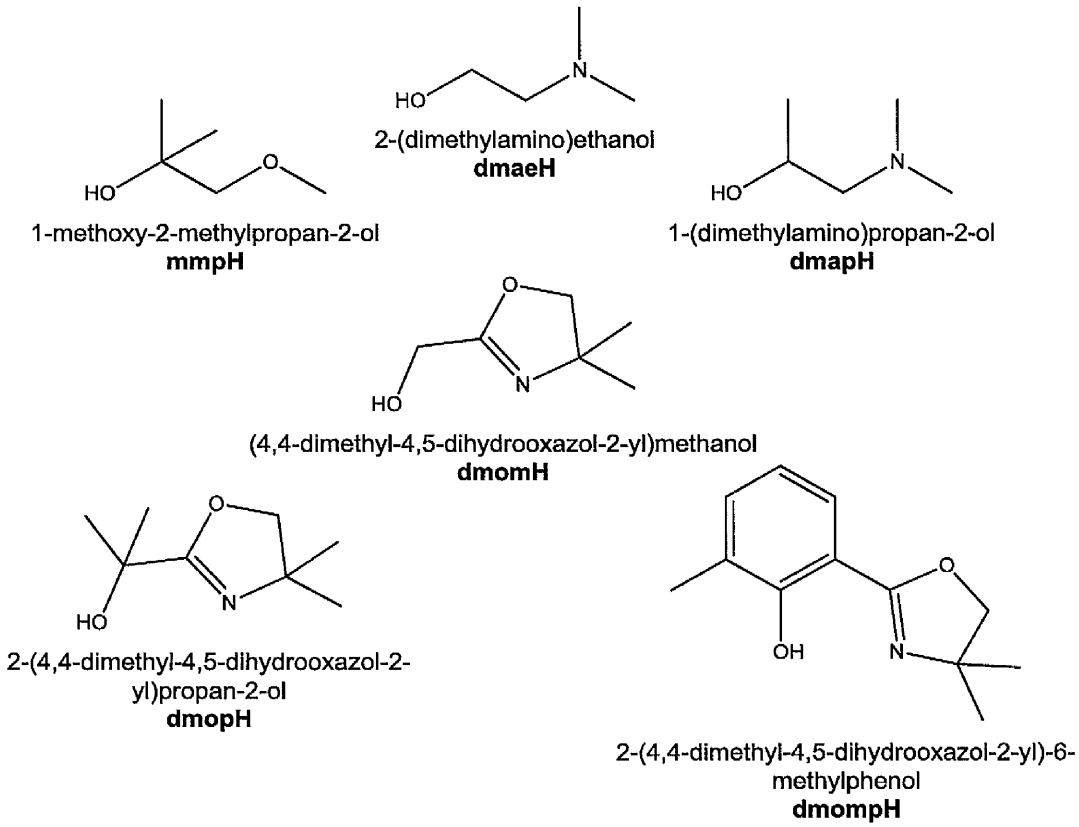

Figure 2.6: Donor-functionalised alcohols used to make monomeric Ce(IV) alkoxide complexes.

Figure 2.6 shows the six ligands used to make new Ce(IV) monomeric complexes. Each binds to the Ce atom via an alcohol oxygen and by either a methoxy O (mmpH), an amine N (dmaeH and dmapH) or an imine N (dmopH, dmomH, dmompH). There will therefore be different strengths of dative bond in each complex. Aside from this, steric effects from the bulky methyl groups will affect whether a complex will be formed and how stable the complex will be.

Cerium complexes with these types of donor-functionalised alcohols are few in number. The only known Ce(IV) complex with an oxazolinyl ligand was reported in 2004 with the ligands 2-(2'-hydroxyphenyl)-4-methyl)oxazoline and 2-(2'-hydroxyphenyl)-4-isopropyl)oxazoline] though these were never structurally characterised (figure 2.7).[43]

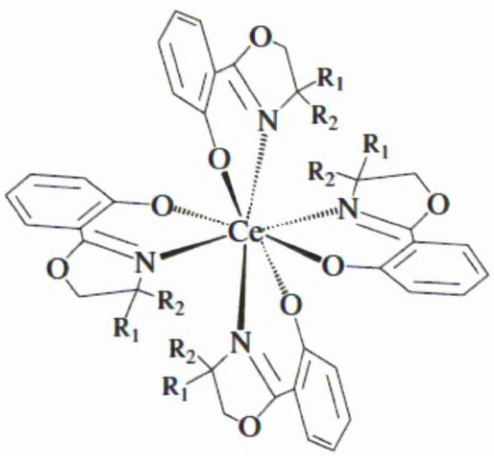

$R_1 = R_2 = Me$ **(1)**

$R_1 = H$, $R_2 = {}^{i}Pr$ **(2)**

Figure 2. 7: Proposed structure of [Ce(Me$_2$oxaz)$_4$] (1) and [Ce(Pr^{i}Hoxaz)$_4$] (2) complexes.

These were made via an alcohol exchange reaction with $[Ce_2(OPr^i)_8(HOPr^i)_2]$ to give monomeric compounds in good yield. The complexes were found to be air stable though complex (1) hydrolyses after two days. These were found to be much less volatile than $[Ce(thd)_4]$.

The dmop ligand has been used previously to make useful precursors of HfO_2 and ZrO_2. $[M(OBu^t)_2(dmop)_2]$[44] (M = Hf, Zr) and $[Hf(dmop)_4]$[45] were shown to grow films of the metal oxides over substrate temperatures of 350-550 °C and were also found to be less reactive to air and moisture than other Zr and Hf alkoxides such

as $[Zr(OBu^t)_4]$ and $[Hf(OBu^t)_4]$. All three structures were determined crystallographically to be six-coordinate and monomeric.

2.2. Results and Discussion.

2.2.1. Synthetic Route to Homoleptic Ce(IV) alkoxides.

2.2.1.1. Preparation and Isolation of $[Ce(OBu^t)_4]$.

$$[NH_4]_2[Ce(NO_3)_6] + 6NaOBu^t \xrightarrow{THF} [Ce(OBu^t)_4][THF] + 6NaNO_3 + 2NH_3 + 2HOBu^t$$

Figure 2.8: Reaction scheme for synthesis of $[Ce(OBu^t)_4]$.

Initially the isolation of $[Ce(OBu^t)_4]$ was attempted following the reaction showed in figure 2.8.[30] Ceric ammonium nitrate (CAN) was stirred in tetrahydrofuran (THF) and 6 equivalents of sodium *tert*-butoxide in THF were added via cannula to cause a salt metathesis at room temperature. The reaction is pushed forward by the formation of ammonia gas and the precipitation of $NaNO_3$ which easily comes out of solution on the addition of sodium *tert*-butoxide. After filtration of the precipitate the volatiles were removed *in vacuo* and the crude material recrystallised from toluene.

Several reactions were tried making the $NaOBu^t$ by refluxing Na metal with *tert*-butanol but given the difficulty of guaranteeing stoichiometry it was determined

that pre-made $NaOBu^t$ would be more useful. The reactions yielded yellow solids but elemental analysis showed C and H content too low for the monomeric $[Ce(OBu^t)_4][THF]$ or complexes containing N (table 2.1). Reactions were also tried in dimethoxyethane (DME) given the greater solubility of CAN and also the possibility of extra "stabilisation" of the monomeric structure by the solvent but results were the same.

Table 2. 1: Elemental analysis of products isolated from reactions of CAN with $NaOBu^t$ (act) compared with theoretical values (theo).

	C %	H %	N %
$[Ce(OBu^t)_4[THF]$ (theo)	41.65	7.64	NA
$[Ce_3(OBu^t)_{10}O]$ (theo)	41.13	7.77	NA
$[Ce(OBu^t)_3(NO_3)]$ (theo)	34.2	6.46	3.32
Reactions in THF (act)	41.62	8.07	NA
	35.15	7.04	NA
	13.87	2.96	7.83

The low C and H content is likely due to the small amount of the desired monomeric $[Ce(OBu^t)_4]$ complex presence as well as a mixture of the trimer and other oxo-clusters and nitrate complexes. It was then deemed that isolation of a *tert*-butoxide complex would not lead to a viable route to make monomeric complexes as has been the issue of other research.[46,47]

2.2.1.2. [Ce(ONep)$_4$] isolation.

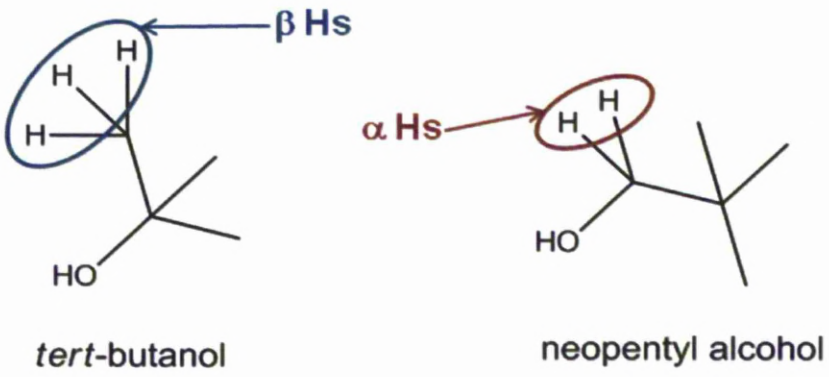

Figure 2. 9: Schematic illustrating the differences between *tert*-butanol and neopentyl alcohol.

Neopentyl alcohol ($HOCH_2C(CH_3)_3$) was used in a similar way to *tert*-butanol to try and make a monomeric Ce alkoxide. The ligand has been used previously for the growth of HfO_2 films using hafnium oxoneopentoxide.[48] Given the presence of β-hydrogens in the *tert*-butanol structure (figure 2.9) there is room for decomposition to occur via β-hydride elimination (figure 2.10). Neopentyl alcohol still has the bulk of a $C(CH_3)_3$ group but only has α-hydrogens and so it is possible that this could lead to a more stable structure. Also, the extra bulk of neopentyl alcohol could make a monomeric complex sterically more favourable.

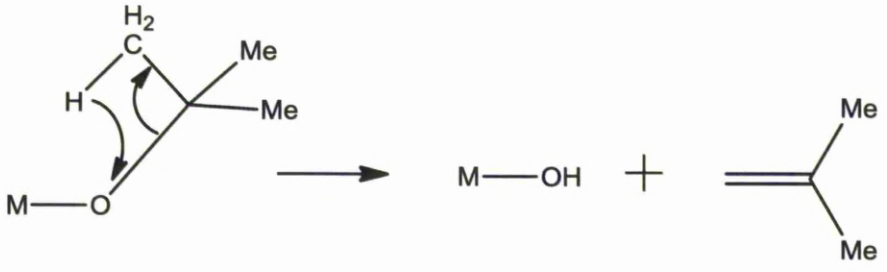

Figure 2.10: Mechanism for β-hydride elimination on a metal with the alkoxide ligand OBu^t.

The alcohol was dissolved in DME or THF and reacted with sodium hydride to form sodium neopentoxide. This was added to CAN in DME or THF with stirring and the reaction left for 3 hours as $NaNO_3$ precipitated out. The mixture was then worked up in the same way as for $[Ce(OBu^t)_4]$. Elemental analysis of the yellow product again showed low C and H percentages against theoretical values (table 2.2).

Table 2. 2: Elemental analysis of solid isolation from reactions of CAN with NaONep (actual), compared with theoretical values (theo).

	C %	H %
$[Ce(ONep)_4]$ (theo)	49.16	9.07
$[Ce(ONep)_4]$THF (theo)	51.4	9.35
Actual	41.93	8.47

2.2.1.3. Use of $[Ce(OBu^t)_4]$ as an in situ intermediate.

A different method was used to try to isolate $[Ce(ONep)_4]$. The route to make a $[Ce(OBu^t)_4]$ derivative was followed up until the precipitation of $NaNO_3$. After filtering off the precipitated $NaNO_3$ the complex was left in solution. Four equivalents of neopentyl alcohol were added and the reaction refluxed for 2 hours. Volatiles were removed *in vacuo* to give a yellow oil. The ^1H NMR spectrum of this oil is shown in figure 2.11.

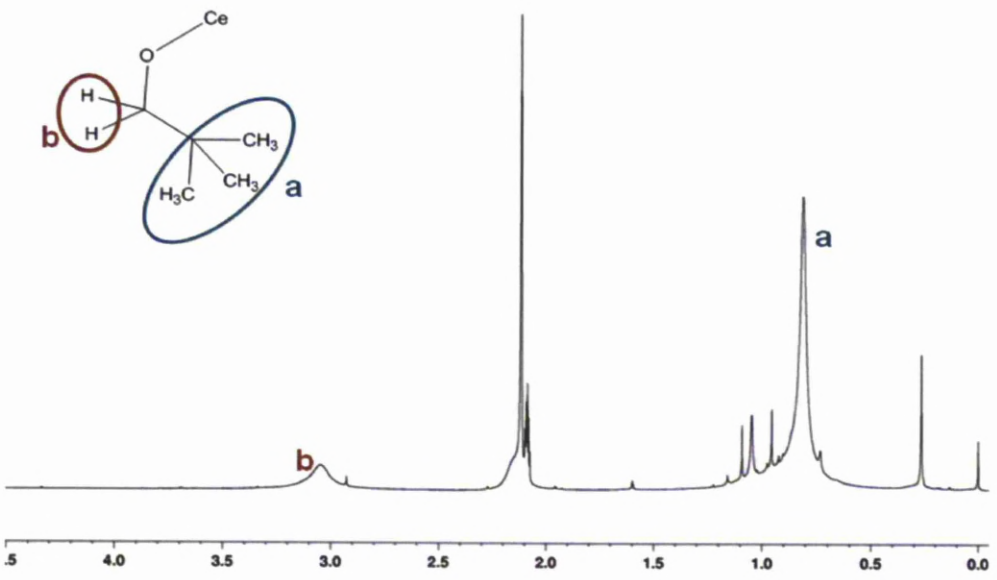

Figure 2.11: ^{1}H NMR spectrum (C_7D_8) of [Ce(ONep)$_4$] trial.

Variable temperature NMR spectroscopy at 193 K did not help to elucidate a structure as the peaks remained broad. Given this broadness it can be deemed there are either neopentoxide groups in different environments or it is a fluxional complex possibly due to the presence of a small amount of H_2O in solution. After a few days at -18 °C in toluene a crystal suitable for X-ray analysis was grown, the structure of which is shown in figure 2.12. The complex was made up of a trimer consisting of three 6-coordinate Ce atoms. Each Ce atom is bonded to 4 neopentoxide groups and an O atom and a *tert*-butoxide linking all 3 Ce atoms together. The complex has a C_3 axis passing though O_1 and O_2 and the structure is analogous to that proposed for $[Ce_3(OBu^t)_{10}O]$[30] by comparison with $[U_3(OBu^t)_{10}O]$.[31] The CHN analysis of the material was found to be too low to match the structure shown crystallographically and so this crystal is not representative of the bulk of the material (table 2.3).

Table 2. 3: table showing elemental analysis comparisons for reaction with neopentyl alcohol (actual) and theoretical values (theo).

	C %	H %
$[Ce(ONep)_4]$ (theo)	49.16	9.07
$[Ce_3(ONep)_9(OBu^t)O]$ (theo)	45.49	8.41
Actual	40.89	7.63

The complex illustrates further the difficulty of isolating a monomeric structure of Ce(IV) using a monodentate ligand. It also proved that using $[Ce(OBu^t)_4]$ as an *in situ* intermediate gave the opportunity to form a different alkoxide network. Neopentoxide itself is not a good ligand for the stabilisation of a monomeric complex but this led to a different synthetic route for other alkoxides.

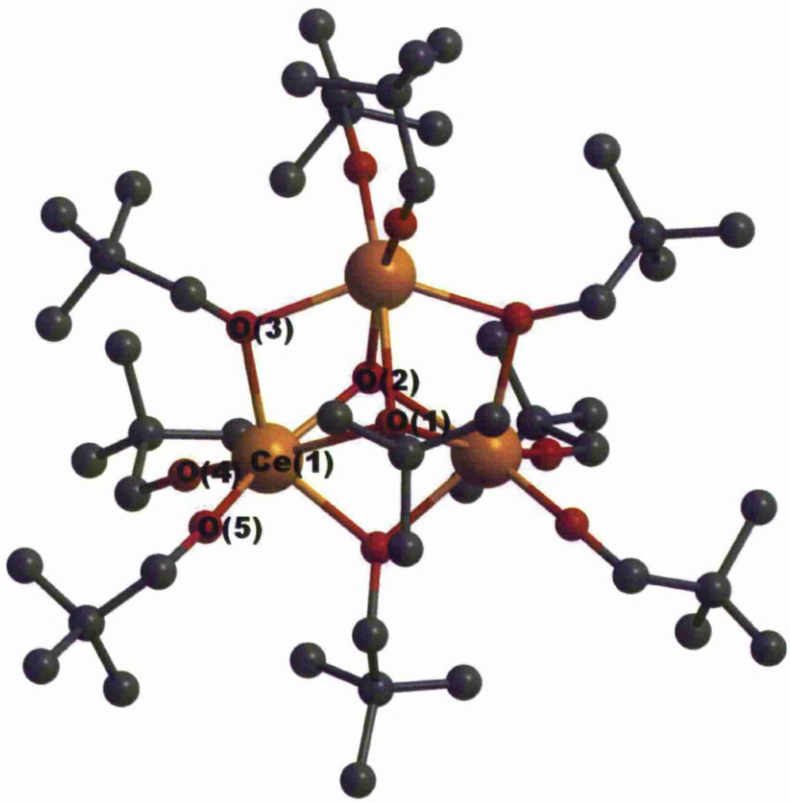

Figure 2. 12: Crystal Structure of $[Ce_3(ONep)_9(OBu^t)O]$.

Table 2. 4: Table showing selected bond lengths and bond angles for $[Ce_3(ONep)_9(OBu^t)O]$.

Bond Atoms	Bond Lengths (Å)
Ce(1)-O(1)	2.530(2)
Ce(1)-O(2)	2.249(5)
Ce(1)-O(3)	2.331(5)
Ce(1)-O(4)	2.054(4)
Ce(1)-O(5)	2.081(4)
Bond Atoms	**Bond Angles (°)**
Ce(1)-O(1)-Ce(1)#1	87.5(2)
Ce(1)-O(3)-Ce(1)#1	98.0(4)
O(4)-Ce(1)-O(5)	99.6(3)

2.2.2. Complexes with donor functionalised ligands.

2.2.2.1. Synthesis of [Ce(mmp)$_4$].

2.2.2.1.1. Reaction with Na(mmp).

The reaction methodology previously laid out by Bradley,[29] Evans[30] and Gradeff[33] was used in an attempt to make a monomeric donor functionalised Ce(IV) alkoxide. The sodium salt of mmpH was made by reaction with sodium hydride in DME. This was added to a solution of CAN in DME and the procedure followed as before. This method consistently gave material that was insoluble in solvents like toluene and/or exhibited much lower C and H content than would theoretically be expected for $[Ce(mmp)_4]$.

2.2.2.1.2. Synthesis via [Ce(OBu^t)$_4$]

[Ce(mmp)$_4$] was made based on the synthetic route attempted for the preparation of [Ce(ONep)$_4$]. After 2 hours of stirring CAN with NaOBu^t the [Ce(OBu^t)$_4$] intermediate was left *in situ*. Four equivalents of mmpH were added and the reaction refluxed for two hours. An oily yellow solid was obtained after removing the volatiles. This was extracted with hexane and the material recrystallised to give [Ce(mmp)$_4$] in 52 % yield. This reaction was repeated on a 50-100 g in SAFC Hitech and gave the complex in 83 %. The yield of reaction decreases to 35 % without the refluxing step.

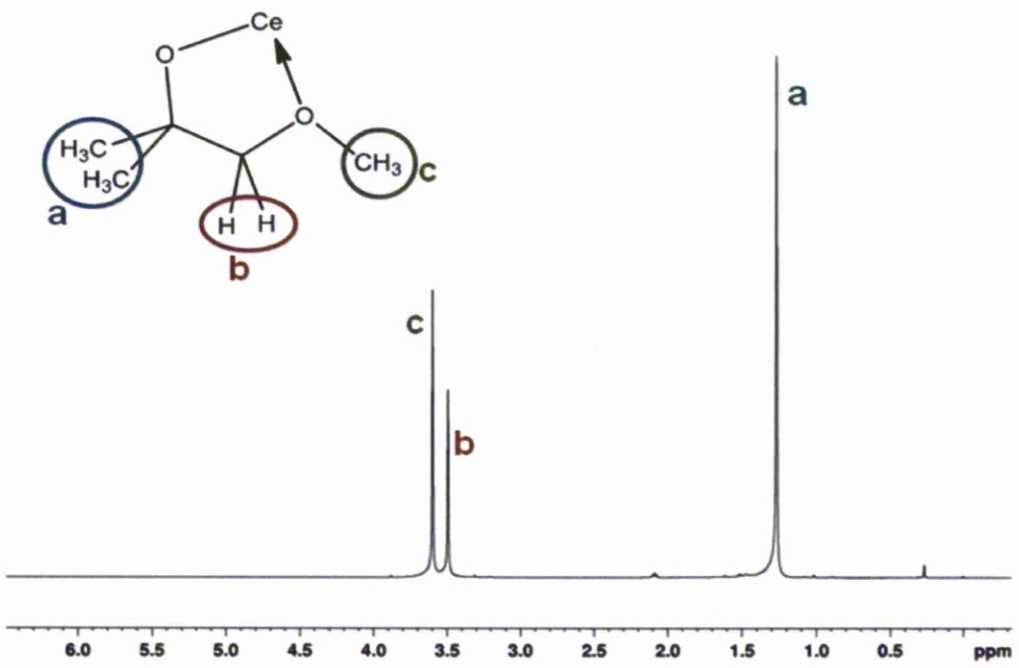

Figure 2. 13: ^{1}H NMR spectrum (C_7D_8) of [Ce(mmp)$_4$].

The sharpness of the 3 singlets in the ^{1}H NMR spectrum of the complex (figure 2.13) indicates the lack of fluxionality of the ligands and variable temperature NMR down to 198 K showed no broadening or splitting of the peaks. In comparing this spectrum to the free ligand also in d^8-toluene there is only a slight change in chemical shift of the singlets from 1.13, 2.93 and 3.07 ppm (figure 2.14).

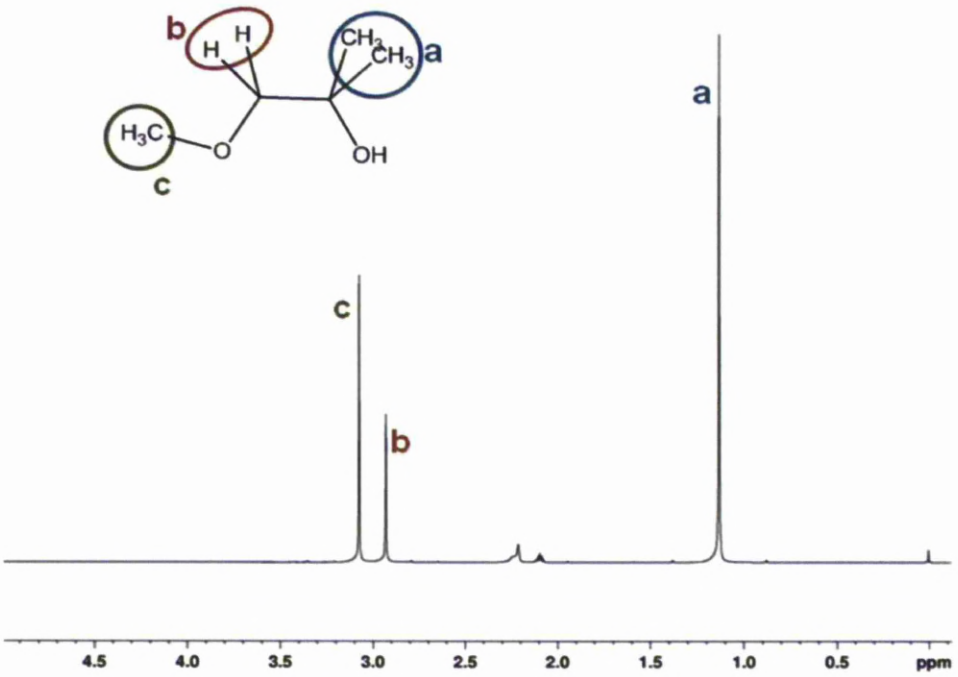

Figure 2. 14: ^{1}H NMR spectrum (C_7D_8) of mmpH.

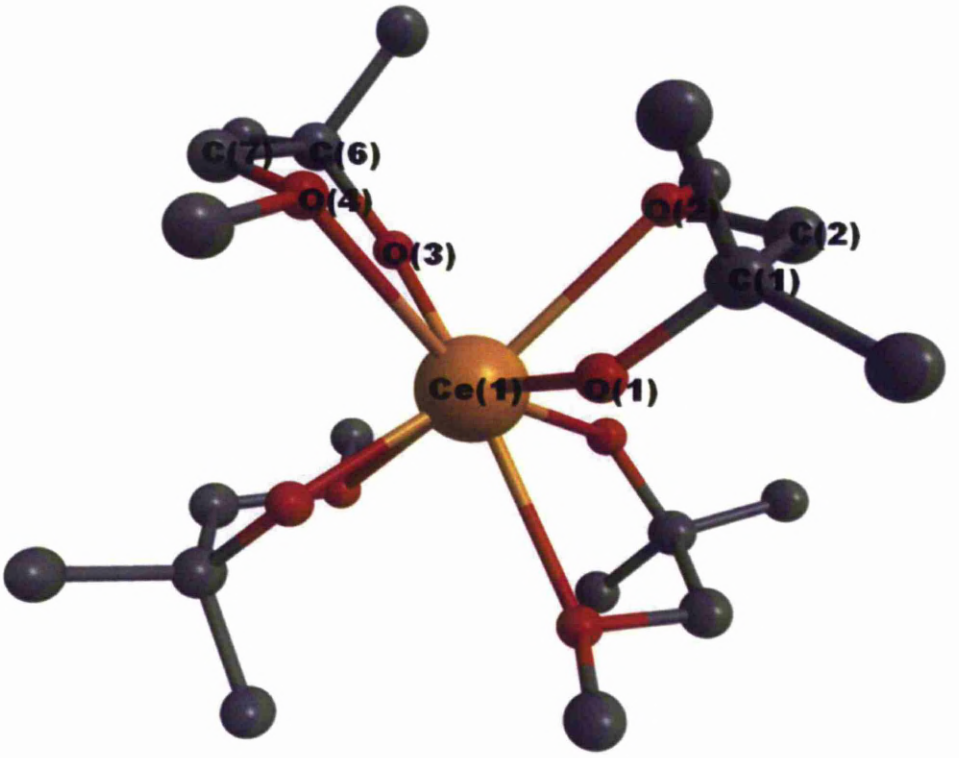

Figure 2. 15: X-ray crystal structure of $[Ce(mmp)_4]$.

Table 2. 5: Selected Bond lengths and angles for $[Ce(mmp)_4]$.

Bond Atoms	Bond Length (Å)
Ce(1) - O(1)	2.155(4)
Ce(1) - O(2)	2.666(4)
Ce(1)-O(3)	2.155(5)
Ce(1)-O(4)	2.684(4)
Bond Atoms	**Bond Angle (°)**
O(1)-Ce(1)-O(2)	64.0(1)
O(1)-Ce(1)-O(3)	96.1(2)
O(1)-Ce(1)-O(4)	153.3(1)
O(1)-Ce(1)-O(1)	105.5(2)
O(4)-Ce(1)-O(2)	140.4(1)
O(4)-Ce(1)-O(3)	76.3(1)
O(1)-C(1)-C(2)-O(2)	46.8(6)
O(3)-C(6)-C(7)-O(4)	48.9(6)

Crystals for X-ray crystallography were grown over a few days in toluene at -18 °C (figure 2.15). The structure shows all 4 mmp ligands coordinated in a distorted square antiprismatic configuration via a Ce-O bond between the mmp alcohol and a dative Ce-OMe bond. The average Ce-OMe dative bond distance in $[Ce(mmp)_4]$ (2.678 Å) is significantly longer than the Ce-$OC(CH_3)_2$ bond distance (2.156 Å). All four ligands are equivalent and all contain a plane of symmetry.

2.2.2.1.3. $[Ce_2(OPr^i)_8(HOPr^i)_2]$ intermediate route

Much like $[Ce(OBu^t)_4]$ the synthesis of $[Ce_2(OPr^i)_8(HOPr^i)_2]$ stems from the reaction between CAN and the sodium salt of the alcohol. Reactions using $[Ce_2(OPr^i)_8(HOPr^i)_2]$ as an intermediate were tried to improve on the $[Ce(OBu^t)_4]$ route for future Ce(IV) alkoxide synthesis. Isopropanol was first reacted with sodium hydride to yield the sodium salt in DME. A solution of ceric ammonium nitrate in DME and $HOPr^i$ was added and $NaNO_3$ precipitated out. MmpH was added to the yellow solution and heated under reflux for 2 hours. Volatiles were removed *in vacuo* and the crude materials recyrstallised from toluene. This reaction did produce $[Ce(mmp)_4]$ but only in 22.9 % yield.

2.2.2.2. Synthesis of $[Ce(dmae)_4]$

$[Ce(dmae)_4]$ was made *via* the same basic route as $[Ce(mmp)_4]$ using 4 equivalents of dmaeH instead of mmpH. After refluxing the intermediate with

dmaeH for 2 hours the volatiles were removed *in vacuo* resulting in a yellow oil. The ^{1}H NMR spectrum of the crude material is shown in figure 2.16 which when compared to the ^{1}H NMR spectrum of the free dmaeH ligand (figure 2.17) is quite similar.

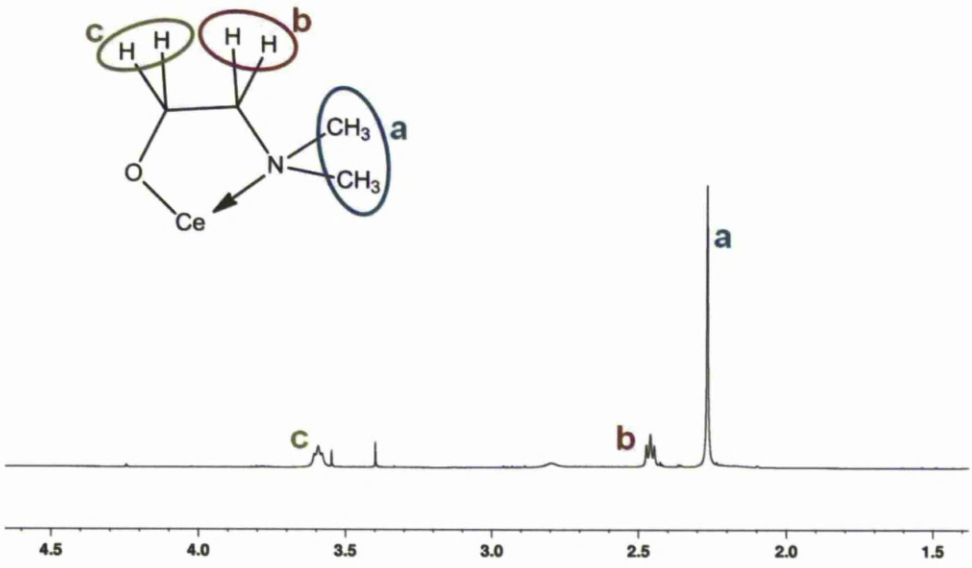

Figure 2. 16: ^{1}H NMR spectrum ($CDCl_3$) of the crude [Ce(dmae)$_4$].

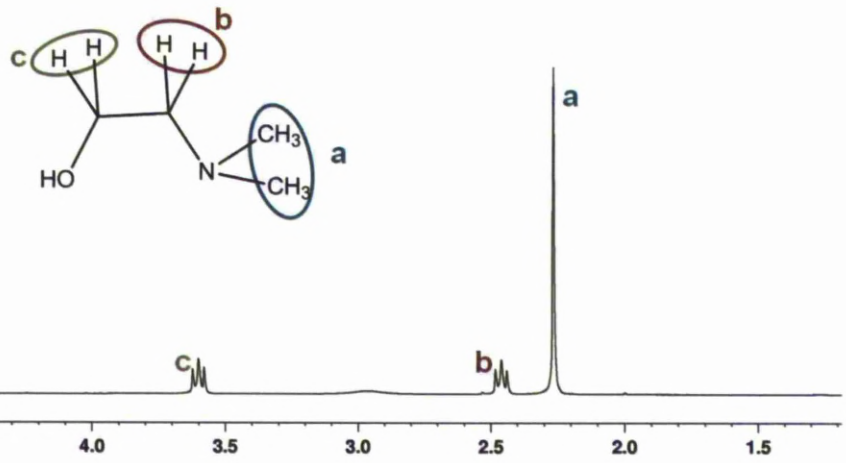

Figure 2. 17: ^{1}H NMR spectrum ($CDCl_3$) of dmaeH in $CDCl_3$.

Very small crystals were obtained after leaving the compound at -18 °C in toluene for a few weeks. These were analysed by X-ray crystallography to give the cluster shown in figure 2.18.

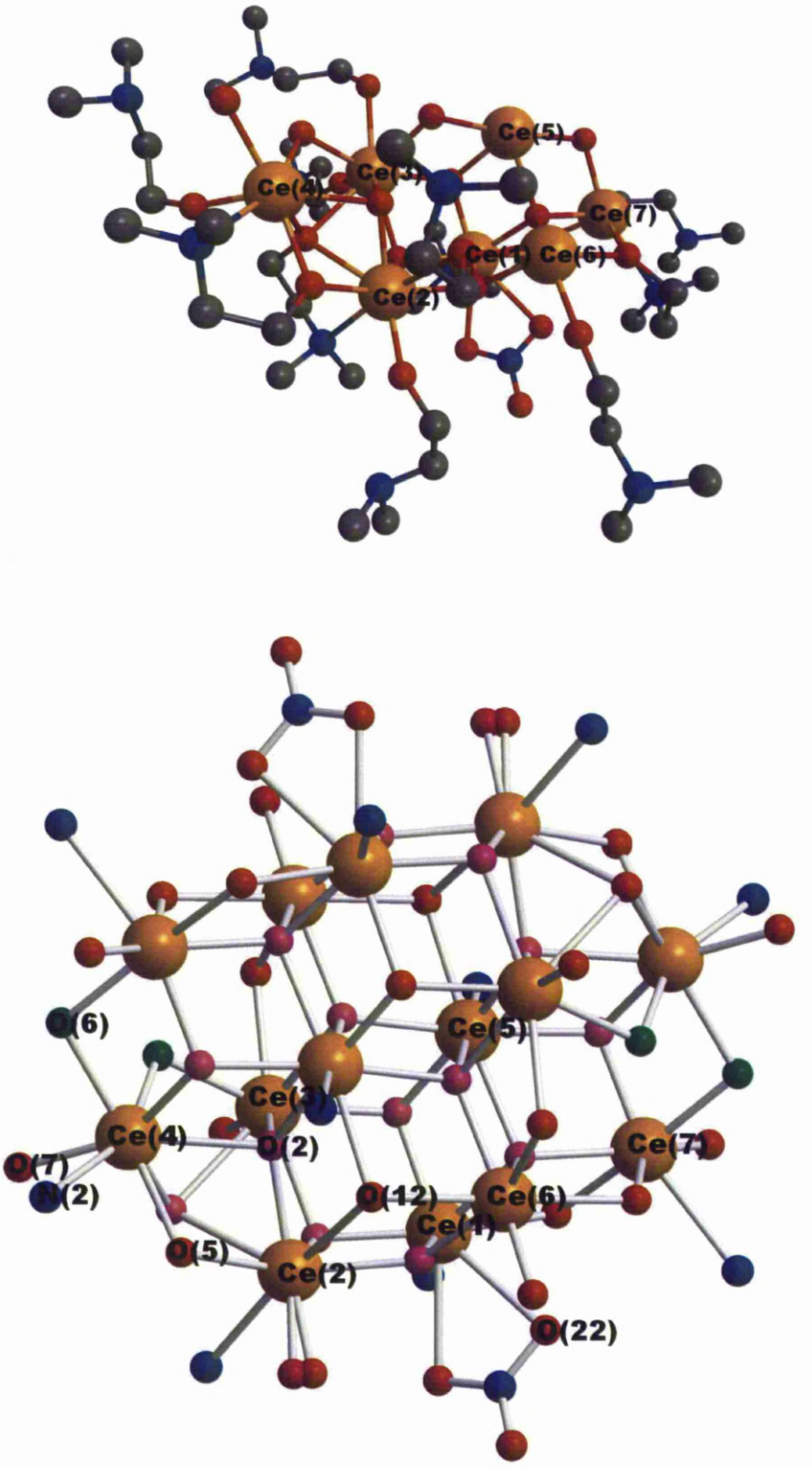

Figure 2.18: Crystal structure of half (top) and the core (bottom) of the cluster $[Ce_{14}(dmae)_{22}(NO_3)_2O_{14}(OH)_4]$. Red = $[O^-]$, pink = $[O^{2-}]$, green = $[HO^-]$.

The cluster consists of 14 Ce^{4+} atoms. The Ce atoms are a mixture of 8-coordinate (10 Ce) and 7-coordinate (4 Ce) and are all bound to each other *via* an oxo-bridge. Out of the 22 dmae ligands there are 12 that are monodentate without the amine N being used in bonding and 10 that are chelating.

Table 2. 6: Table for selected bond lengths and angles for $[Ce_{14}(dmae)_{22}(HNO_3)_2O_{18}]$.

Bond Atoms	Bond Lengths (Å)	O Bond Type
O(7)-Ce(4)	2.104(7)	μ_1
O(5)-Ce(2)	2.406(1)	μ_2
O(3)-Ce(2)	2.626(1)	μ_3
N(5)-Ce(1)	2.649(2)	
Bond Atoms	**Angle (°)**	**O Bond Type**
Ce(2)-O(5)-Ce(4)	101.1(5)	μ_2
Ce(2)-O(12)-Ce(6)	98.7(7)	μ_3
Ce(2)-O(2)-Ce(3)	104.2(0)	μ_4

The reaction was attempted again with addition of the dmaeH at 0 °C with stirring for 2 hours. The crude product gave a complicated ^1H NMR spectrum with broad peaks. The material was distilled for purification leading to the volatilisation of a pale yellow oil that was shown by mass spectrometry to be free dmaeH. The oily residue had the ^1H NMR spectrum shown in figure 2.19. The CHN analysis of this material was within 0.18 % of theoretical values for $[Ce(dmae)_4]$ indicating that $[Ce(dmae)_4]$ exists with the ligand in different environments. Reaction of the dmae ligand at 0 °C was then deemed too low a temperature for the synthesis to go to completion.

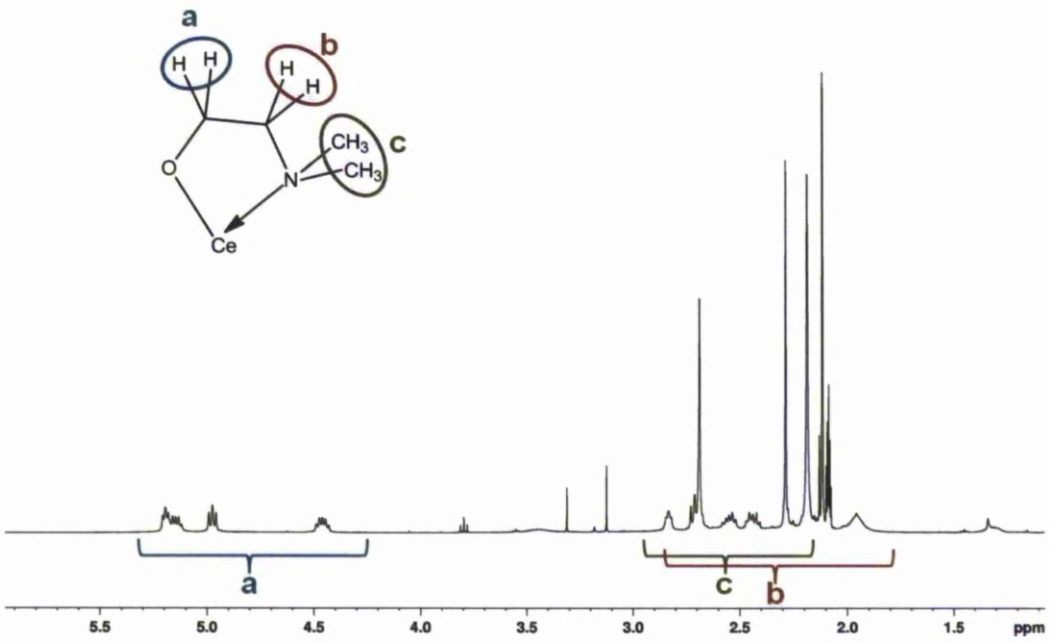

Figure 2. 19: ^{1}H NMR spectrum (C_7D_8) [Ce(dmae)$_4$] sublimed residue.

Repeating the synthesis of [Ce(dmae)$_4$] gave different results sometimes giving the ^{1}H NMR spectra shown in figures 2.16 and 2.19 and other times spectra with very broad peaks and material with low CHN content. Hence, [Ce(dmae)$_4$] does not demonstrate the same structural stability as was found with [Ce(mmp)$_4$] which has a very reproducible synthesis. This is due to the lack of methyl groups at the α-position next to the alcohol oxygen. Sterically the mmp ligand allows for more stability to decomposition than dmae.

2.2.2.3. Synthesis of [Ce(dmap)$_4$].

In view of the instability of the complex with dmae the dmap ligand was considered. Its structure is very similar to dmaeH only differing by the presence of a methyl group in the α-position. This gives the ligand a chiral centre which could lead to the synthesis of different isomers (figure 2.20). A racemic mixture was used in this study.

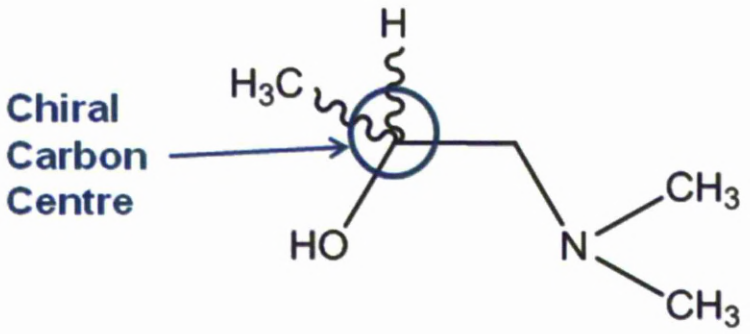

Figure 2. 20: Schematic showing the chiral carbon centre of the dmapH alcohol.

Addition of dmapH to the [Ce(OBu^t)$_4$] intermediate at room temperature resulted in a crude yellow oil that was recrystallised in toluene to give [Ce(dmap)$_4$] as yellow crystals. Altering the temperature of the reaction did not increase the yield from 45 %. The ^{1}H NMR spectrum shown in figure 2.21 is of the crystals grown for x-ray crystallographic analysis. The peaks are sharp and comparable to those of the free ligand (figure 2.22). This indicates that a single highly symmetrical diasteromer was present in solution.

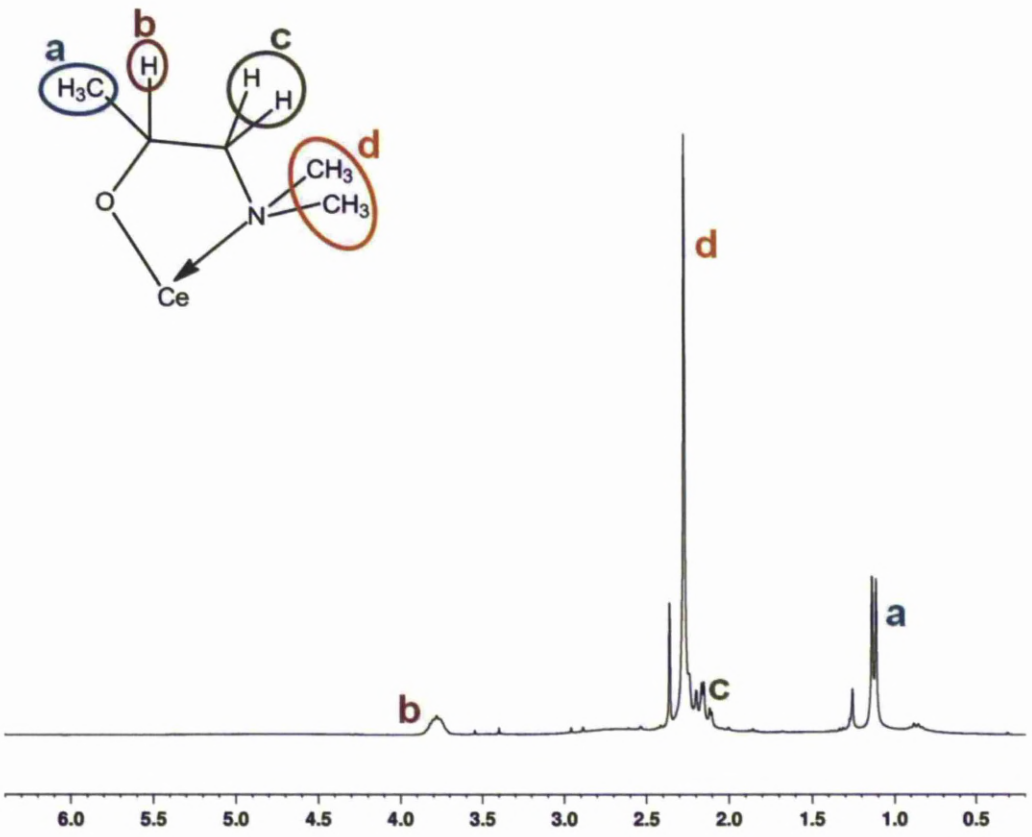

Figure 2. 21: ^{1}H NMR spectrum ($CDCl_3$) of [Ce(dmap)$_4$] crystals for x-ray crystallography.

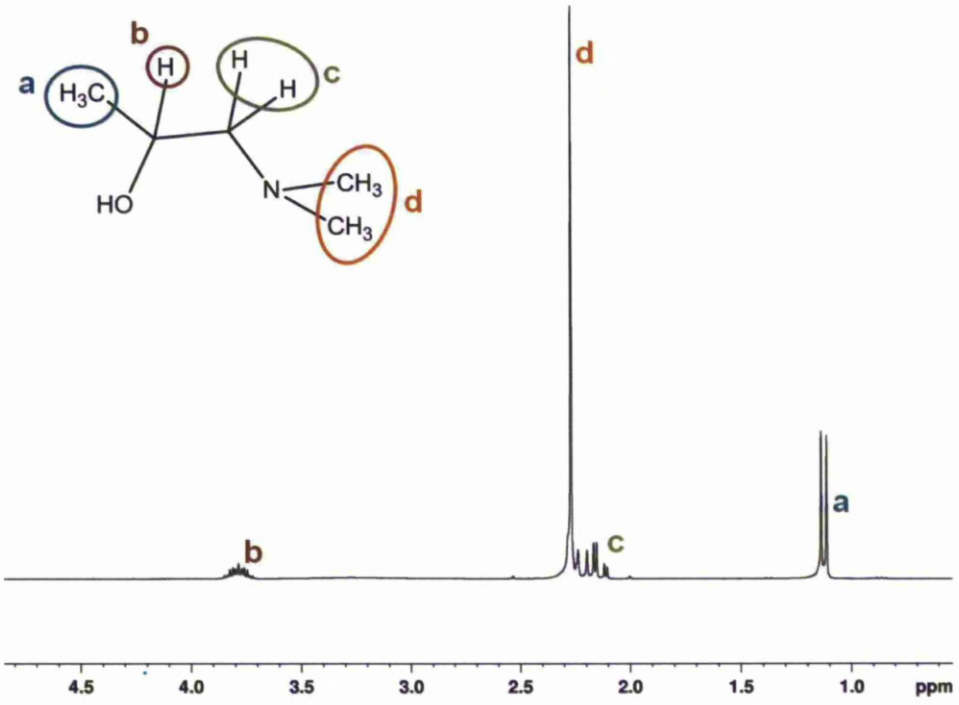

Figure 2. 22: ^{1}H NMR spectrum ($CDCl_3$) of dmapH.

The crystal structure for [Ce(dmap)$_4$] is shown in figure 2.23. All four dmap ligands are chelating to the Ce centre in a square-antiprismatic geometry. The complex contains two *R*- (N2,O2,N2#,O2#) and two *S*-dmap (N1,O1,N1#,O1#) ligands. Despite this, the complex crystallises in the rare chiral, hexagonal, space group P6$_1$22 (figure 2.24). The dihedral angles of 44.9(1) and -45.8(4) (table 2.7) of the *S*- and *R*- ligands show their coplanarity. The Ce-O bonds (~2.17 Å) are siginificantly shorter than the dative Ce-N(CH$_3$)$_3$ bonds (~2.82 Å).

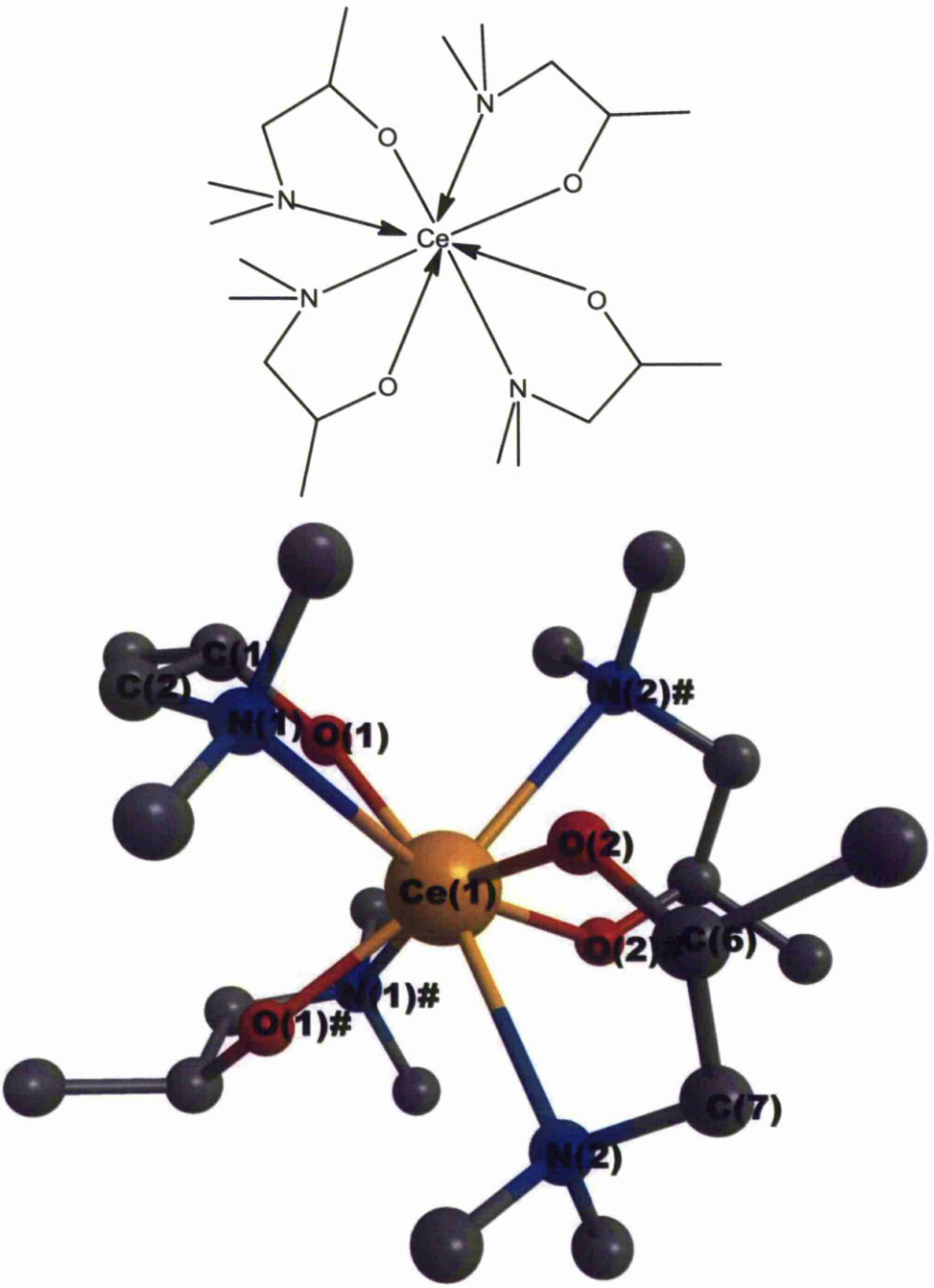

Figure 2. 23: Crystal Structure of [Ce(dmap)$_4$].

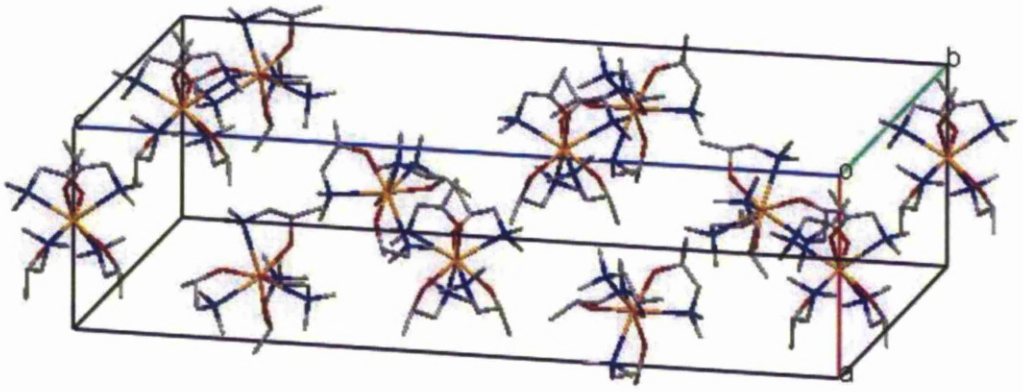

Figure 2. 24: Unit cell packing of $[Ce(dmap)_4]$ in its $P6_122$ space group.

Table 2. 7: Selected bond lengths and angles for $[Ce(dmap)_4]$ crystal structure.

Bond Atoms	Bond Length (Å)
Ce(1)-O(1)	2.165(9)
Ce(1)-O(2)	2.170(9)
Ce(1)-N(1)	2.783(7)
Ce(1)-N(2)	2.851(4)
Bond Atoms	**Bond Angles (°)**
O(1)-Ce(1)-O(2)	126.2(6)
O(1)-Ce(1)-N(1)	64.5(1)
O(2)-Ce(1)-N(2)	77.5
N(1)-Ce(1)-N(2)	99.9(5)
O(2)-C(6)-C(7)-N(2)	-45.8(4)
O(1)-C(1)-C(2)-N(1)	44.9(1)

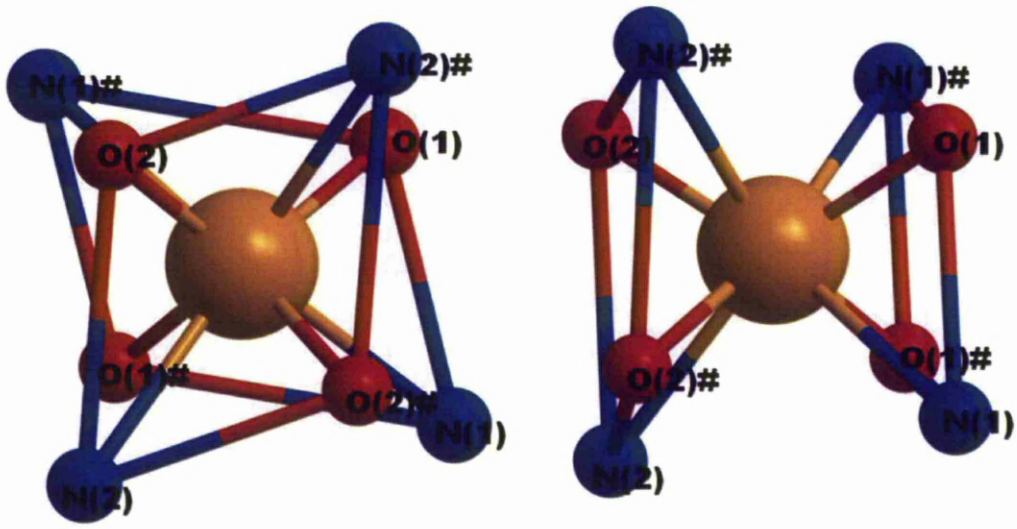

Figure 2. 25: Diagram demonstrating the symmetry of [Ce(dmap)$_4$] (C omitted for clarity).

Figure 2.25 shows a simplified view of the C_2 axis of [Ce(dmap)$_4$]. This demonstrates how the two parallelograms defined as N(1)O(1)N(1)#O(1)# and N(2)O(2)N(2)#O(2)# are twisted by ~84 ° with respect to each other. This renders the complex chiral at the Ce atom.

[Ce(dmap)$_4$] was sublimed at 0.8 Torr. The crystals were seen to melt at 83 °C to a yellow/orange oil and then began a reduced pressure distillation at ~120 °C. As the temperature increased more yellow crystals formed on the condenser. These were analysed by ^{1}H NMR spectroscopy and CHN analysis and confirmed to be the [Ce(dmap)$_4$]. Along with the crystalline material a dark oily residue also remained. This had the elemental analysis shown in table 2.8 and the ^{1}H NMR spectrum in figure 2.26. The material was dissolved in toluene and crystal growth attempted at -

18 °C though no crystals were formed. [Ce(dmap)$_4$] therefore has good volatility but is perhaps less thermally stable than [Ce(mmp)$_4$].

Table 2. 8: Elemental analysis data for sublimation material of [Ce(dmap)$_4$].

	C %	H %	N %
[Ce(dmap)$_4$]	43.78	8.82	10.21
Sublimed Crystals	43.62	8.99	10.11
Sublimation Residue	37.39	7.89	7.55

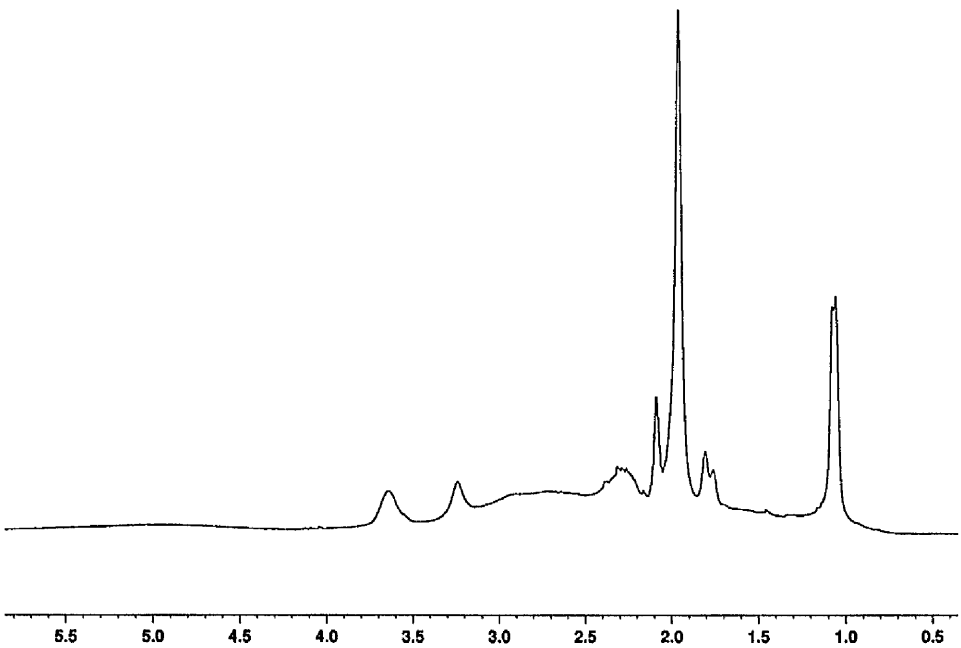

Figure 2. 26: ^{1}H NMR spectrum (C_7D_8) of the sublimation residue of [Ce(dmap)$_4$].

2.2.3. Complexes with oxazolinyl ligands.

2.2.3.1. Synthesis of oxazolinyl ligands.

2.2.3.1.1. Synthesis of 2-(4,4-dimethyl-4,5-dihydrooxazol-2-yl)propanol (dmopH).

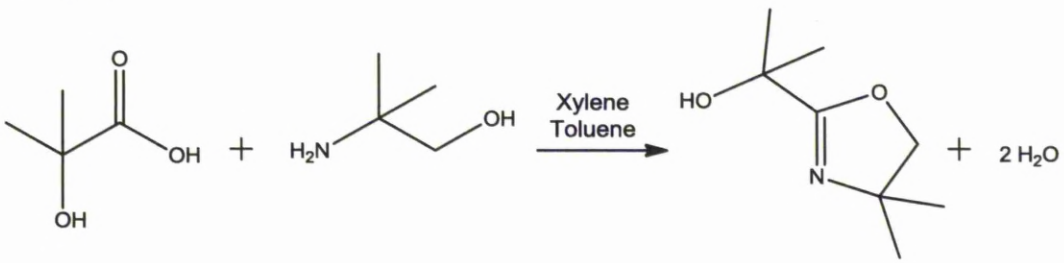

Figure 2. 27: Reaction scheme for synthesis of dmopH.

The dmopH ligand was made following a well known procedure.[49,50] 2-hydroxyisobutyric acid was stirred in xylene at room temperature. 2-amino-2-methyl-propanol was added and the reaction flask fitted with a Dean-Stark apparatus. The mixture was heated to reflux for several days until the desired amount of water was collected. Xylene was distilled off and the resulting yellow oil purified using a kugelrohr to yield dmopH as needle-like white crystals. The reported yield for this reaction is 25 % though only as little as 9 % was obtained. Due to the volatility of dmopH it is likely that some material is lost during the distillation of xylene and also in the Kugelrohr process.

Due to the difficulty of removing the xylene solvent from the reaction mixture a slightly different route was adopted. The amine was added to the acid in solution with toluene and the reaction mixture heated with the Dean-Stark apparatus for 4

days or until over half the theoretical amount of water was collected. Fifty percent of the toluene was then distilled off and xylene was added to the reaction so the toluene and xylene were in a 2:1 ratio. The reaction was then heated for a further 2 days. The solvents were removed *in vacuo* and the crude oil purified as before using a kugelrohr. This increased the reaction yield to 20.8 %. Attempts at SAFC Hitech were unsuccessful in improving the reaction yield.

2.2.3.1.2. Synthesis of (4,4-dimethyl-4,5-dihydrooxazol-2-yl)methanol (dmomH).

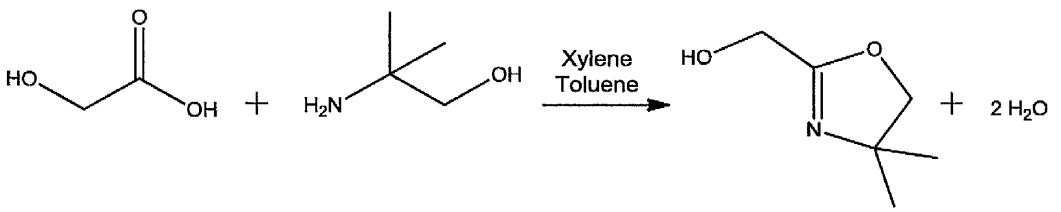

Figure 2. 28: Reaction scheme for the synthesis of dmomH.

DmomH was made in a similar way to dmopH using glycolic acid instead of 2-hydroxyisobutyric acid. The resulting brown oil was purified by Kugelrohr distillation to give dmomH as a low melting pale solid.

2.2.3.1.3. Synthesis of 4,4-dimethyl-4,5-dihydrooxazol-2-yl)-6-methylphenol (dmompH).[51]

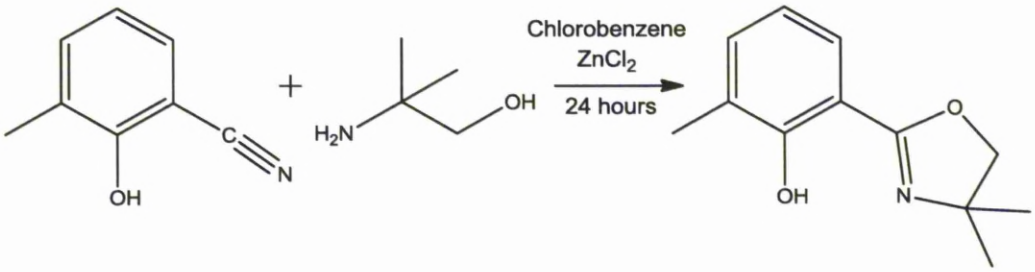

Figure 2. 29: Reaction scheme for the synthesis of dmompH.

The synthesis of dmompH involves a cyclisation reaction between 2-amino-2-methyl propanol and 2-hydroxy-3-methylbenzonitrile catalysed by $ZnCl_2$. The $ZnCl_2$ is first activated by heating under vacuum for 20 minutes. Chlorobenzene is added followed by the nitrile and the amine and the reaction mixture is refluxed for 24 hours. After removing the volatiles and dissolving the crude product in DCM the mixture is washed with H_2O and the resulting yellow oil purified by column chromatography to give dmompH in a 36.4 % yield.

2.2.3.2. Preparation of [Ce(dmop)$_4$]

[Ce(dmop)$_4$] was synthesised using the alcohol exchange reaction with [Ce(OBu^t)$_4$] used previously to make [Ce(mmp)$_4$] (figure 2.29). After the formation of [Ce(OBu^t)$_4$] as an *in-situ* intermediate 4 equivalents of dmopH in DME were added at room temperature giving an alkoxy exchange reaction to yield [Ce(dmop)$_4$].

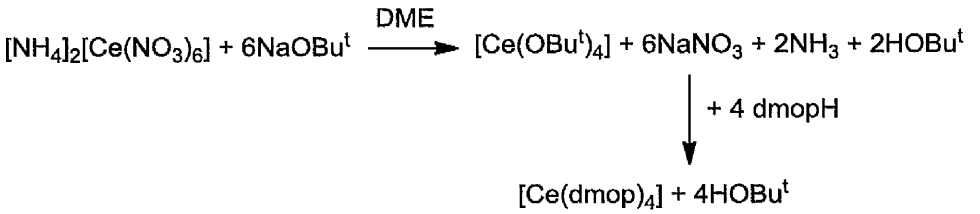

Figure 2. 30: Reaction scheme for synthesis of $[Ce(dmop)_4]$.

Recrystallisation of the crude solid from toluene gave yellow crystals of $[Ce(dmop)_4]$ in 45% yield. The ^1H NMR spectrum of $[Ce(dmop)_4]$ shows 3 singlets in a 6:6:2 ratio (figure 2.31). The two different methyl groups of the ligand are very close in chemical shifts differing from the spectrum of the free dmop ligand (figure 2.32). The plane of symmetry through dmop is retained in the complex.

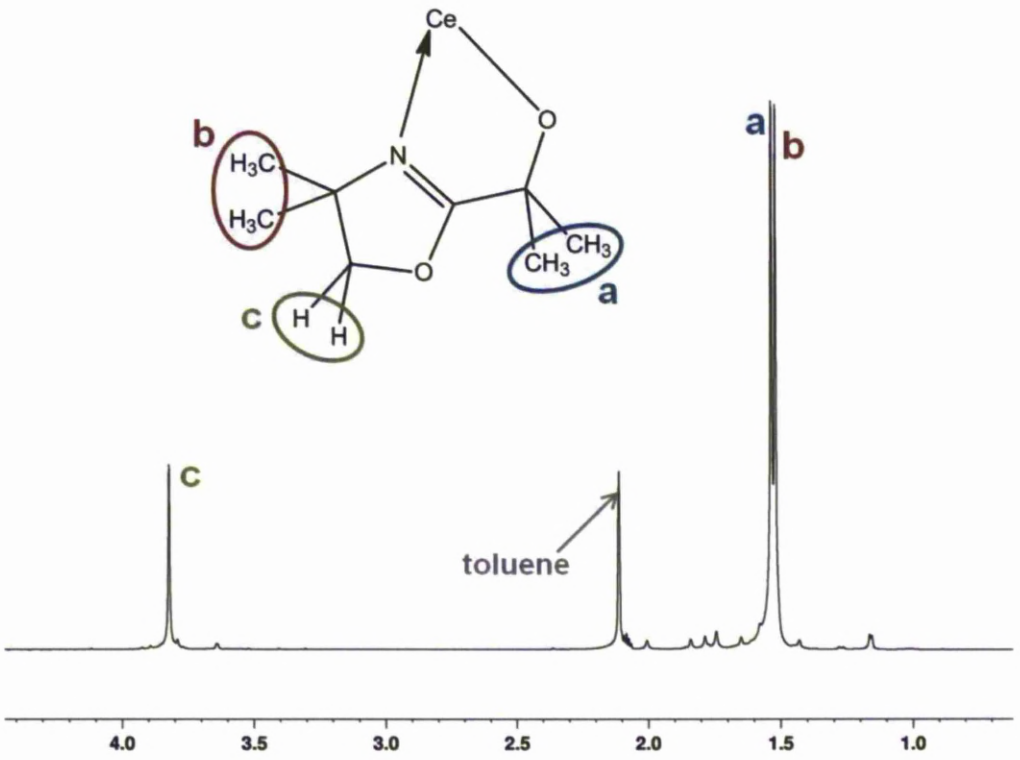

Figure 2. 31: ^{1}H NMR spectrum (C_7D_8) of [Ce(dmop)$_4$].

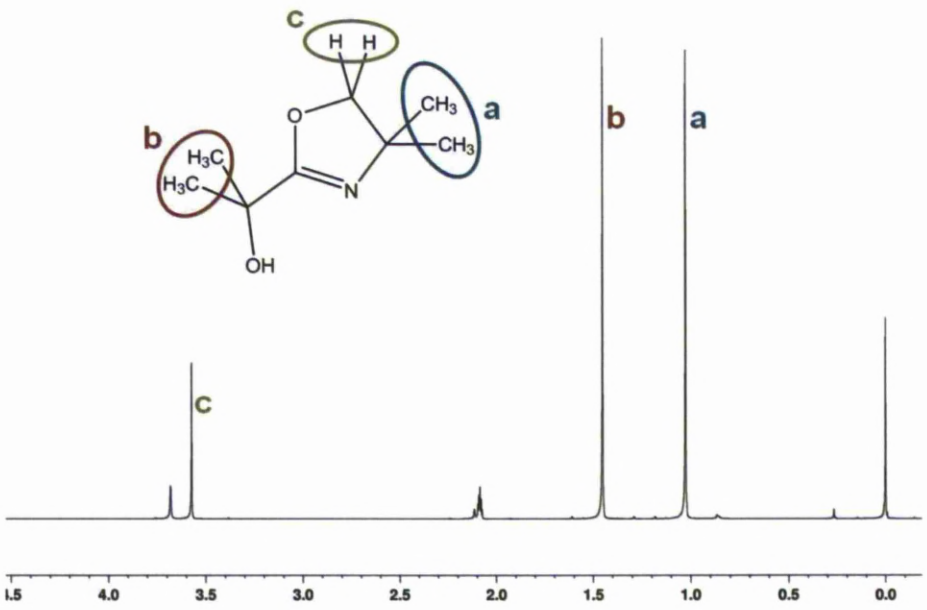

Figure 2. 32: ^{1}H NMR spectrum (C_7D_8) of dmopH.

The crystal structure of $[Ce(dmop)_4]$ shows the dmop ligands sitting with the imine N atoms *cis* to each other. All four ligands are chelating to the Ce atom. The Ce-O bonds are shorter with an average of 2.184 Å than the dative Ce-N bonds with an average length of 2.714 Å. The donor atoms of two of the chelating dmop ligands are close to coplanar (N(1), O(1), N(3), N(5)) as are those of the other two ligands (N(2), O(3), N(4), O(7)). As shown in figure 2.34 the two planes are twisted by ~ 51 ° with respect to each other making the complex chiral but the unit cell has a plane of symmetry meaning that both enantiomeric forms of $[Ce(dmop)_4]$ are present.

Table 2. 9: Selected bond lengths and angles for $[Ce(dmop)_4]$.

Bond Atoms	**Bond Lengths (Å)**
Ce(1)-O(1)	2.174(2)
Ce(1)-O(5)	2.182(2)
Ce(1)-O(3)	2.183(2)
Ce(1)-O(7)	2.195(2)
Ce(1)-N(1)	2.658(2)
Ce(1)-N(2)	2.715(2)
Ce(1)-N(4)	2.723(2)
Ce(1)-N(3)	2.758(2)
Bond Atoms	**Bond angles (°)**
O(1)-Ce(1)-N(1)	64.71(6)
O(7)-Ce(1)-N(3)	78.16(6)
O(3)-Ce(1)-N(2)	63.88(6)
O(5)-Ce(1)-N(4)	75.81(5)
O(1)-C(1)-C(2)-N(1)	5.2(3)
O(3)-C(9)-C(10)-N(2)	-0.4(3)
O(5)-C(17)-C(18)-N(3)	-14.6(3)
O(7)-C(25)-C(26)-N(4)	-13.7(3)

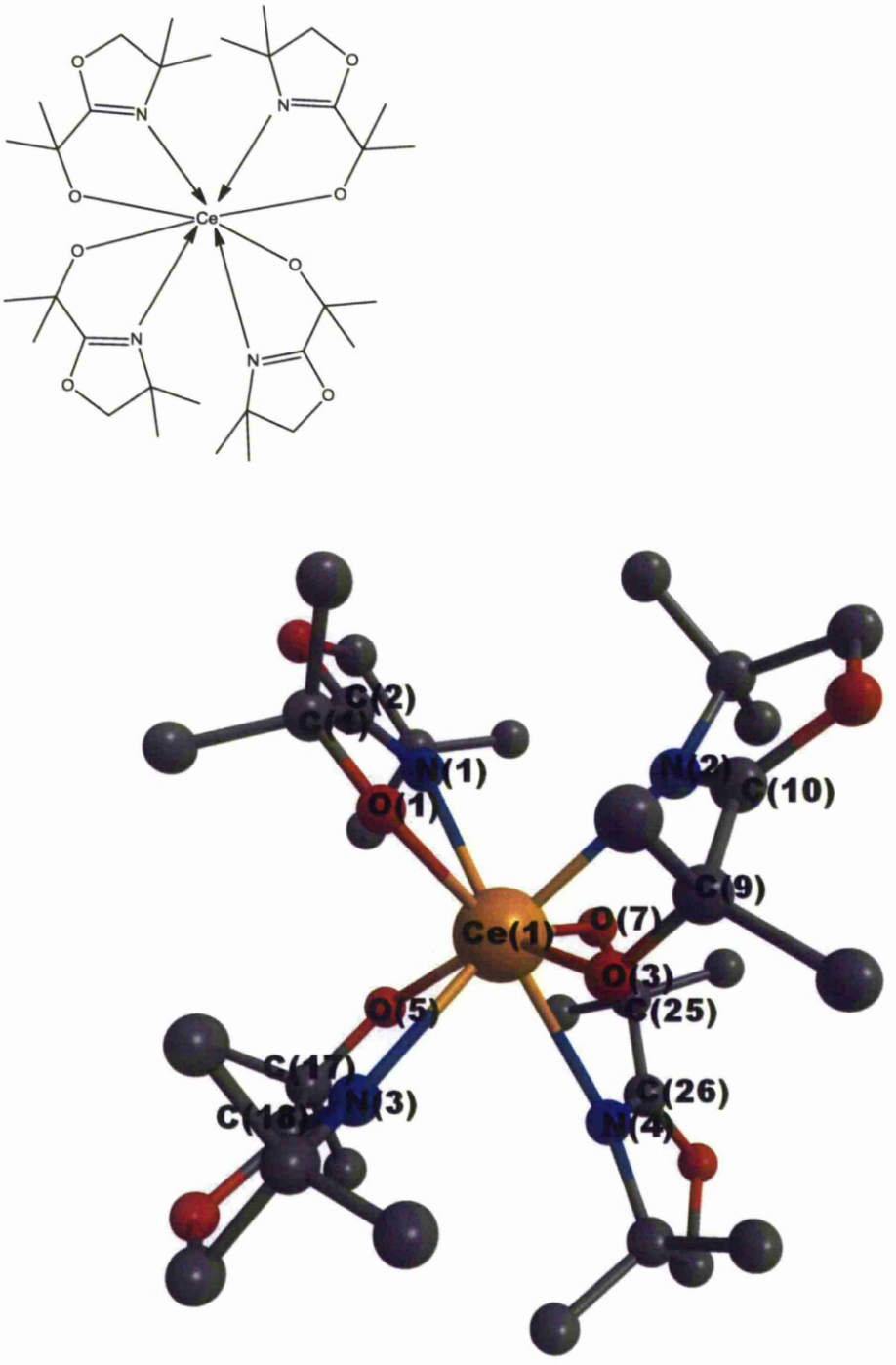

Figure 2. 33: X-ray crystal structure of [Ce(dmop)$_4$].

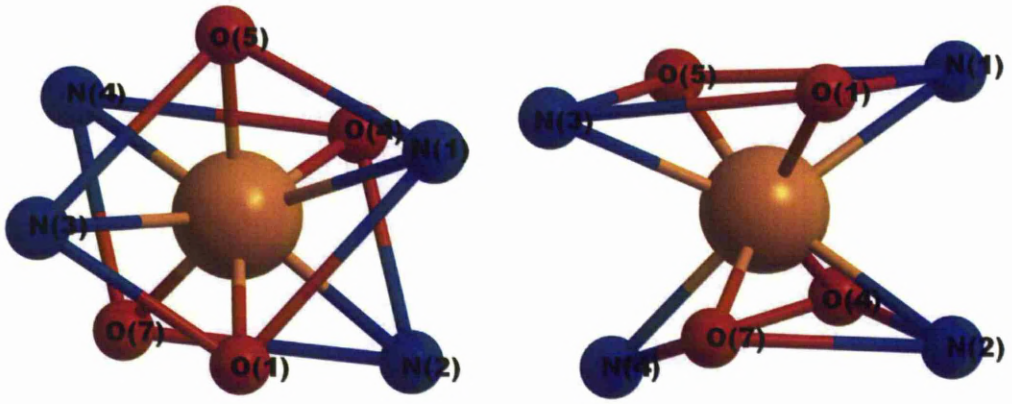

Figure 2. 34: The coordination sphere of one enantiomeric form of [Ce(dmop)$_4$] (C omitted for clarity).

Attempted sublimation of [Ce(dmop)$_4$] yielded in white needle-like crystals condensing at 133 °C. These were determined by ^{1}H NMR spectroscopy to be dmopH. The yellow residue gave the ^{1}H NMR spectrum shown in figure 2.35. This ^{1}H NMR spectrum has also been seen when the synthetic mixture was refluxed. It appears that there are several environments for the dmop ligands. CHN analysis of the material matched the theoretical values for the dimeric [Ce$_2$(dmop)$_6$O]. It is possible that the application of heat to the monomeric [Ce(dmop)$_4$] causes the complex to decompose and form this dimer with the loss of two dmopH ligands.

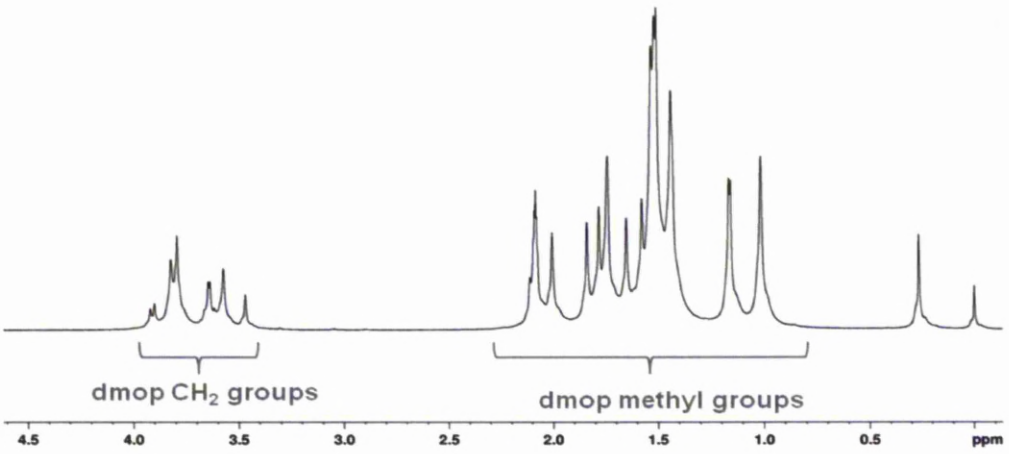

Figure 2. 35: ^{1}H NMR spectrum (C_7D_8) of residue from attempted sublimation of [Ce(dmop)$_4$].

2.2.3.3. Attempted preparation of [Ce(dmom)$_4$].

The synthesis of [Ce(dmom)$_4$] was attempted using a range of different reaction temperatures and times. In most cases the crude material formed was a sticky solid which would decompose in a matter of hours to an insoluble sandy solid. The crude material from the reaction attempted at room temperature gave the ^{1}H NMR spectrum shown in figure 2.36.

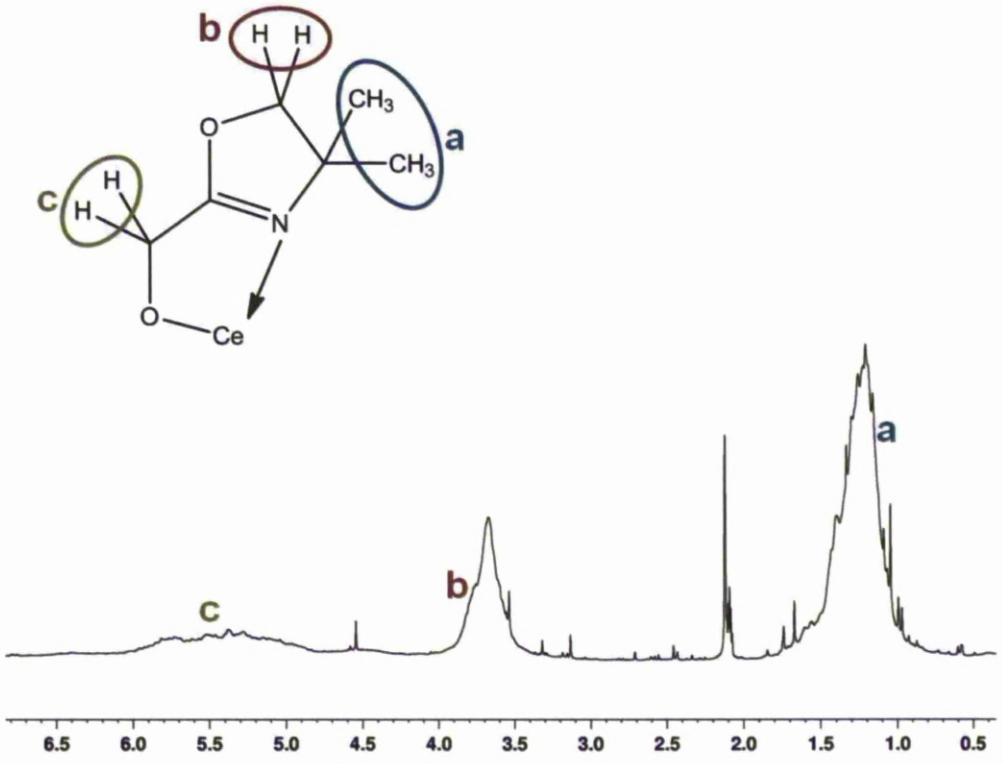

Figure 2. 36: ^{1}H NMR spectrum (C_7D_8) of crude material for the synthesis of [Ce(dmom)$_4$].

The peaks in the spectrum are unexceptional. This material decomposed quickly, precipitating out of the deuterated toluene solution. It would seem the desired complex did form but is very unstable and so further analysis of the material was difficult. This could be due to the lack of an α-methyl group next to the alcohol of the ligand. The steric bulk of the ligand is hence smaller than compared to dmop reducing its ability to stabilise the complex. Further attempts to make [Ce(dmom)$_4$] were abandoned.

2.2.3.4. Preparation of [Ce(dmomp)$_4$].

[Ce(dmomp)$_4$] was made using the intermediate [Ce(OBu^t)$_4$]. On addition of four equivalents of dmompH in DME to [Ce(OBu^t)$_4$] at room temperature a colour change from yellow to deep red was seen. After 2 hours of stirring, the volatiles were removed under vacuo to give a red, dusty solid. This material was found to be less soluble in toluene than previous complexes. Attempts to crystallise the solid from toluene at -18 °C, 5 °C and room temperature gave only red solid coming out of solution. The ^{1}H NMR spectrum of this solid in deuteurated chloroform is shown in figure 2.37.

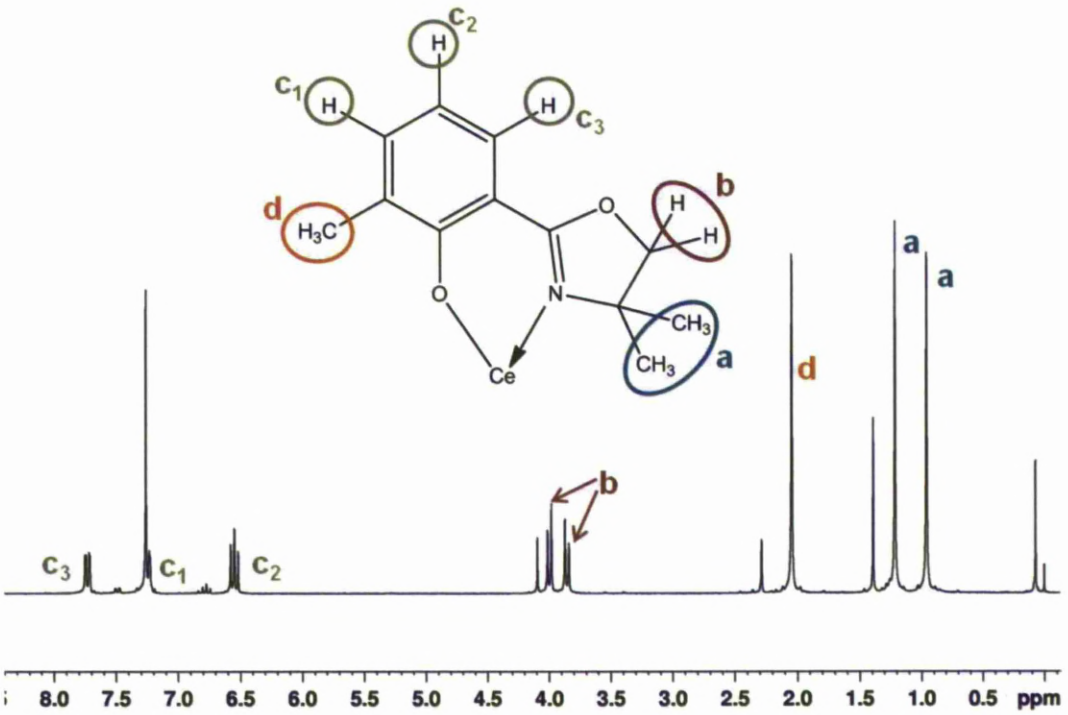

Figure 2. 37: ^{1}H NMR spectrum ($CDCl_3$) of [Ce(dmomp)$_4$].

The two oxazoline ring methyls are seen as two separate singlets and the protons of the oxazoline ring have been split into AB doublets with a coupling constant of $J = 7.90$ Hz. The dmomp ligand has lost its symmetry in coordination to Ce causing this splitting of peaks. All peaks are in the ratio 3:3:3:1:1:1:1:1. The other peaks in this spectrum are attributed to the free dmompH ligand as an impurity. The material was also analysed by mass spectroscopy to give a dominant peak of 956.3 correlating to the $[M^+]$.

$[Ce(dmomp)_4]$ appeared to have low solubility in toluene in comparison to more polar solvents such as THF or DCM when comparing solutions of 0.025 M concentration. Given that the precursors used for liquid-injection MOCVD are made into solutions in toluene the compound looked unfavourable for deposition. Even though the complex demonstrated better solubility in THF and DCM it was observed that after 48 hours in DCM and 120 hours in THF the solutions went from dark red to yellow with a sand coloured precipitate. This occurrence was found to be independent of temperature or light. The ^1H NMR spectrum of this precipitate is shown in figure 2.38.

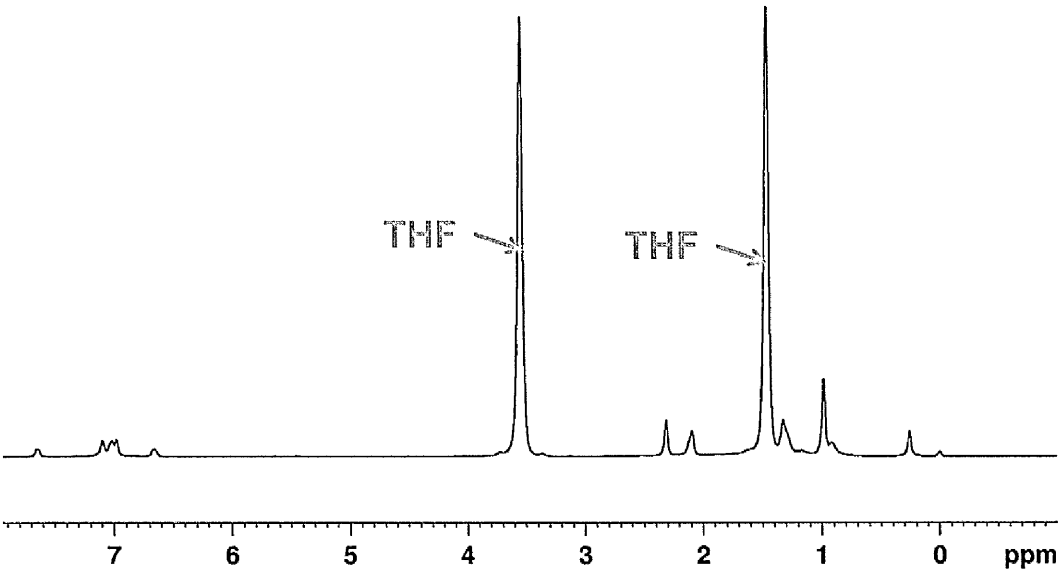

Figure 2. 38: ^{1}H NMR spectrum (C_7D_8) of yellow solution after [Ce(dmomp)$_4$] degradation.

Given that the ^{1}H NMR spectrum is not of a paramagnetic complex it was deemed that degradation to a Ce^{3+} complex had not occurred. The broadening of the peaks suggests cleavage of a dmomp ligand to give fluxionality or perhaps oligomerisation. The material soon became insoluble in several solvents tried and so further characterization was difficult.

2.2.4. Heteroleptic Ce(IV) alkoxide complexes

2.2.4.1. Complexes with β-diketonates

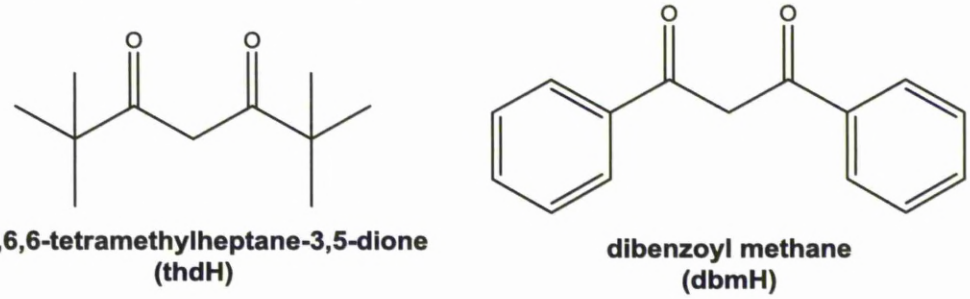

2,2,6,6-tetramethylheptane-3,5-dione (thdH)

dibenzoyl methane (dbmH)

Figure 2. 39: Structures of the β-diketonates thdH and dbmH.

The β-diketones thdH and dbmH (figure 2.39) have shown promise as ligands for monodentate Ce (IV) complexes[52-54] but they lack the reactivity necessary for better deposition of CeO_2 given their low Brønsted bascitiy. Making complexes with these ligands and alkoxides was attempted.

2.2.4.1.1. 2,2,6,6,-tetramethylheptane-3,5-dione (thdH).

Given the usefulness of $[Ce(thd)_4]$, thd was used to make heteroleptic derivatives of the compound with mmpH and dmapH alcohols. Due to the strong chelating ability of the β-diketonate, reactions were tried starting with $[Ce(mmp)_4]$ and $[Ce(dmap)_4]$. In all reactions the starting complex was dissolved in toluene and two equivalents of thdH in toluene were added to the solution. Reactions were tried at varying temperatures ranging from -80 °C to room temperature and in all cases $[Ce(thd)_4]$ was synthesised. The thdH ligand is therefore a much stronger ligand than the alkoxides and so making heteroleptic complexes was difficult.

2.2.4.1.2. Dibenzoylmethane (dbmH).

2.2.4.1.2.1. Synthesis of [Ce(mmp)$_2$(dbm)$_2$].

2 equivalents of dbmH in toluene was added to [Ce(mmp)$_4$] stirring in toluene at 0 °C. The yellow solution was seen to turn orange on immediate addition of the β-diketonate and the reaction was stirred for 2 hours allowing warming to room temperature. Removing the volatiles under *vacuo* gave an orange oil residue. Attempts to crystallise this material in toluene gave a very low melting point orange solid in 31.2 % yield.

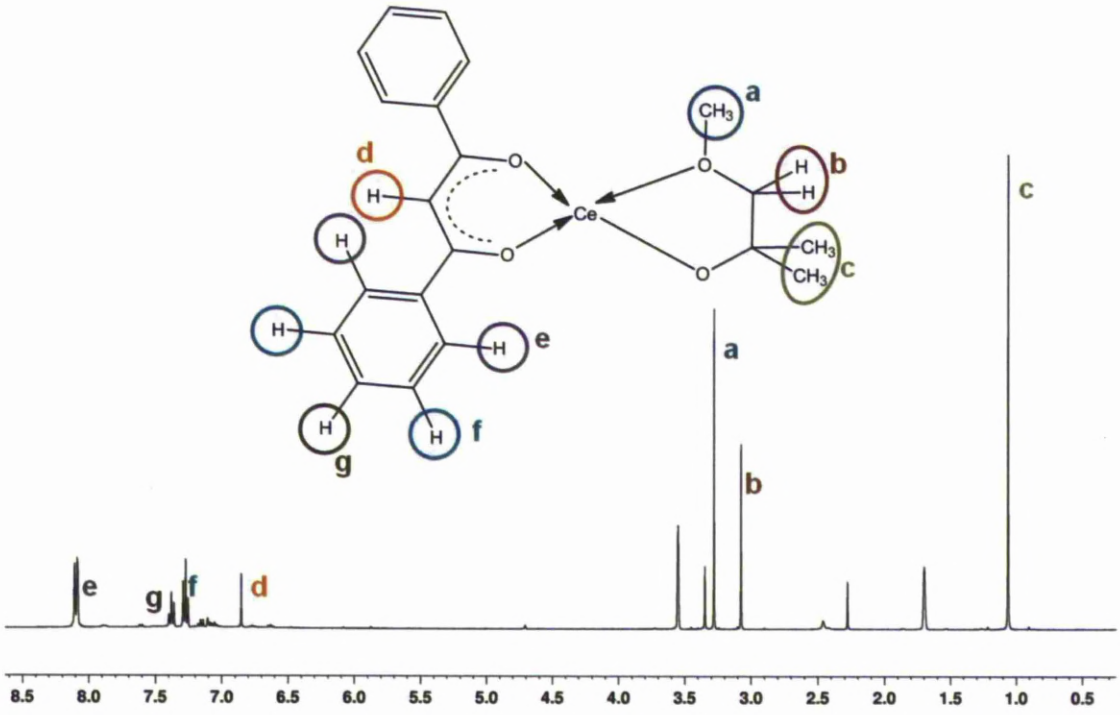

Figure 2. 40: ^{1}H NMR spectrum (C_7D_8) of [Ce(mmp)$_2$(dbm)$_2$].

Sublimation attempts of this material led to the darkening in colour from deep orange to red with no volatilisation up to 180 °C. This material was shown by ^{1}H NMR spectroscopy to resemble $[Ce(dbm)_4]$.

2.2.4.1.2.2. Synthesis of $[Ce(dmap)_2(dbm)_2]$.

$[Ce(dmap)_2(dbm)_2]$ was synthesised by the addition of 2 equivalents dbmH in toluene to $[Ce(dmap)_4]$. Performing the reaction above -15 °C saw the yellow solution become immediately dark red in colour and $[Ce(dbm)_4]$ was made. At -15 °C the solution remained yellow orange and gave a sticky orange solid. CHN analysis of the material was within 0.19 % of theoretical values.

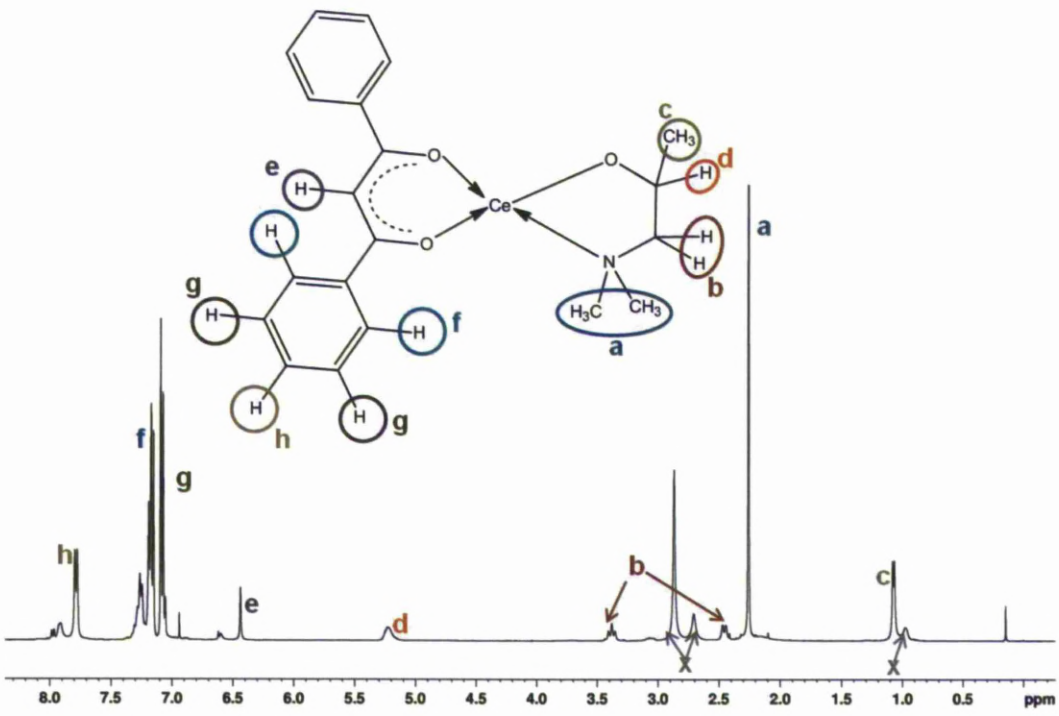

Figure 2. 41: ^{1}H NMR spectrum ($CDCl_3$) of $[Ce(dmap)_2(dbm)_2]$.

Figure 2.41 shows the ^{1}H NMR spectrum with proposed peak assignments. The integrations for the dbm ligand peaks are 2:1 in ratio with the dmap peaks. In the ^{13}C NMR spectrum there are 10 peaks for the ligand whereas theoretically there should be 6. This could be explained if the dbm ligand has lost its symmetry in coordination to Ce and the aromatic groups are no longer equivalent. The dmap ligand peaks labelled (a), (b), (c) and (d) are in the correct ratios for one ligand and were shown by COSY spectroscopy to be related to each other. The peaks labelled "x" may be due to a dmap ligand in a different geometry though a peak for an extra amine group is not visible.

Attempts to sublime this material also led to the formation of $[Ce(dbm)_4]$. This shows that under higher temperatures the compound decomposes causing the thermodynamically more stable homoleptic complex to form.

2.2.4.2. Heteroleptic Alkoxide Complexes with mmp.

2.2.4.2.1. Attempted synthesis of [Ce(mmp)$_2$(dmop)$_2$].

The synthesis of the heteroleptic [Ce(mmp)$_2$(dmop)$_2$] was attempted by adding 2 equivalents of dmopH in toluene to [Ce(mmp)$_4$] stirring in toluene at 0 °C. After stirring for 2 hours the volatiles were removed under *vacuo* and the crude product was recrystallised from toluene. The crystals were characterised by x-ray crystallography and found to be the dimer [Ce(dmop)$_4$(mmp)$_2$(O)] (figure 2.42).

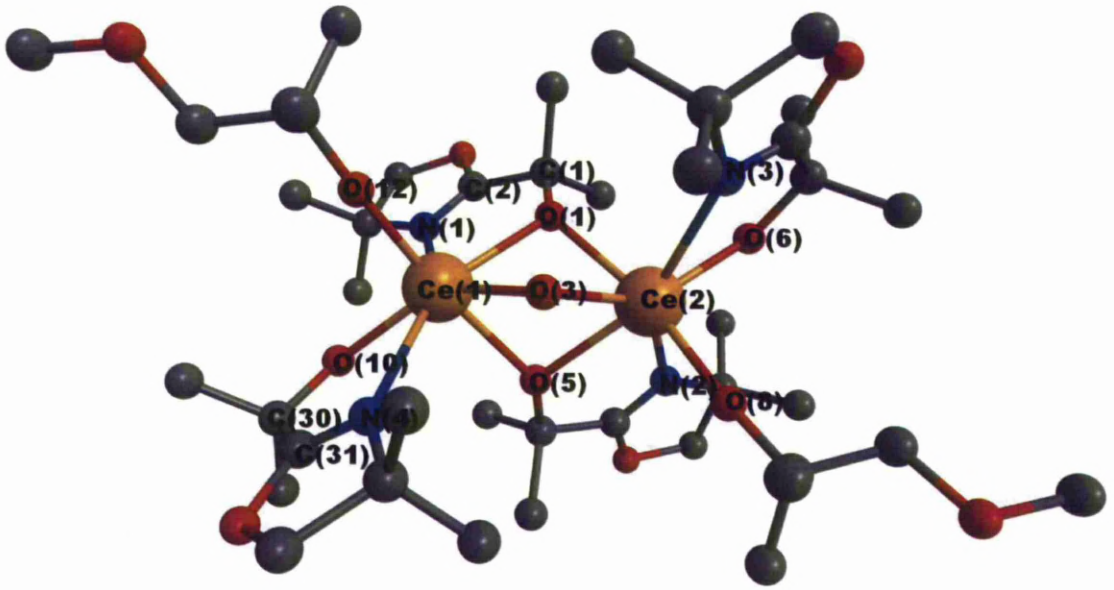

Figure 2. 42: X-ray crystal structure of [Ce$_2$(mmp)$_2$(dmop)$_4$(O)].

The dimer exists with each Ce atom bound to one monodentate mmp ligand and one chelating dmop ligand demonstrating again that the OMe group is not a powerful donor. The crystal is in the chiral space group $P2_1$. There is also a second dmop ligand creating an oxo-bridge between the two Ce atoms via its alcohol O. Another oxygen bridges the two Ce atoms as well making each Ce atom 7-coordinate. The bond lengths (table 2.10) of the mmp and dmop ligands are different to those of $[Ce(mmp)_4]$ and $[Ce(dmop)_4]$. The Ce-O bond of the mmp alcohol is shorter in the dimer than the monomer (2.08 Å and 2.16 Å respectively). The dmop Ce-N dative bonds are similar lengths of ~ 2.6 Å whereas the alcohol Ce-O bonds are much longer in the dimer at ~ 2.4 Å compared to $[Ce(dmop)_4]$ (2.2 Å).

Table 2. 10: selected bond data for $[Ce_2(mmp)_2(dmop)_4(O)]$.

Bond Atoms	Bond Length (Å)
Ce(1)-O(1)	2.406(5)
Ce(1)-O(3)	2.395(5)
Ce(1)-O(5)	2.106(5)
Ce(1)-O(10)	2.238(6)
Ce(1)-O(12)	2.078(5)
Ce(1)-N(1)	2.603(5)
Ce(1)-N(4)	2.620(6)
Bond Atoms	**Bond Angle (°)**
Ce(1)-O(1)-Ce(2)	89.9(2)
Ce(1)-O(5)-Ce(2)	106.7(2)
Ce(1)-O(3)-Ce(2)	88.3(2)
O(1)-Ce(1)-N(1)	63.7(2)
O(10)-Ce(1)-N(4)	64.7(2)
O(10)-C(30)-C(31)-N(4)	1(1)
O(1)-C(1)-C(2)-N(1)	0(1)

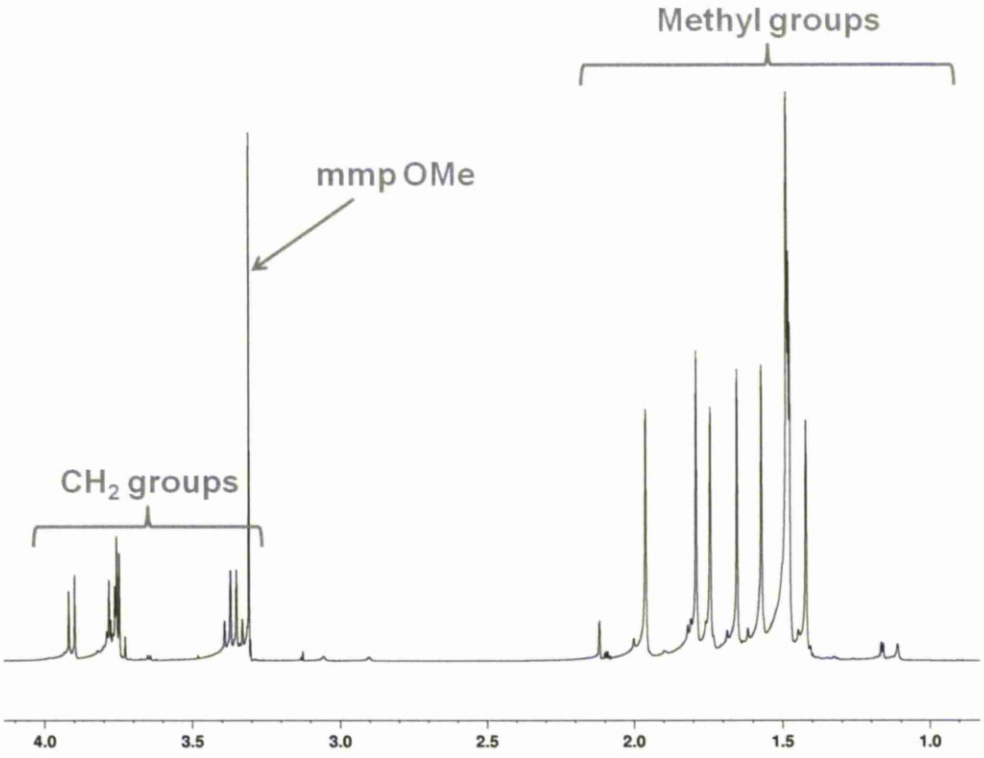

Figure 2. 43: ^{1}H NMR spectrum (C_7D_8) of the dimer $[Ce_2(mmp)_2(dmop)_4(O)]$.

The ^{1}H NMR spectrum of $[Ce_2(mmp)_2(dmop)_4(O)]$ shows 7 peaks in the chemical shift range 1.42 ppm to 3.39 ppm in the ratio 3:12(m):3:3:3:3:3 (figure 2.43). This accounts for the 8 different methyl groups on the four dmop ligands and the 2 different methyl groups on the two mmp ligands. The singlet at 3.30 ppm represents the methoxy of mmp.

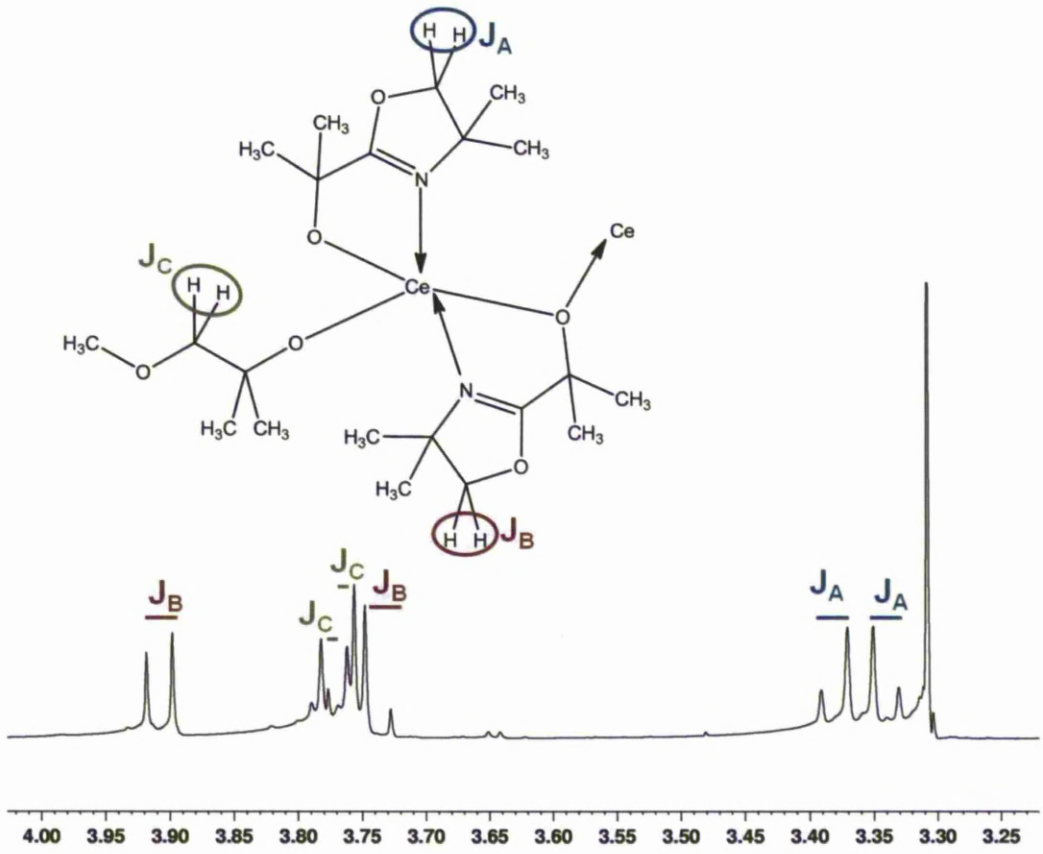

Figure 2. 44: ^{1}H NMR spectrum (C_7D_8) expansion of $[Ce_2(mmp)_2(dmop)_4(O)]$.

The spectrum in figure 2.44 shows the peaks due to the geminal CH_2 protons of the ligands. The AB doublets with coupling constants J_A and J_B are the protons for the two dmop ligands in different environments. The coupling constants are both equal to 8.08 Hz. The doublets with the coupling constant J_C are from the geminal protons of the mmp ligand and has a value of 2.24 Hz. All the doublets are 1:1 in ratio and are 1:3 in ratio with the singlet peaks of the methyl groups.

The ^{1}H NMR spectrum of the crude reaction mixture suggests that a monomer does initially form. The crude material was dissolved in deuterated toluene and

flame-sealed in a glass NMR tube. A spectrum was run initially, after 1.5 hours and then after several hours. The results of which are shown in figure 2.45.

In the initial spectra there are 6 predominant peaks in a 6:6:6:2:3:2 ratio which would be theoretically expected for the $[Ce(mmp)_2(dmop)_2]$ complex. After 1.5 hours the peaks have changed dramatically and there is obvious conversion to a different complex. After 6 hours the ^1H NMR spectrum is beginning to resemble that in figure 2.43. This shows that there may be initial formation of the monomer which converts over time to the thermodynamically more stable dimer.

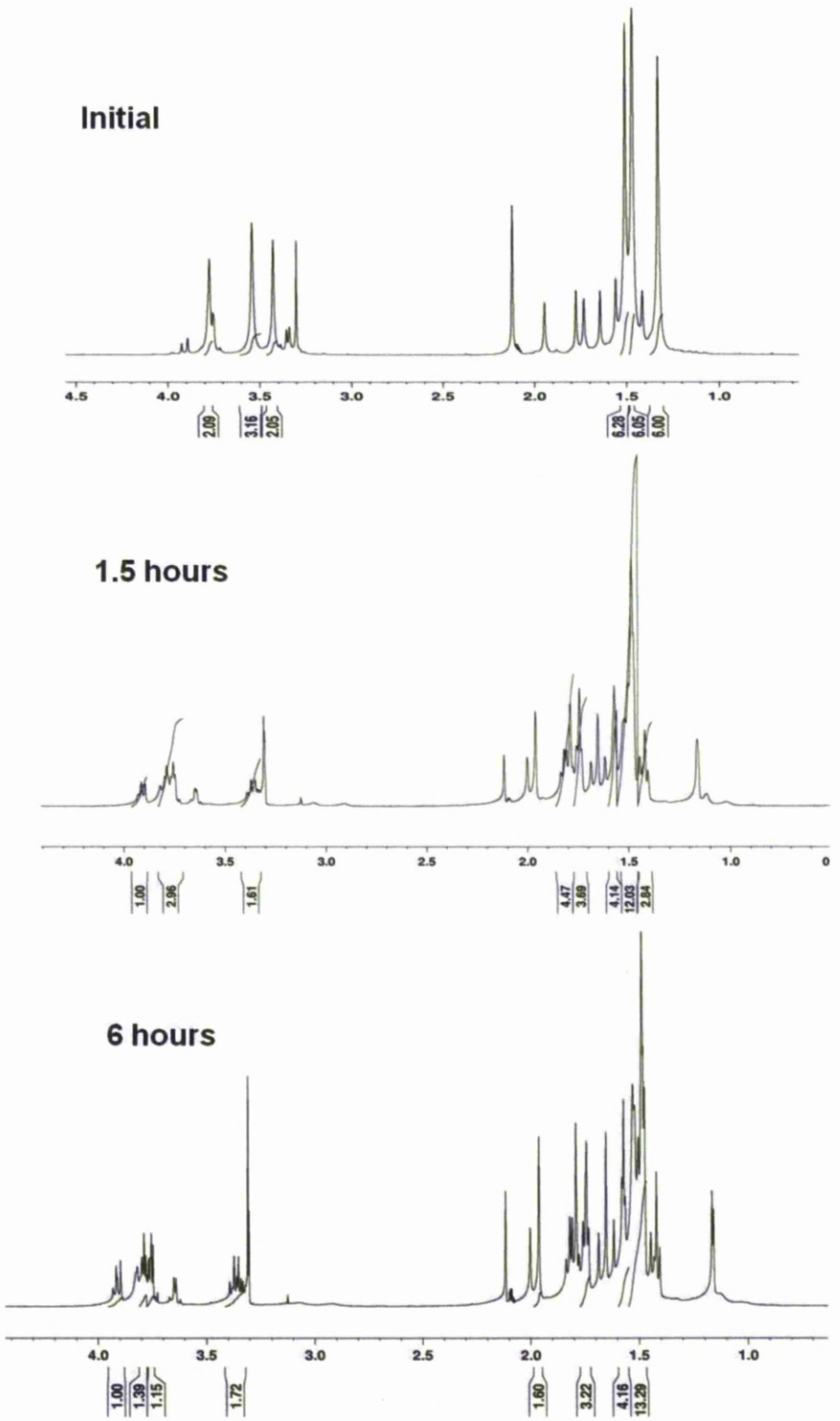

Figure 2. 45: ^{1}H NMR spectra (C_7D_8) of $[Ce(mmp)_2(dmop)_2]$ conversion to $[Ce_2(dmop)_4(mmp)_2(O)]$.

2.2.4.2.2. Synthesis of [Ce(mmp)$_2$(dmom)$_2$].

[Ce(mmp)$_4$] was dissolved in toluene and stirred with cooling to 0 °C. Two equivalents of dmomH in toluene were added slowly to the yellow solution and the reaction was stirred for 2 hours maintaining the temperature at 0 °C. There was no visible change in the solution during this time. Removal of the volatiles gave a yellow oil, the ^{1}H NMR spectrum of which is shown in figure 2.46.

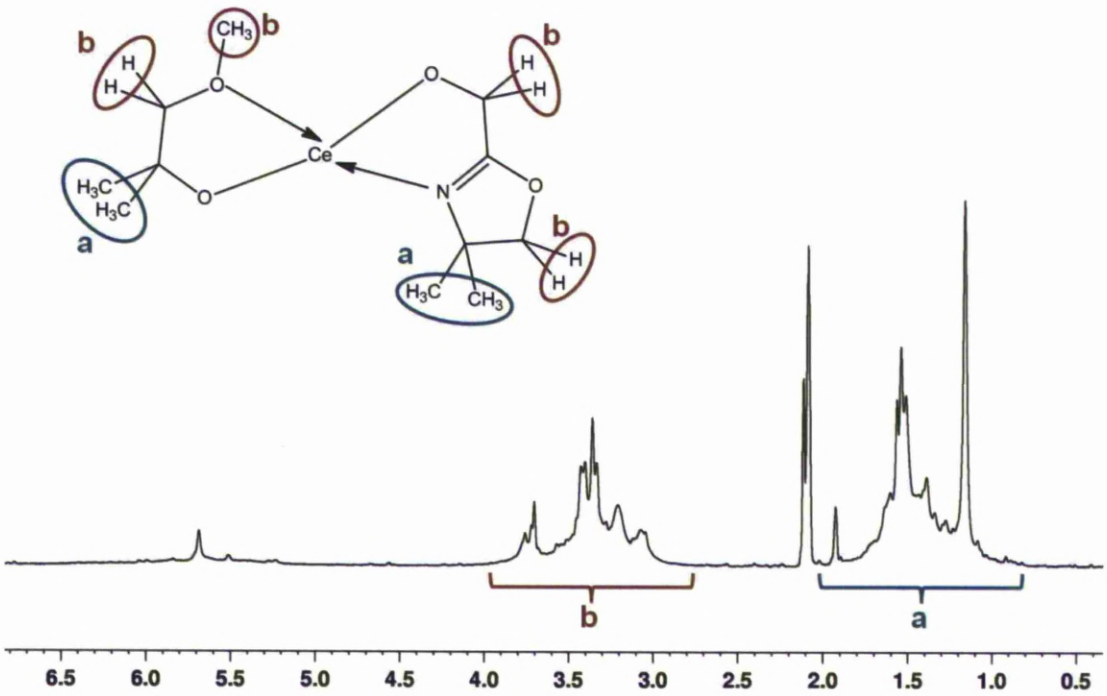

Figure 2. 46: ^{1}H NMR spectrum (C_7D_8) of [Ce(mmp)$_2$(dmom)$_2$].

After several weeks at -18 °C in toluene some crystals suitable for x-ray diffraction were obtained. These gave the structure shown in figure 2.47. The

structure is that of a dimer consisting of two Ce atoms, six mmp ligands, four dmom ligands and two Na atoms.

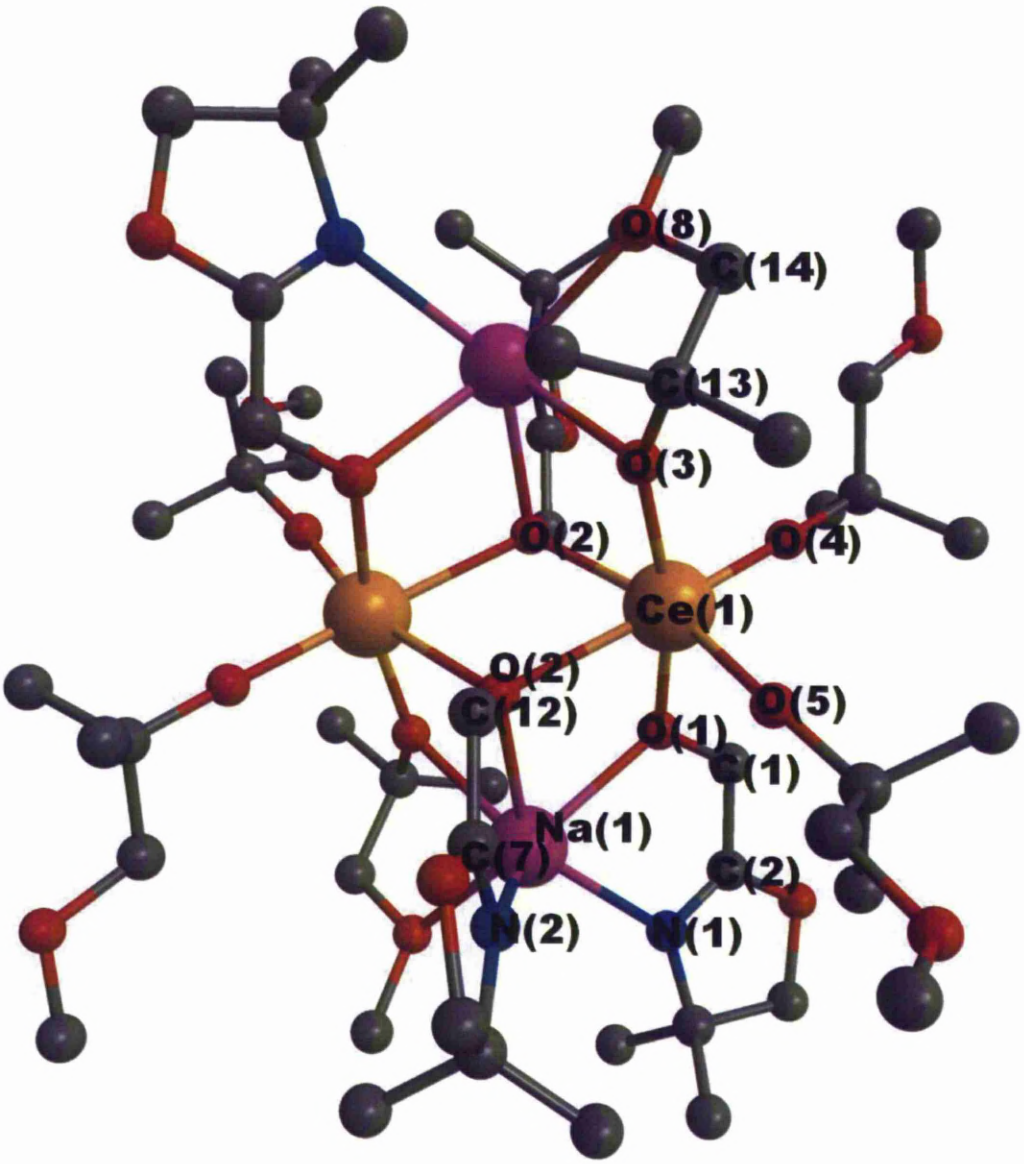

Figure 2. 47: Crystal structure of $[Ce_2(dmom)_4(mmp)_6Na_2]$.

Each Ce atom in the structure is 6-coordinate. They are bound to the O atoms of two dangling mmp ligands. The third mmp is bonded to the Ce via its alcohol O

and is also chelating to a Na atom with both of its oxygens. Two dmom ligands are also bonded to Ce with its alcohol O and chelating to a Na atom via its O and its imine N. The two Ce atoms are bridged via the dmom O(2) alcohol atom.

The longest Ce-O bond is the bridging Ce(1)-O(2) at ~2.42 Å, the next being Ce(1)-O(1) of ~ 2.22 Å which also belongs to a dmom ligand. All Ce-O mmp bonds are approximately the same at ~ 2.1 Å though the chelating mmp ligand is slightly longer (table 2.11).

Table 2. 11: Selected bond lengths and angles for crystal structure of $[Ce_2(dmom)_4(mmp)_6Na_2]$.

Bond Atoms	**Bond Length (Å)**
Ce(1)-O(1)	2.220(1)
Ce(1)-O(2)	2.4184(8)
Ce(1)-O(3)	2.1695(9)
Ce(1)-O(4)	2.0945(8)
Ce(1)-O(5)	2.100(1)
Na(1)-O(1)	2.3899(9)
Na(1)-O(2)	2.488(1)
Na(1)-O(3)	2.498(1)
Na(1)-N(1)	2.508(1)
Na(1)-N(2)	2.567(1)
Bond Atoms	**Bond Angle (°)**
O(2)-Ce(1)-O(2)#	71.82(3)
O(2)-Ce(1)-O(3)	83.77(3)
O(3)-Ce(1)-O(4)	97.75(3)
O(4)-Ce(1)-O(5)	100.64(4)
O(5)-Ce(1)-O(1)	92.27(3)
Ce(1)-O(2)-Na(1)	96.56(3)
Ce(1)-O(3)-Na(1)	103.06(4)
O(3)-C(13)-C(14)-O(8)	56.8(1)
N(1)-C(2)-C(1)-O(1)	6.7(2)
N(2)-C(7)-C(12)-O(2)	-1.3(2)

Attempts to sublime the material led to its decomposition at low temperatures (~ 60 °C). This suggests the complex is not very thermally stable.

2.2.4.2.3. Synthesis of [Ce(mmp)$_2$(dmomp)$_2$].

The reaction between [Ce(mmp)$_4$] and 2 equivalents of dmompH gave [Ce(dmomp)$_4$] when performed at room temperature or higher. At 0 °C the ^{1}H NMR spectrum of the product resembled that shown in figure 2.37 for [Ce(dmomp)$_4$]. The mass spectrum of the complex does not give a peak for the [M+] of either [Ce(dmomp)$_4$] or [Ce(mmp)$_2$(dmomp)$_2$]. The dominant peak is at M/Z 753.21 which would correlate to [Ce(dmomp)$_3$ + H].

The reaction was repeated at -83 °C. On addition of the ligand to the yellow solution a colour change to deep orange was seen. After stirring at low temperature for one hour the colour remained the same. The volatiles were removed under *vacuo* to give a deep orange oil the ^{1}H NMR spectrum of which is seen in figure 2.48.

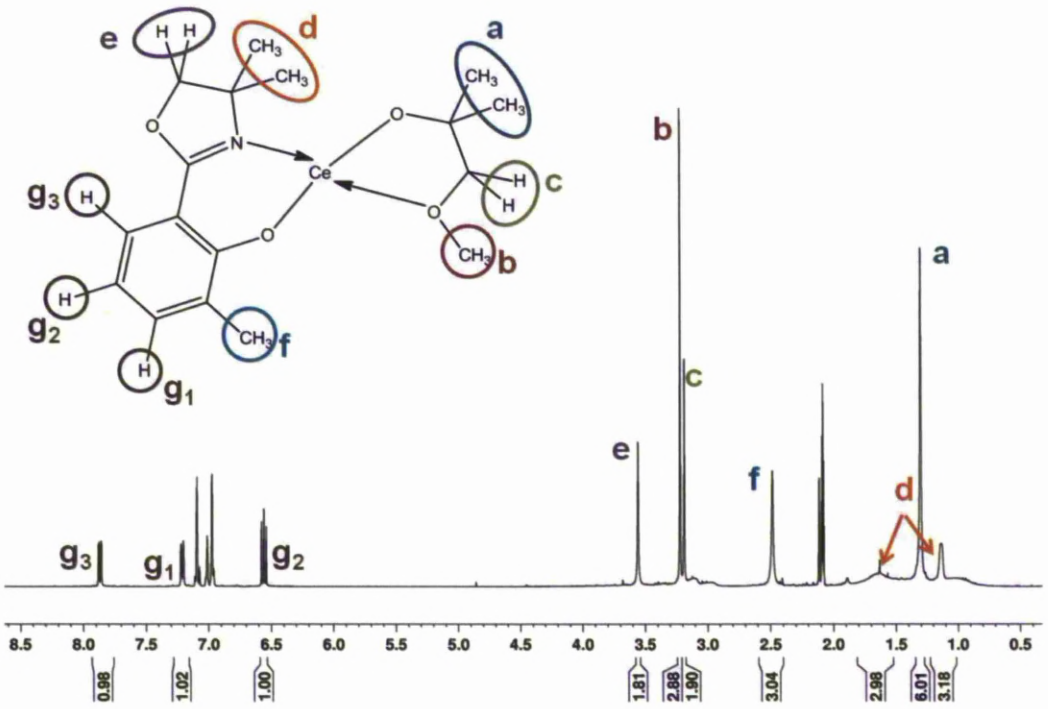

Figure 2. 48: ^{1}H NMR spectrum (C_7D_8) of [Ce(mmp)$_2$(dmomp)$_2$].

From the spectrum we can see the peaks for the mmp ligand are still sharp singlets and the peaks for the methoxy group (b) and CH_2 (c) are closer in chemical shift than other mmp complexes. The methyl groups in position (d) of the dmomp ligand have been split in to two different peaks both of which appear as broad singlets. This indicates that the ligand has lost its symmetry in the complex.

Attempts to grow crystals of the compound led to the precipitation of a partially soluble solid. This was shown by ^{1}H NMR spectroscopy to be the monomer [Ce(dmomp)$_4$]. A spectrum of the complex in solution for a few hours shows the conversion of the heteroleptic complex to the more stable monomer. The complex threfore exhibits a very low shelf-life.

2.3. Conclusion

The difficulty of using monodentate alkoxides ligands to make Ce(IV) homoleptic complexes was proved further by investigation with *tert*-butoxide and neopentoxide. The use of these materials led to a synthetic route to make a range of monomeric Ce(IV) donor functionalised materials. $[Ce(mmp)_4]$, $[Ce(dmap)_4]$, $[Ce(dmop)_4]$ and $[Ce(dmomp)_4]$ were found to be easily made and stable complexes. $[Ce(dmae)_4]$ and $[Ce(dmom)_4]$ were synthesised but were susceptible to decomposition and synthesis of the complexes was unreliable. This is due the lack of steric stability in the α-position of the ligand next to the alcohol.

The thdH ligand was unsuitable as a coligand for heteroleptic complexes with mmp and dmap though the dbm ligand was used to make $[Ce(mmp)_2(dbm)_2]$ and $[Ce(dmap)_2(dbm)_2]$. Even though these were easily synthesised they lacked thermal stablility when attempting sublimation decomposing to give $[Ce(dbm)_4]$.

$[Ce(mmp)_4]$ was used to make a range of heteroleptic alkoxide complexes. The monomeric $[Ce(mmp)_2(dmop)_2]$ was difficult to isolate leading to the dimer $[Ce_2(mmp)_2(dmop)_4(O)]$. $[Ce(mmp)_2(dmom)_2]$ and $[Ce(mmp)_2(dmomp)_2]$ were made though the bonding strength of the dmomp ligand gives $[Ce(mmp)_2(dmomp)_2]$ a low shelf-life.

Chapter 3. Liquid-injection MOCVD and ALD of CeO_2.

3.1. Introduction.

3.1.1. CeO_2.

CeO_2 has many attractive properties, such as resistance to high temperatures and chemical reactions, which have made it a very suitable oxide for use in applications such as catalytic oxidation reactions[55] and capacitors.[56] CeO_2 has also been used as a buffer layer preventing chemical reactions at the film/substrate surface for $YBa_2Cu_3O_{7-\delta}$ (YBCO) films used as components for high-power applications such as fault current limiters.[57] Thin films of CeO_2 have been deposited by using physical techniques like laser ablation[7] but MOCVD and ALD are better methods for producing uniform, pure films.

Lanthanide oxides generally occur as the sesquioxide Ln_2O_3, though Ce_2O_3 is only formed under strong reducing conditions. The oxidation of Ce^{3+} or Ce^{4+} gives CeO_2 which adopts a fluorite structure (figure 3.1).

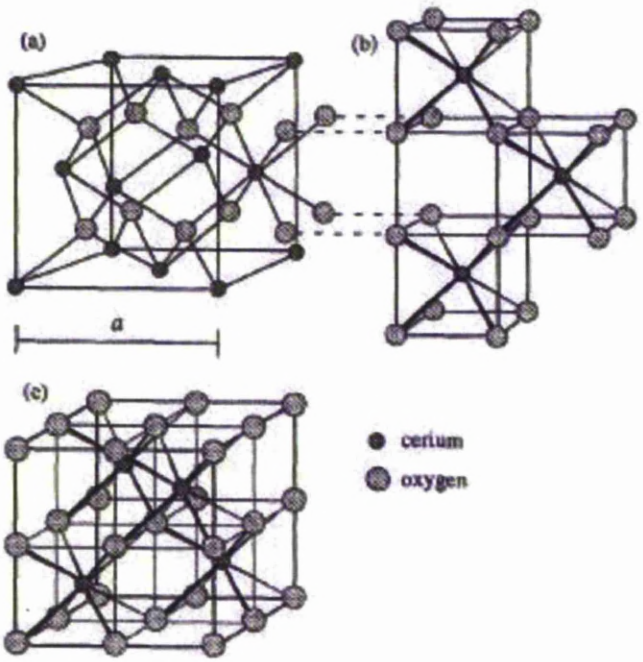

Figure 3. 1: The crystal structure of CeO_2 a) unit cell as a ccp array of cerium atoms. The ccp layers are prallele to the [111] planes of the fcc unit cell. b) and c) are the same structure redrawn as a primitive cubic array of oxygens. [58]

The flourite structure exhibits a face-centred cubic unit cell (f.c.c.). Each cerium cation is coordinated by eight equivalent nearest-neighbour oxygen anions. The structure can be seen as a ccp array of cerium ions with oxygens occupying all the tetrahedral holes. There are large octahedral holes which are important when considering the movement of ions through the structure. This helps explain its higher dielectric constant when compared to SiO_2.

3.1.2. Precursors of CeO_2.

3.1.2.1. Ce^{3+} Precursors.

Ce^{3+} precursors like $[Ce(hfac)_3(diglyme)]$ utilise a chelating β-diketonate ligand and a neutral diglyme preventing oligomerisation of the complex (figure 3.2). Aside from this the fluorine groups increase volatility by the reduction of intermolecular attractions and hence increases its usefulness as a precursor. Unfortunately complexes like these can easily lead to fluorine contamination of the films outweighing the volatility benefits of the ligand.[28,59]

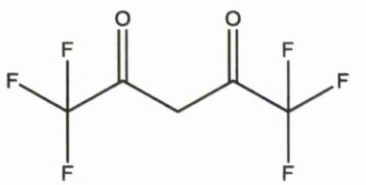

1,1,1,5,5,5-hexafluoropentane-2,4-dione
(hfacH)

1-methoxy-2-(2-methoxyethoxy)ethane
(diglyme)

Figure 3. 2: Schematic showing structures of the ligands hfacH and diglyme.

3.1.2.2. β- diketonates - $[Ce(thd)_4]$.

Currently the most common precursor used for the liquid-injection MOCVD or ALD of thin films of CeO_2 is $[Ce(thd)_4]$ shown in figure 3.3. The presence of the three methyl groups either side of the β-diketonate centre removes the possibility for

β-hydride elimination making the complex quite stable and so [Ce(thd)$_4$] can be easily synthesised as a monomeric complex in good yield. It also exhibits a long shelf-life and good volatility.[41,42,53]

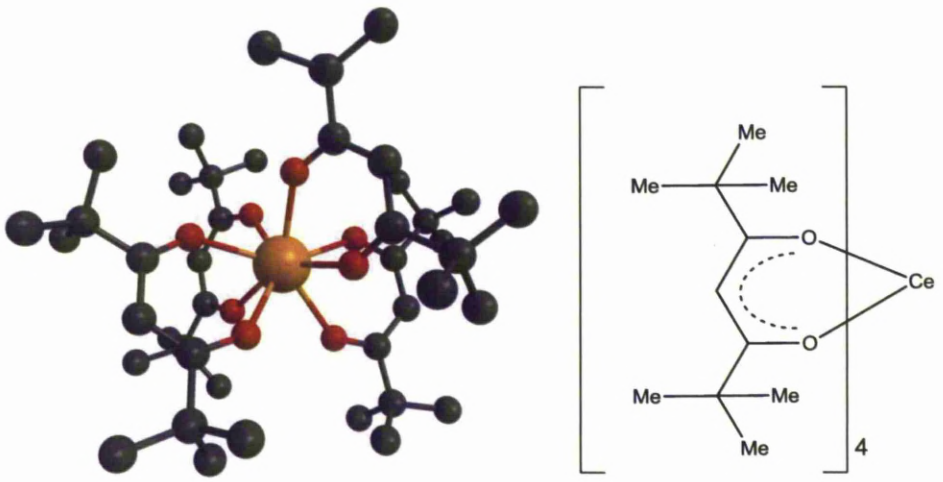

Figure 3. 3: [Ce(thd)$_4$] crystal structure and diagram of bonding.

[Ce(thd)$_4$] sublimes above 145 °C and the TGA curve in figure 3.4 shows its evaporation at just above 200 °C with full decomposition occurring at 300 °C. These results have been found in other studies.[52,60] The stability of the compound has also been demonstrated after leaving a sample exposed for 30 days in air. The data collected for the exposed sample was very similar when compared to a fresh one.[12]

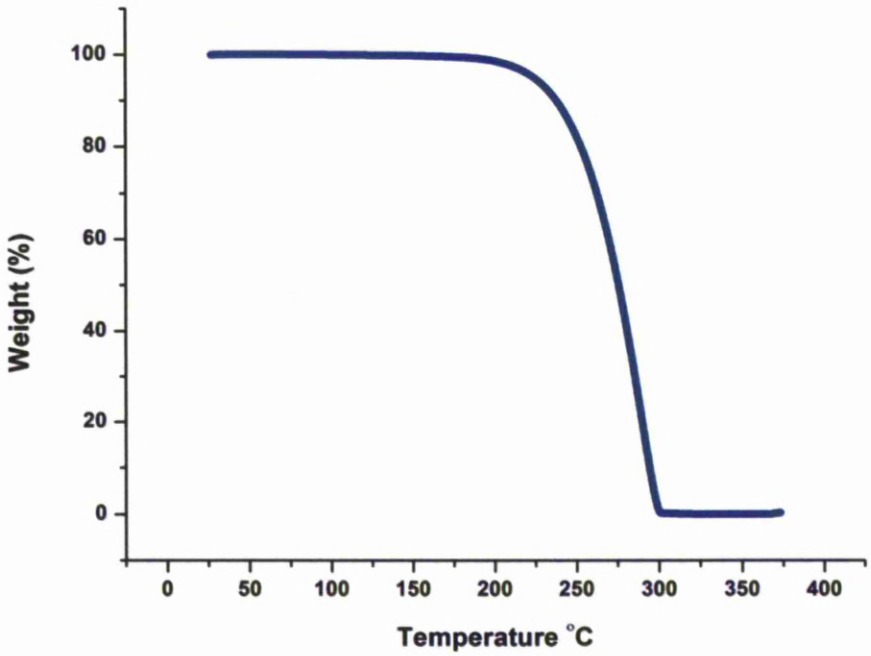

Figure 3. 4: TGA data for $[Ce(thd)_4]$ of N_2 with a heating rate of 10 °C min^{-1} at atmospheric pressure.

Even though this stability is a useful characteristic for a precursor it also has its downfalls. Frequently films of CeO_2 made using $[Ce(thd)_4]$ are contaminated with carbon. In the case of ALD, H_2O is not sufficiently Brønsted acidic to interact with the complex and so ozone must be used. This can cause the formation of a SiO_2 interfacial layer between the substrate and film which has a low permittivity reducing the ability of current to pass through the film.[61]

Films grown by MOCVD using $[Ce(thd)_4]$ as the precursor have been successful between 400 – 900 °C on $SrTiO_3$, yttria stabilized zirconia (YSZ) and MgO substrates. The growth rates of this study were around 0.2 μm/hr over the temperature range though the uniformity of the coating was found to be quite poor in

some experiments.[62] In ALD [Ce(thd)$_4$] has demonstrated a narrow temperature window between 175 and 250 °C when growing CeO_2 on Si(100). Although these gave good films with low impurities, ozone is required as the oxygen source.[41]

Since the β-diketonate complexes are so stable the need for a monomeric Ce (IV) complex that is thermally stable but reactive enough to oxygenation is highly sought out.

3.1.2.3. Alkoxides – [Ce(OC(CH$_3$)$_2$Pr^i)$_4$].

[Ce(OC(CH$_3$)$_2$Pr^i)$_4$] has also been tested for use as a CeO_2 precursor and exists as a dimer in the solid state (figure 3.5). The low pressure CVD of CeO_2 on a silicon surface using [Ce(OC(CH$_3$)$_2$Pr^i)$_4$] has reportedly grown films at temperatures from 270-530 °C with O_2 as a dual source precursor. These films were uniform with a 3 % carbon impurity.[36] There is no reported use of this precursor for the ALD of CeO_2.

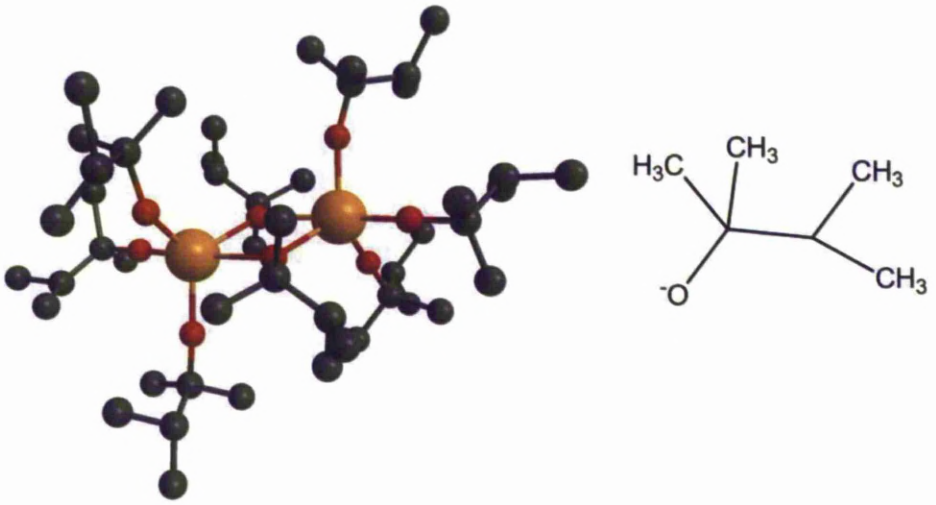

Figure 3. 5: Crystal structure of $[Ce(OC(CH_3)_2Pr^i)_4]_2$.

3.2. Thermogravimetric Analysis of Ce(IV) Complexes.

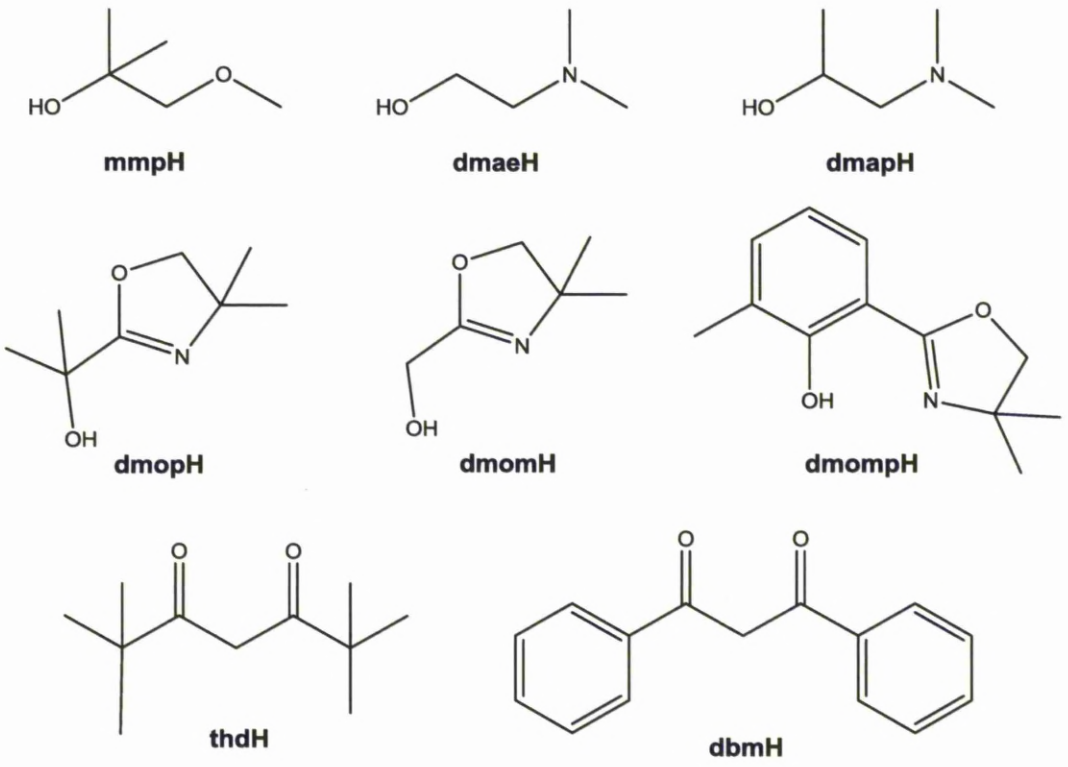

Figure 3. 6: Structures of alcohols and β-diketonates used as ligands.

Figure 3.6 shows the structures of ligands used to make Ce(IV) alkoxide complexes that were tested thermogravimetrically to determine whether they would be feasible precursors for the growth of CeO_2.

3.2.1. TGA of donor-functionalised alkoxide complexes.

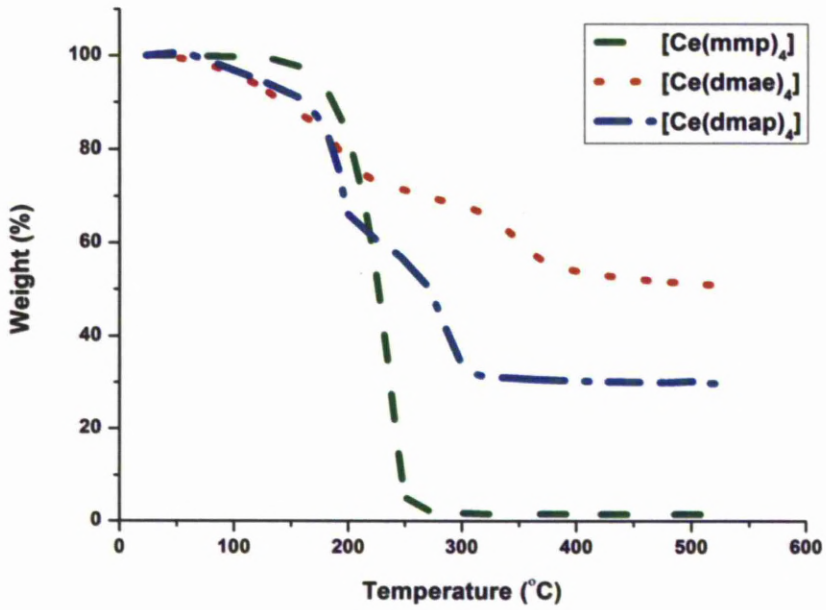

Figure 3. 7: TGA analysis of Ce(IV) alkoxide complexes with donor-functionalised ligands. All TGAs were run under the flow of N_2 with a heating rate of 10 °C min^{-1} at atmospheric pressure.

As shown by the TGA in figure 3.7 $[Ce(mmp)_4]$ demonstrates a good evaporation curve. Starting at ~144 °C the complex has a large mass loss up to ~250 °C where it leaves a 1.48 % residue. This is ~ 50 °C less than the evaporation temperature observed for $[Ce(thd)_4]$.

The other two complexes do not exhibit as smooth a pathway. $[Ce(dmae)_4]$ shows decomposition starting at the beginning of the TGA run. The first step in the

curve down to ~166 °C correlates approximately to a loss of one dmae ligand. There is then gradual mass loss down to ~61 % representative of another dmae ligand. A large residue of 51 % remains at the end of the run with a molecular weight of 251 which corresponds approximately to CeO_2 with a dmae ligand.

$[Ce(dmap)_4]$ also has a gradual mass loss indicating decomposition rather than evaporation. The first loss up to 150 °C is equivalent in mass to an $N(CH_3)_2$ group. Next there is a steeper loss up to ~197 °C with a mass of 132 and then a loss of mass 170 up to 294 °C. These losses are equal to organic decomposition. The compound continues to gradually lose mass resulting in a residue of 30 %. This is approximately equivalent to the mass of CeO_2 relative the $[Ce(dmap)_4]$ complex.

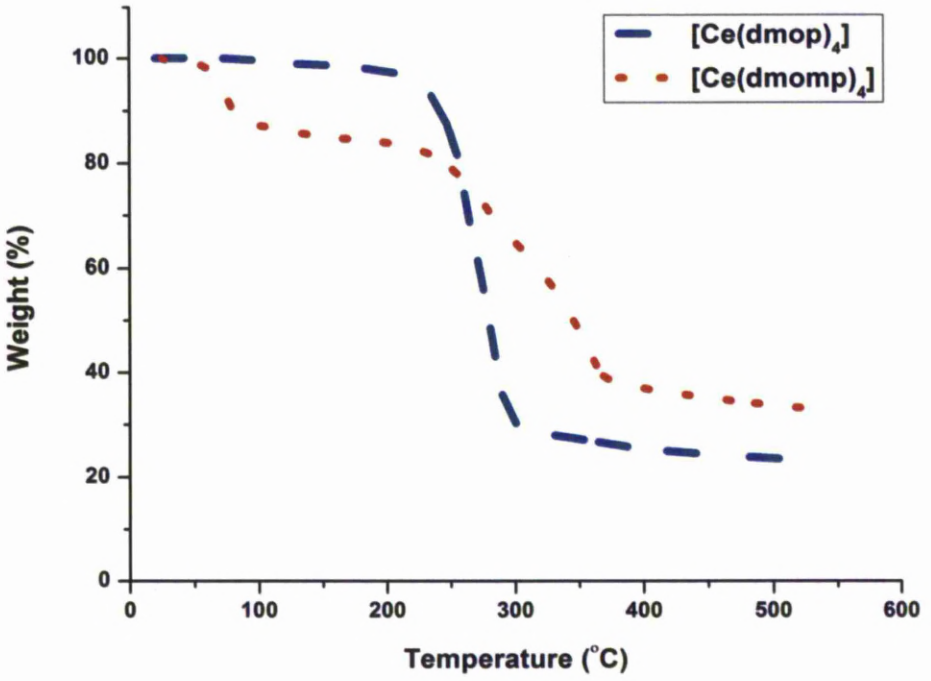

Figure 3. 8: TGA analysis of Ce(IV) alkoxide complexes with oxazolinyl ligands. All TGAs were run under the flow of N_2 with a heating rate of 10 °C min^{-1} at atmospheric pressure.

$[Ce(dmop)_4]$ has a large mass loss when decomposition occurs from ~204 °C up to 291 °C (figure 3.8). The complex then shows very gradual loss eventually leaving a residue of 23 % which is approximately the mass of CeO_2. $[Ce(dmomp)_4]$ has a less smooth curve. The first loss is ~ 10 % of the complex weight which is equivalent to an oxazolinyl-ring of the dmomp ligand. There is then a larger loss from 83 – 366 °C equivalent to the decomposition of two dmomp ligands. Gradual loss then ensues leaving a residue of 33 %, nearly double what would be expected for CeO_2.

3.2.2. TGA of Ce(IV) heteroleptic Complexes.

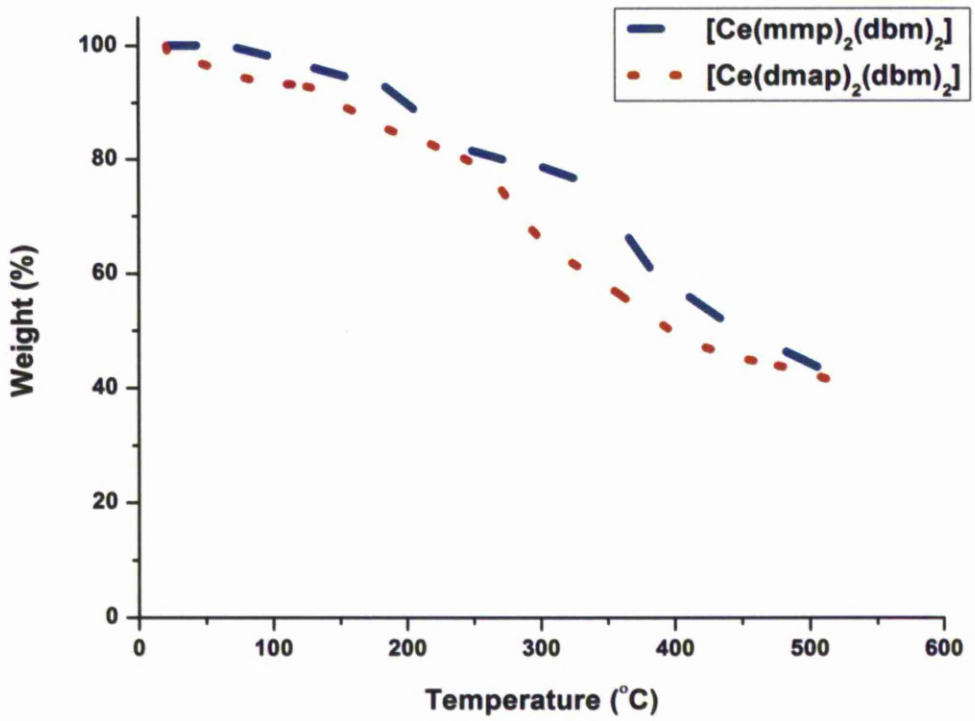

Figure 3. 9: TGA analysis of heteroleptic Ce(IV) alkoxide complexes with the dbm ligand. All TGAs were run under the flow of N_2 with a heating rate of 10 °C min^{-1} at atmospheric pressure.

$[Ce(mmp)_2(dbm)_2]$ and $[Ce(dmap)_2(dbm)_2]$ follow a similar decomposition path in their TGAs. Neither complex is volatile enough for evaporation. Both have a very gradual decomposition pathway down to 93 % mass, ~ 75 % and leaving a residue of ~39.6 % in each case. These residues are nearly 20 % higher than that expected for CeO_2 relative to the mass of each complex.

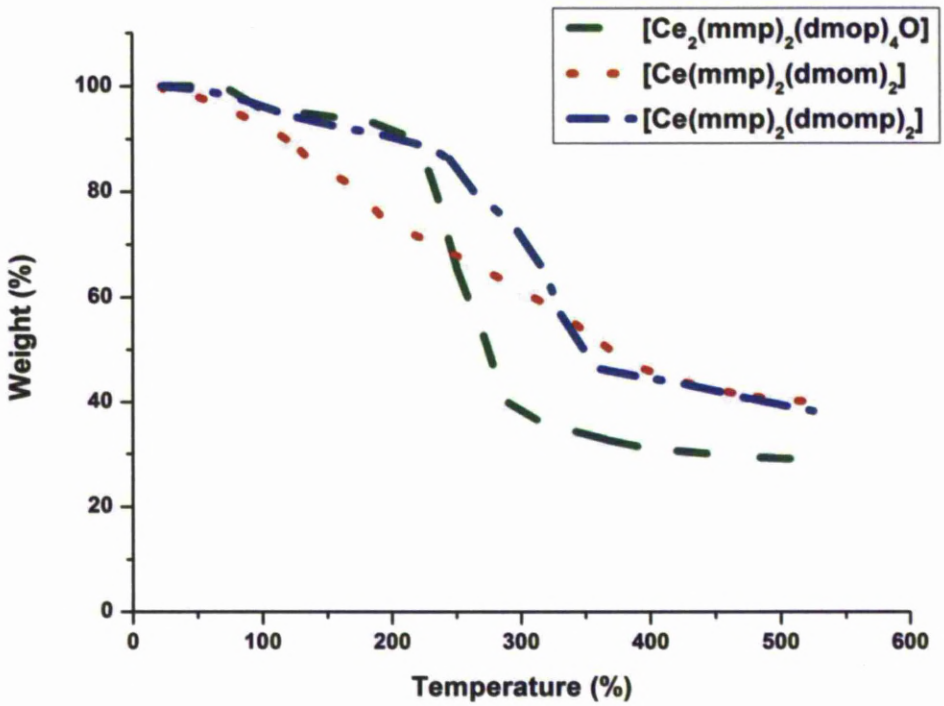

Figure 3. 10: TGA analysis of heteroleptic Ce(IV) alkoxide complexes with the mmp ligand. All TGAs were run under the flow of N_2 with a heating rate of 10 °C min^{-1} at atmospheric pressure.

$[Ce_2(mmp)_2(dmop)_4O]$ exhibits gradual mass loss up to 200 °C where it evaporates with its greatest loss of 50.4 % ending at 286 °C. This is approximately equivalent to the loss of three dmop ligands and one mmp. The compound then slowly decomposes leaving a residue of 28.9 %. This is greater than what would be expected for CeO_2 (15.3 %) so organic matter must still be left in the materials.

$[Ce(mmp)_2(dmom)_2]$ shows no evaporation characteristics slowly decomposing over the temperature range leaving a residue of ~ 40 %.

$[Ce(mmp)_2(dmomp)_2]$ leaves a similar residue though has a mass loss of ~ 38 % between 238 and 352 °C which is equivalent to the loss of a dmomp ligand and most of an mmp. These three complexes leave quite high residues and so were deemed not suitable for growth study.

3.3. Sublimation Data.

All attempts to sublime the heteroleptic complexes of Ce(IV) led to their decomposition either without a sublimate or with the sublimation of a free ligand. This was also observed for $[Ce(dmomp)_4]$, $[Ce(dmop)_4]$ and $[Ce(dmae)_4]$. $[Ce(mmp)_4]$ and $[Ce(dmap)_4]$ were found to volatilise at a low temperature and produce a pure crystalline product.

$[Ce(mmp)_4]$ was shown by ^1H NMR spectroscopy to sublime intact at 120 °C with a pressure of 0.8 torr leaving no residue behind. Crystals of $[Ce(dmap)_4]$ were seen to melt at 83 °C and sublime at 125 °C also at 0.8 torr. The sublimed material was confirmed as $[Ce(dmap)_4]$ by CHN analysis. A dark residue was also left during sublimation which gave a low CHN content. Given their ability to sublime at such temperatures $[Ce(mmp)_4]$ and $[Ce(dmap)_4]$ were thus seen as promising precursors for growth of CeO_2.

In comparison to the sublimation data of other known Ce^{4+} precursors it is clear that $[Ce(mmp)_4]$ and $[Ce(dmap)_4]$ are the most volatile precursors found to date. (table 3.1)

Table 3. 1: Sublimation data for precursors of CeO_2

Compound	Sublimation Temperature (°C)	Sublimation Pressure (torr)
$[Ce(mmp)_4]$	120	0.8
$[Ce(dmap)_4]$	125	0.8
$[Ce(thd)_4]$[59]	135-140	0.1
$[Ce(OC(CH_3)_2Pr^i)_4]$[29]	132	0.05
$[Ce_2(OPr^i)_8(HOPr^i)_2]$[63]	160-170	0.05

3.4. Growth of CeO_2 by liquid-injection MOCVD.

(Majority of growth studies performed by Kate Black, Matt Werner and Paul Marshall, Department of Engineering Centre for Materials and Structures, University of Liverpool)

Table 3. 2: Growth conditions used for the deposition of CeO_2 by liquid-injection MOCVD and ALD.

General Growth Condition	
Solvent	Toluene
Precursor Conc.	0.05 M
Evaporator Temperature	100 °C
Reactor Pressure	1 mbar
Argon Flow Rate	200 cm^3 min^{-1}
MOCVD Growth Conditions	
Substrates Temps	200-600 °C
Oxygen Flow rate	100 cm^3 min^{-1}
ALD Growth Conditions	
Substrates Temps	100-350 °C
Oxygen Source	H_2O ([Ce(mmp)$_4$], [Ce(dmap)$_4$], [Ce(OC(CH$_3$)$_2$Pr^i]) O_3 ([Ce(thd)$_4$])
Number of cycles	300
Pulse Sequence (sec.) Precursor/purge/oxygen source/purge/	2/2/0.5/3.5

3.4.1. Oxide film growth against temperature.

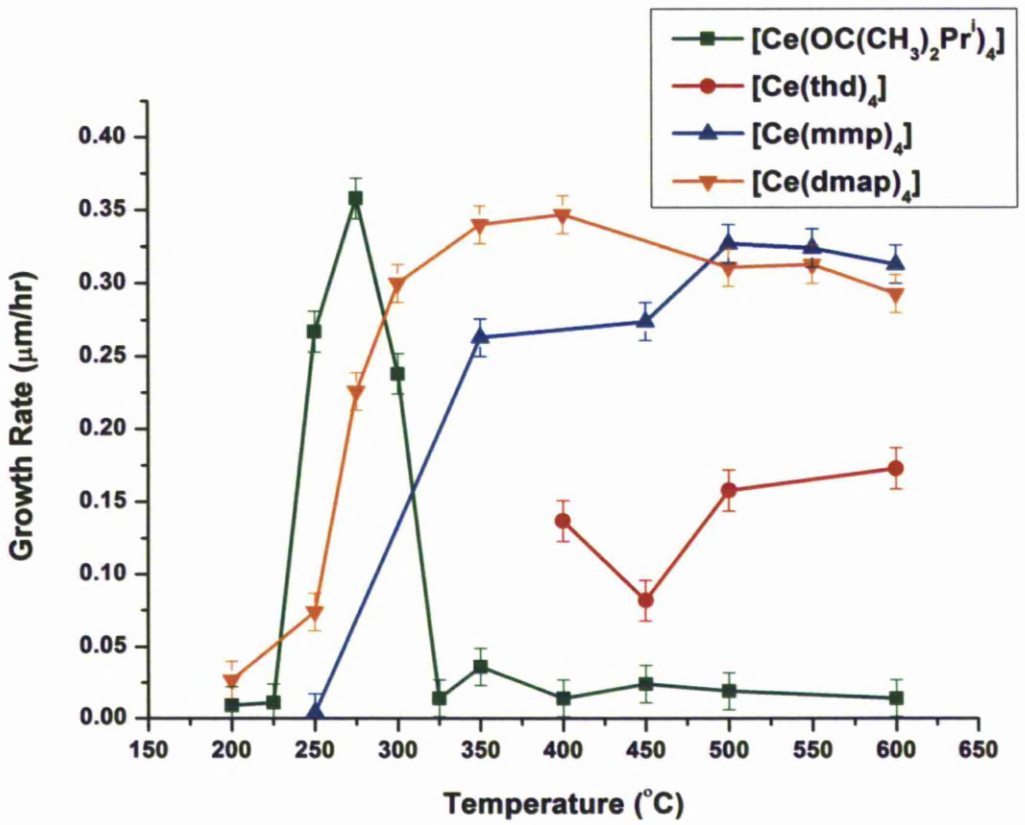

Figure 3. 11: Liquid-injection MOCVD growth curves for deposition of CeO_2 using the precursors $[Ce(OC(CH_3)_2Pr^i)_4]$, $[Ce(thd)_4]$, $[Ce(mmp)_4]$ and $[Ce(dmap)_4]$ as 0.05 M solutions in toluene with O_2.

The growth curves for the four different CeO_2 precursors are shown in figure 3.11. It is clear from the data that $[Ce(mmp)_4]$ and $[Ce(dmap)_4]$ exhibit better growth than the two previously known precursors. $[Ce(thd)_4]$ showed disappointing results given its common usage. Below 400 °C the precursor proved difficult to handle as

precipitation occurred in the reactor injectors. Even though the precursor was difficult to use it did maintain its growth at higher temperatures at rates similar to those previously reported.[62]

$[Ce(OC(CH_3)_2Pr^i)_4]$ shows kinetic control up to 250 °C leading to a high growth rate of 0.35 μm/hr in the precursor controlled region at 275 °C. The compound only demonstrates a very narrow growth window between 250 and 300 °C. Above 275 °C thin film growth is determined by the depletion of the precursor. Here the growth rate decreasing dramatically from 0.24 μm/hr to 0.02 μm/hr at the temperatures 300 and 325 °C respectively. $[Ce(OC(CH_3)_2Pr^i)_4]$ therefore has a very narrow window between evaporation and decomposition for growth to occur. This would explain the little use of this precursor for CeO_2 deposition reported in the literature.

The two new precursors, $[Ce(mmp)_4]$ and $[Ce(dmap)_4]$, both show very promising results in comparison to $[Ce(thd)_4]$ and $[Ce(OC(CH_3)_2Pr^i)_4]$. $[Ce(mmp)_4]$ has a kinetic region spread between 250 and 350 °C where it begins precursor controlled growth. It shows thermal stability up to 600 °C maintaining a high growth rate at 0.30 μm/hr, nearly double the rate of $[Ce(thd)_4]$ at the same temperature. In contrast to other mmp based precursors $[La(mmp)_3]$[64] and $[Gd(mmp)_3]$[65] show a rapid decrease in oxide growth rate above 500 °C due to thermal depletion of the precursors on the reactor walls.

CeO_2 growth using $[Ce(mmp)_4]$ was also tried at temperatures of 350 and 500 °C without the use of O_2 gas. This gave growth rates of 0.021 and 0.038 μm/hr respectively differing greatly from the rates of 0.263 and 0.327 μm/hr obtained with O_2 gas. This shows that $[Ce(mmp)_4]$ would not be a useful single-source precursor.

$[Ce(dmap)_4]$ interestingly shows growth at 200 °C which continues to 300 °C spanning the kinetically controlled region. Diffusion controlled growth has a window of 150 °C giving growth rates higher than the other 3 precursors at the same temperatures. Depletion of the precursor begins above 450 °C though high thermal stability is still seen by $[Ce(dmap)_4]$ much like $[Ce(mmp)_4]$.

CeO_2 growth with $[Ce(dmap)_4]$ was also attempted at 400 °C without the use of O_2 gas. This gave the growth rate of 0.20 μm/hr, lower than that obtained in the presence of O_2 gas (0.347 μm/hr). Even though the rate is lower there is still enough oxygen present in the ligand to give some single-source CeO_2 growth.

3.4.2. Oxide film growth activation energies.

In the kinetic region, control of growth is governed by the substrate temperature in an Arrhenius type fashion. Using Arrhenius plots the activation energies of the precursors can be calculated.

$$k = A \times e^{-E/RT} \tag{3.1}$$

k = reaction rate, A = frequency factor, E = activation energy, R= gas constant, T = temperature (K)

$$\ln k = -\frac{E}{TR} + \ln A \tag{3.2}$$

The Arrhenius equation (3.1) in logarithmic form (3.2) allows the activation energies to be calculated by the determination of gradients from the straight lines in the Arrhenius plot in figure 3.12. The graph is of the natural log of the growth rate versus the reciprocal of the temperature. Multiplying the measured gradient by the gas constant yields the activation energy ($R = 8.31$ J mol^{-1} K^{-1}).

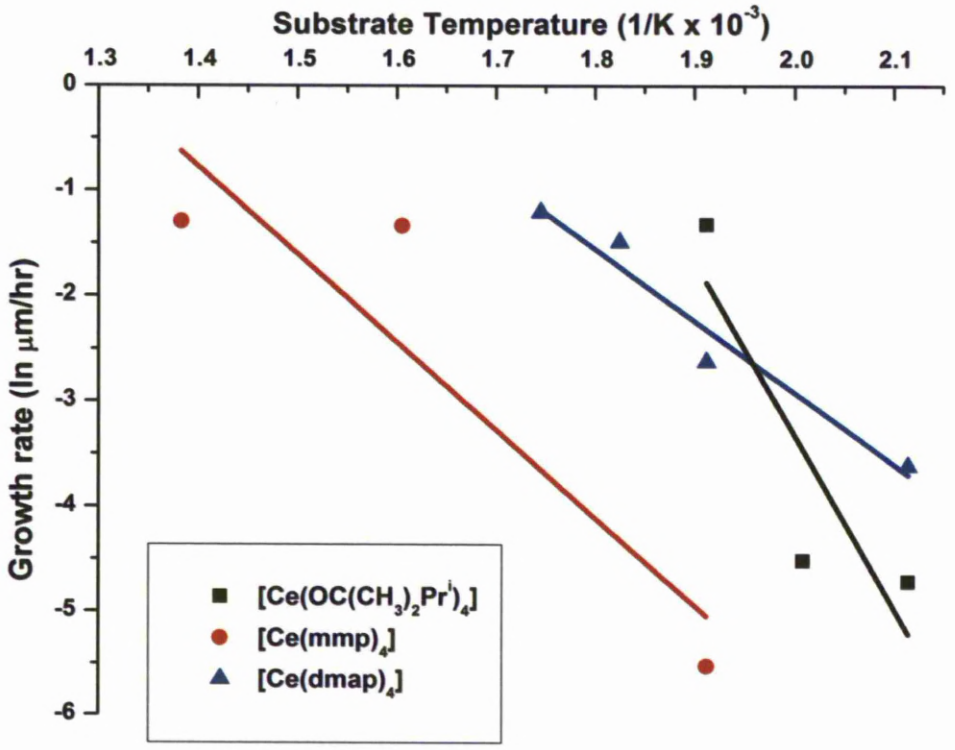

Figure 3. 12: Arrhenius plots of $[Ce(OC(CH_3)_2Pr^i)_4]$, $[Ce(mmp)_4]$ and $[Ce(dmap)_4]$.

Table 3. 3: Precursor activation energies.

Precursor	$[Ce(OC(CH_3)_2Pr^i)_4]$	$[Ce(mmp)_4]$	$[Ce(dmap)_4]$
Activation energy ($kJmole^{-1}$)	122	72	54

$[Ce(OC(CH_3)_2Pr^i)_4]$ has a greater activation energy than $[Ce(mmp)_4]$ and $[Ce(dmap)_4]$. $[Ce(dmap)_4]$ has the lowest of the three and is hence a more reactive precursor requiring less energy for growth to occur. This explains its growth at the lower temperatures and better growth rates when compared with $[Ce(mmp)_4]$.

3.5. Growth of CeO_2 by ALD.

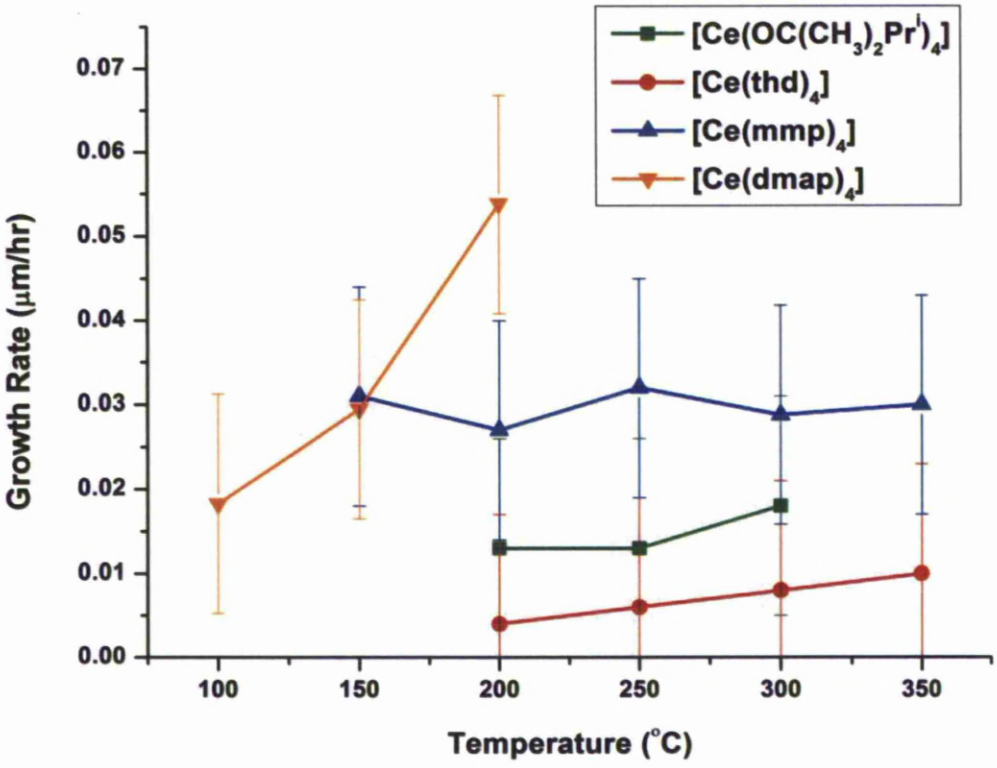

Figure 3. 13: ALD growth curves for deposition of CeO_2 using the precursors $[Ce(OC(CH_3)_2Pr^i)_4]$, $[Ce(mmp)_4]$ and $[Ce(dmap)_4]$ with H_2O and $[Ce(thd)_4]$ with O_3.

$[Ce(OC(CH_3)_2Pr^i)_4]$ and $[Ce(thd)_4]$ both show low growth rates for ALD of CeO_2 though they appear to be self-limiting. As temperatures reach 300 °C the growth rates only increase gradually. $[Ce(mmp)_4]$ shows a greater growth rate in comparison to $[Ce(OC(CH_3)_2Pr^i)_4]$ and $[Ce(thd)_4]$. The rate remains steady at ~0.03 μm/hr over the temperature 150 to 350 °C indicating it is a self-limiting precursor. $[Ce(dmap)_4]$ is the most reactive precursor giving growth at temperatures as low as 100 °C. The rate of growth increases quickly up to 200 °C which can be attributed to

the thermal decomposition of [Ce(dmap)$_4$] consistent with the onset of thermal MOCVD at 200 °C.

3.6. CeO_2 film characterisation.

3.6.1. Films grown using [Ce(mmp)$_4$].

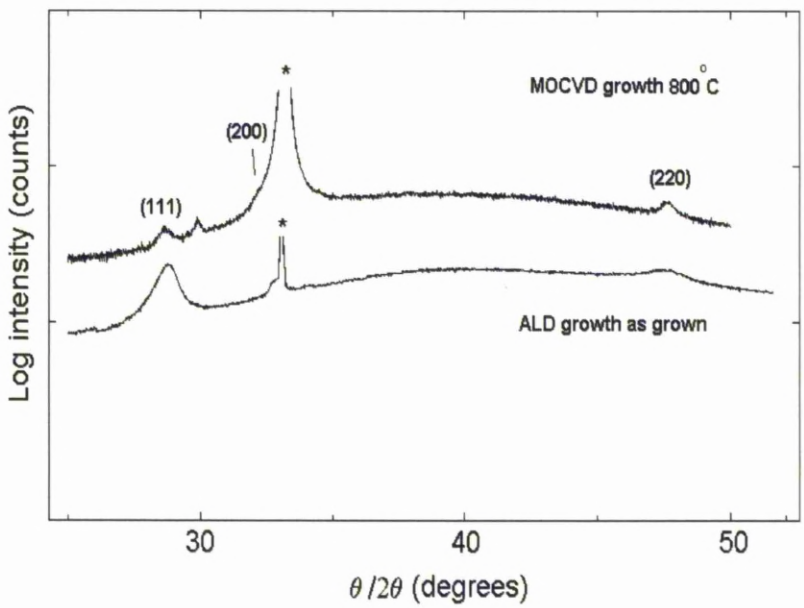

Figure 3. 14: XRD data for CeO_2 films grown on Si(100) using [Ce(mmp)$_4$] and O_2 gas via by liquid injection MOCVD (top trace) and ALD (bottom trace). Substrate peaks are shown with a (*).

Figure 3.14 shows the X-ray diffraction data for the CeO_2 films. Films deposited by ALD (growth temperature = 300 °C) were analysed as-deposited, and the CeO_2 films deposited by MOCVD (growth temperature = 450 °C) were analysed after annealing at 800 °C in air for 15 min. Peaks marked with a star are due to the Si

substrate. The films grown by ALD exhibited crystalline diffraction features consistent with the cubic ceria phase. The CeO_2 film deposited by MOCVD showed evidence of crystallinity in the XRD spectrum. The film crystallised into the cubic phase on annealing in air at 800 °C for 15 min.

Analysis of the MOCVD and ALD grown CeO_2 films by Auger electron spectroscopy (AES) collected from the bulk of the film (depth>12nm) showed that films grown by MOCVD (450 °C) and ALD (250, 350 °C) were high purity with carbon levels below the AES detection limit (~0.5 at.-%).

3.6.2. Films grown using [Ce(dmap)$_4$].

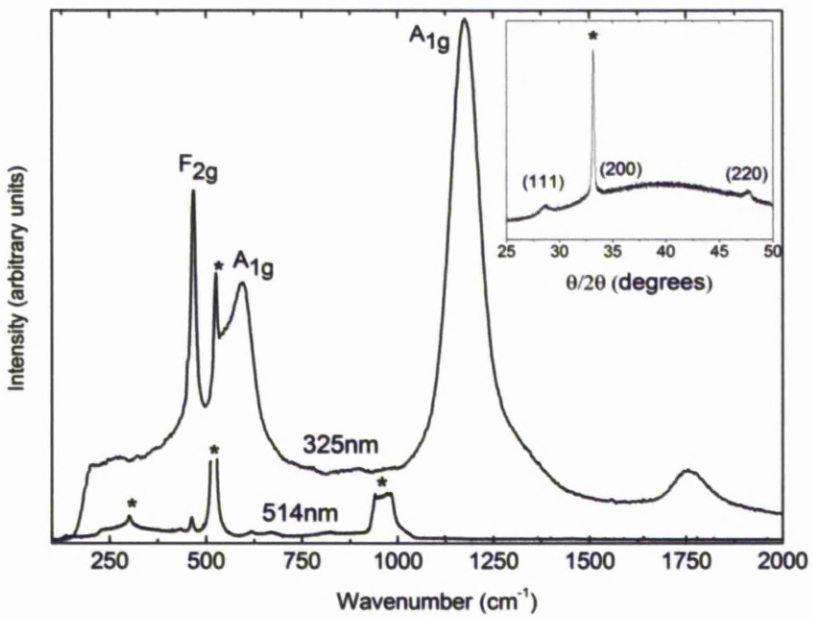

Figure 3. 15: Raman spectroscopy and XRD data (inset) of CeO_2 thin film grown on Si(100) by MOCVD using 0.05 M [Ce(dmap)$_4$] and O_2 at 400 °C at 325 and 514 nm. Substrate peaks are shown with a (*).

Figure 3.15 shows the Raman measurements at 325 nm and 514 nm for the 400 °C as grown film using [Ce(dmap)$_4$] and O_2. The triply-degenerate Raman mode at ~465 cm^{-1} with F_{2g} symmetry is indicative of CeO_2 and is present from both laser sources. A_{1g} modes seen at ~600 cm^{-1} and ~1180 cm^{-1} are second-order modes and are only seen by the 325 nm source. Neither trace shows evidence of the characteristic D and G carbon bands at ~1350 cm^{-1} and ~1600 cm^{-1} respectively demonstrating minimal carbon inclusion in the deposition. These measurements and the XRD plot in the inset show the films were cubic as grown and this was found for all the films in the 300-600 °C temperature window.

3.7. Conclusion.

[Ce(mmp)$_4$] and [Ce(dmap)$_4$] were chosen to be tested as precursors for the MOCVD and ALD of CeO_2 and the results compared to the known compounds [Ce(thd)$_4$] and [Ce(OC(CH$_3$)$_2$Pr^i)$_4$]. Both complexes were more volatile than the known precursors and gave deposition of CeO_2 over the wide temperature range 200 – 600 °C in MOCVD. This makes [Ce(mmp)$_4$] and [Ce(dmap)$_4$] a more practical choice for use as precursors as their deposition window is greater and could be more useful when tailoring experiments with other precursors e.g. doping studies. [Ce(mmp)$_4$] was a self-limiting precursor for ALD between the temperatures of 150-350 °C. [Ce(dmap)$_4$] showed ALD growth at 100 °C though began to decompose due to CVD processes at higher temperatures.

Chapter 4. Ti(IV) alkoxide complexes

4. 1. Introduction

4.1.1. TiO_2

TiO_2 has developed into an extremely useful material for several different applications. It is an n-type semiconductor (excess of negative charge carriers) that is useful in different devices, for example, in photovoltaics a high surface area TiO_2 film deposited on conducting glass together with a charge transfer dye can give quantitative conversion of visible light photons into electric current.[66] It can also act as a photoanode[67,68] responding to light that has a larger energy than its band gap (E_g – 3.0 eV) though this could be enhanced with doping making it an applicable material for photoelectrochemical and optoelectronic applications.[69-71]

Other uses of TiO_2 involve the increased efficiency of photocatalytic hydrogen production for renewable energy purposes,[72,73] photodegradation of other species under UV light irradiation,[74,75] black light,[76] solar energy conversion applications,[77] and BTSO ($Bi_{1-x-y}Ti_xSi_yO_z$) for the production of dynamic random access memory storage capacitors (DRAMs).[78] In more recent studies the use of TiO_2 and ultrasound has been found as a possible treatment for cancer.[79]

4.1.1.1. TiO_2 phases

TiO_2 can exist in several different forms, the three most important being brookite, rutile and anatase. Rutile and anatase are more abundant than brookite and have more useful characteristics since brookite demonstrates no photocatalytic activity. Rutile is the most common natural form of TiO_2 and is very useful in industry as powdered rutile is used as a white pigment in paints and nanoparticulate rutile is found in sunscreens due to its ability to absorb ultraviolet light. The anatase phase is the most photocatalytic of the three and is used in self-cleaning glass where ultraviolet irradiation creates surface oxygen vacancies in the structure allowing for better water adsorption,[73,80] though rutile has also shown examples of this too.[73,81] In mixed-phase titania the presence of pure-rutile phase crystallites is helpful to the photocatalytic behaviour of the anatase phase by acting as an antenna to extend the photoactivity into visible wavelengths. This happens by the stabilization of charges produced on rutile through electron transfer to lower energy anatase lattice trapping sites.[82]

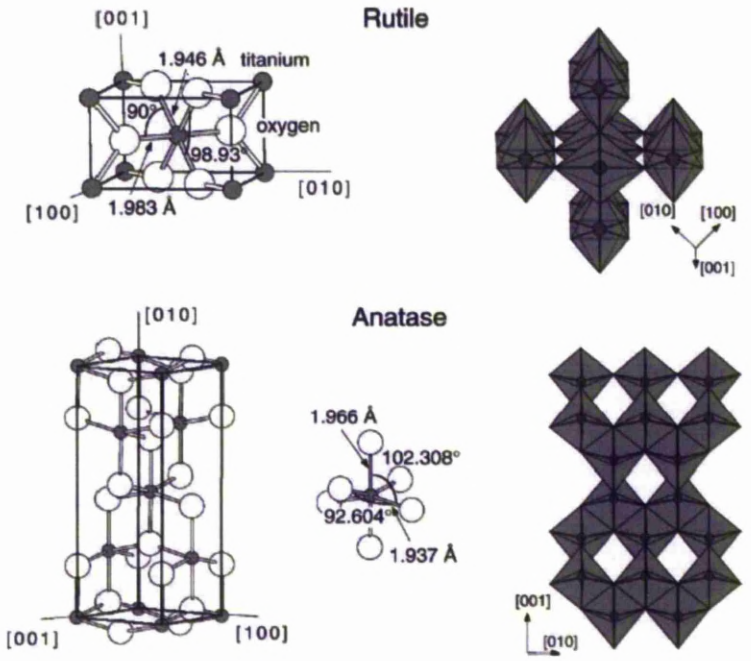

Figure 4. 1: Crystal structures of different phases of TiO_2 top) rutile, bottom) anatase[83]

The basic building block of both structures consists of a Ti^{4+} cation surrounded by 6 oxygen atoms in a distorted octahedral configuration. Anatase can be viewed as a distorted ccp array of O^{2-} with Ti^{4+} in half of the octahedral holes. Rutile on the other hand is a distorted hcp array of O^{2-}. The consequences of this are different angles between bond lengths. The two bonds between the titanium and the oxygen atoms in the [010] plane of the octahedron are slightly longer. Anatase exhibits a large angle between this bond and the [100] plane (102.308 °) whereas the angle for rutile is closer to 90 ° (98.93 °) (figure 4.1). Moving from bulk anatase to rutile requires rotation of half the Ti octahedra. The structural energy of rutile and anatase is quite similar though rutile is known as the stable phase.[84]

Anatase films also differ in electronic properties from rutile. The conduction band of anatase films can undergo metallic transitions whilst these do not exist in

rutile structures making anatase a better electrical conductor. Rutile films also have a smaller gap for absorption than anatase.[85] This explains the greater use of anatase for photocatalytic procedures given its ability to absorb more light than rutile.

4.1.1.2. TiO_2 Phase Transformation

Under ambient conditions macrocrystalline rutile is thermodynamically stable relative to anatase or brookite but if the particle diameters reach below 14 nm anatase becomes the more stable phase. Heating nano-meter sized titania leads to alteration of phase stabilities and anatase will convert to rutile. Phase stability decreases from rutile > brookite > anatase so anatase may either transform directly to rutile or to brookite first.[86]

Several studies have been performed in order to understand what the governing factors are for phase transformation from anatase to rutile. The transformation rate increases dramatically between 465 and 525 °C when the reacting anatase phase is finely crystalline. Given the smaller crystal size, more nucleation sites are available allowing for a greater rate of transformation.[87] The rate was slow below 610 °C, rapid above 730 °C and was second-order with respect to remaining anatase. Repeating the experiment *in vacuo* gave same results as those conducted in air so it was surmised that the transition is not reliant on the atmosphere but dependent on time and temperature.[88]

4.1.1.3. Effect of CVD Conditions on the Phase of TiO_2

During CVD experiments a first-order dependence on precursor pressure was noted with TiO_2 film grown on a Si(100) substrate where polycrystalline anatase grew below 650 °C and rutile around 700 °C.[89] In a different study TiO_2 thin films grown on SiO_2/Si surface were anatase phase above 600 °C and 800 °C annealing though on a Pt/Si substrate the same films became rutile[90] demonstrating the substrate used in deposition can alter the phase.

Different precursors can also change the film phase. $[Ti(OPr^i)_4]$ gives anatase films at temperatures of 450-550 °C, and a mixture of anatase and rutile between 550 and 650 °C whereas $TiCl_4$ gives exclusively rutile between 550-650 °C and no growth below 550 °C. This difference could be explained by the mechanisms of decomposition of each precursor.

$[Ti(OPr^i)_4]$ is broken down in the MOCVD chamber by direct thermolysis (eq. a, b) or hydrolysis (eq. c).[91,92]

$$[Ti(OPr^i)_4] \longrightarrow TiO_2 + 2CH_3CH{=}CH_2 + 2HOPr^i \quad \textbf{(a)}$$

$$[Ti(OPr^i)_4] \longrightarrow TiO_2 + 4CH_3CH{=}CH_2 + 2H_2O \quad \textbf{(b)}$$

$$[Ti(OPr^i)_4] \xrightarrow{H_2O} TiO_2 + 4HOPr^i \quad \textbf{(c)}$$

Figure 4. 2: Equations showing possible decomposition mechanisms of $[Ti(OPr^i)_4]$ to form TiO_2: (a), (b) direct thermolysis, (c) hydrolysis.

This intramolecular mechanism utilising the O in its own structure leads to the direct formation of TiO_2 nanoparticles. Surface studies have also suggested that a

Si(100) surface acts as a support for the intramolecular chemistry. If the Ti precursor was used as dual source with water or oxygen intermolecular reactions could also occur given a faster decomposition rate. Since there is no oxygen present in $TiCl_4$ intermolecular mechanisms must cause TiO_2 formation which would be significantly slower than the decomposition of $[Ti(OPr^i)_4]$. The different rates of decomposition could explain the resulting phases.[93]

4.1.1.4. Nanostructure growth

As well as thin films of TiO_2, there has been a great increase in interest in the production of TiO_2 nanostructures since the larger surface area of nanostructures compared to thin films will improve the efficiency of the photocatalytic activity.[75] Preparation of nanostructures varies widely from nanotubes and fibres,[94] nanowalls,[70] nanopetals,[95] tree-like structures[96] and simpler nanocrystals.[97] Similar to growing films of TiO_2 the temperature and time of growth has an effect on the size and morphology of the nanostructures.[98]

4.1.2. Ti(IV) alkoxides as precursors for MOCVD

Ti(IV) alkoxides have shown use in several different applications. They are used in reductive cross-coupling reactions in organic chemistry,[99] catalysts for the manufacture of polyolefins and esters, precursors to make electroceramic materials and $SrTiO_3$ and $(Ba,Sr)TiO_3$ high-*k* dielectric layers for DRAM applications, and $Pb(Zr,Ti)O_3$ ferroelectric film.[100] They are also precursors for sol–gel deposition of titania–silica catalysts and mesoporous titanium(IV) oxides.

4.1.2.1. $TiCl_4$ and $[Ti(OPr^i)_4]$

Typically the MOCVD of TiO_2 thin films and nanostructures has been performed using titanium tetrachloride, $TiCl_4$[101,102] or homoleptic titanium alkoxides $[Ti(OR)_4]$ (R= Et, Pr^i). Originally $TiCl_4$ was classed as the best CVD precursor for thin films of TiO_2 forming films from either hydrolysis or direct oxidation of the precursor. Unfortunately precursors of this nature tend to result in halogen contamination in the films and also require higher deposition temperatures that exceed the temperatures of typical processing requirements (<500 °C).

In more recent years, titanium alkoxides, such as $[Ti(OPr^i)_4]$, have been more widely used. An alkoxide precursor allows for deposition at low temperature and also removes the problem of halide contamination of the film. However, one drawback is the presence of a sterically unsaturated four-coordinate Ti^{4+} metal ion that gives the complexes moisture sensitivity creating storage issues and the possibility of the precursor reacting in the MOCVD chamber before deposition occurs.

4.1.2.2. Heteroleptic alkoxides

To increase the coordination of the Ti^{4+} centre heteroleptic alkoxides with bulkier ligands have been researched. $[Ti(OPr^i)_2(thd)_2]$ [100,103] is a good example of such stabilised complexes useful for depositing ferroelectric oxides with lead and

zirconium. $[Ti(OPr^i)_2(tbaoac)_2]$ (figure 4.3) has also been used in deposition tests for studies of TiO_2 and $SrTiO_3$ films.[104]

2,2,6,6-tetramethylheptane-3,5-dione
(thdH)

tert-butyl acetoacetate
(tbaoacH)

Figure 4. 3: Structures of the ligands thdH and tbaoacH.

Compounds containing amides have also shown promise. A range of complexes with the ligands NR_2 (R = Me, Et) and malonate derivatives all demonstrated good thermal stabilities.[105] Other precursors with donor-functionalised ligands containing and O and a N donor atom are common like bdmapH ($HOCH(CH_2NMe_2)_2$ and tdmapH ($HOC(CH_2NMe_2)_3$ with OEt and OPr^i ligands. $[Ti(OEt)_3(bdmap)]$ was use for aerosol assisted CVD (figure 4.4).[106]

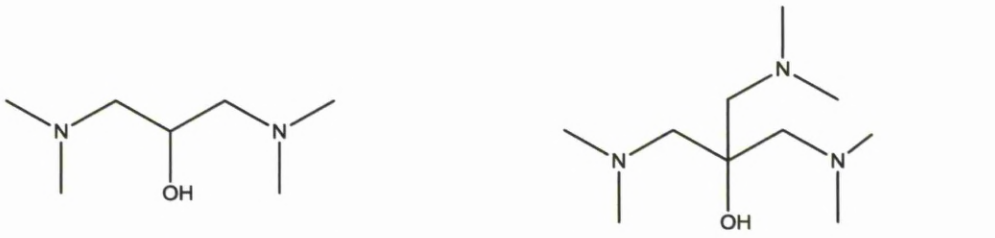

1,3-bis(dimethylamino)propan-2-ol
(bdmapH)

1,3-bis(dimethylamino)-2-((dimethylamino)methyl)
propan-2-ol **(tdmapH)**

Figure 4. 4: Structures of the ligands bdmapH and tdmapH.

4.1.3. Ligands for Precursor Synthesis.

All ligands used in this study are donor-functionalised alcohols shown in figure 4.5. Each binds to Ti via an alcohol oxygen and a dative bond from a methoxy

oxygen (mmp), an amine nitrogen (dmae) or the nitrogen found as an imine in an oxazoline ring (dmop and dmom).

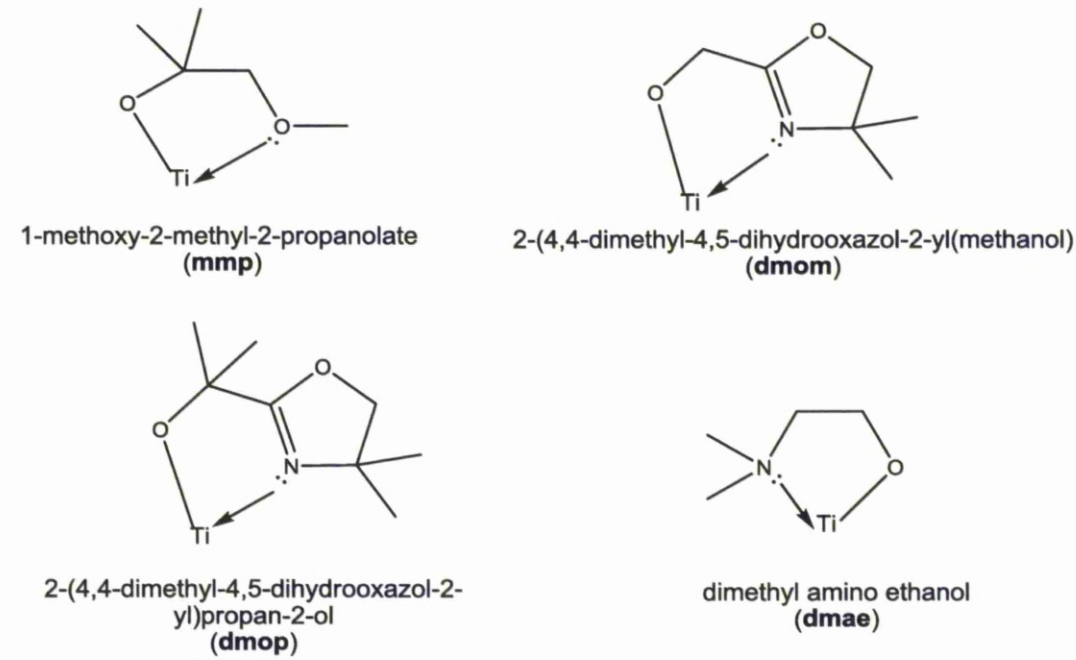

Figure 4. 5: Donor-functionalised alcohols used for Ti complex synthesis.

Each ligand therefore has different donor strengths for the dative bond. Lone pair donor strength increases as following: OMe < N=C <$N(CH_3)_2$. Dmop and dmom should therefore have similar strength donor bonds but given the extra methyl groups on dmop steric hindrance may have more of an effect on its coordination to the metal centre.

The dmae ligand has been used previously to make Ti (IV) heteroleptic alkoxides with two diolate ligands: ethylene glycolate ($(OCH_2)_2$) and pinacol ($(OCMe_2)_2$).[107] The compound $[Ti((OCMe_2)_2)(dmae)_2]_2$ was successful in growing thin films of TiO_2 using MOCVD between 325 - 450 °C whereas $[Ti((OCH_2)_2)(dmae)_2]_2$ gave inconsistent and highly variable growth.

$[Ti(OPr^i)_2(dmae)_2]$ and $[Ti(OPr^i)_3(dmae)]$ have also been made previously via reaction of $[Ti(OPr^i)_4]$ with 2 or 3 equivalents of dmaeH respectively. In their use for growing thin films of TiO_2 on a Si(100) surface via MOCVD it was found that the complex with 2 dmae groups had a greater thermal stability with higher growth up to 600 °C though both precursors were able to grow TiO_2 films at low substrate temperatures (300 – 550 °C).[108] $[Ti(OPr^i)_2(dmae)_2]$ has also been used to grow smooth uniform films via ALD. The precursor becomes self-limiting at temperatures of 100-300 °C.[109] Ti (IV) alkoxides with dmaeH were therefore used as the starting point of this study.

4.2. Results and Discussion

For the synthesis of heteroleptic Ti (IV) alkoxides the reaction scheme in figure 4.6 was adopted. The reaction is an alkoxy exchange displacing two of the isopropoxide or *tert*-butoxide groups with two bidentate ligands increasing the coordination number of titanium to 6.

$$[Ti(OR)_4] + 2HL \longrightarrow [Ti(OR)_2L_2] + 2HOR$$

Figure 4. 6: Basic reaction scheme for heteroleptic Ti (IV) alkoxides. R = OBu^t, OPr^i.

For complexes with an octahedral geometry there is the possibility of structural isomers. These complexes have the general formula $[Ti(OR)_2(O\text{-}L)_2]$ and so will have 5 possible structural isomers with 3 existing as enantiomers (figure 4.7).

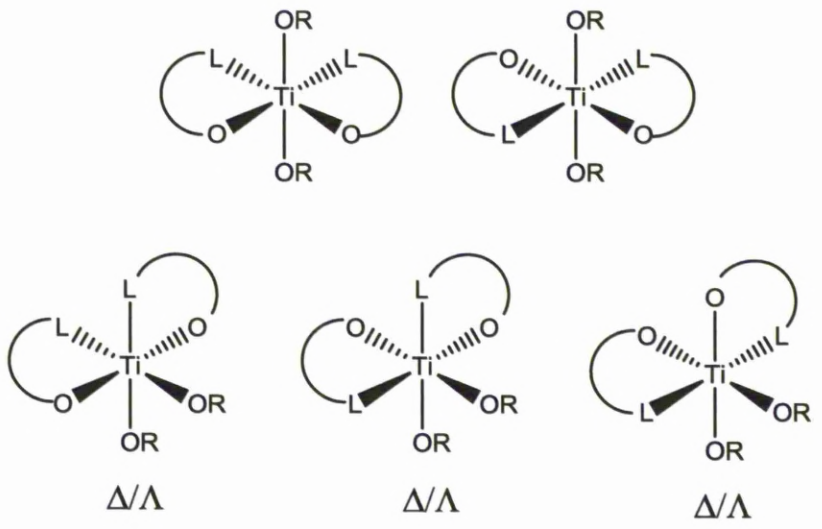

Figure 4. 7: Possible structural isomers for complexes with an octahedral geometry and general formula $[Ti(OR)_2(O\text{-}L)_2]$ were R = OPr^i, OBu^t and L = O, N. The complexes annotated Δ and Λ have enantiomers.

4.2.1. Reaction of $[Ti(OPr^i)_4]$and $[Ti(OBu^t)_4]$ with 2 eq. dmaeH.

Following the alkoxy exchange procedure shown in figure 4.6 $[Ti(OPr^i)_4]$ was dissolved and stirred in hexane at room temperature. Two equivalents of dmaeH were added and the reaction refluxed for 2 hours. After removing the volatiles under *vacuo* the resulting oil was purified via distillation. The ^1H NMR spectrum for $[Ti(OPr^i)_2(dmae)_2]$ is concordant to that reported previously (figure 4.8).[108] Proceeding in the same way as above $[Ti(OBu^t)_2(dmae)_2]$ was synthesised giving a ^1H NMR spectrum that would be as predicted (figure 4.9). This suggests that the complex is either highly fluxional or the structure exists with a plane of symmetry. A combination of the Ray-Dutt and Bailar twist mechanisms[110,111] would lead to rapid isomerisation of the complex and result in a plane of symmetry through the

chelate ligands giving the simple spectra observed. This fluxional process was not frozen out by low temperature ^{1}H NMR spectroscopy.

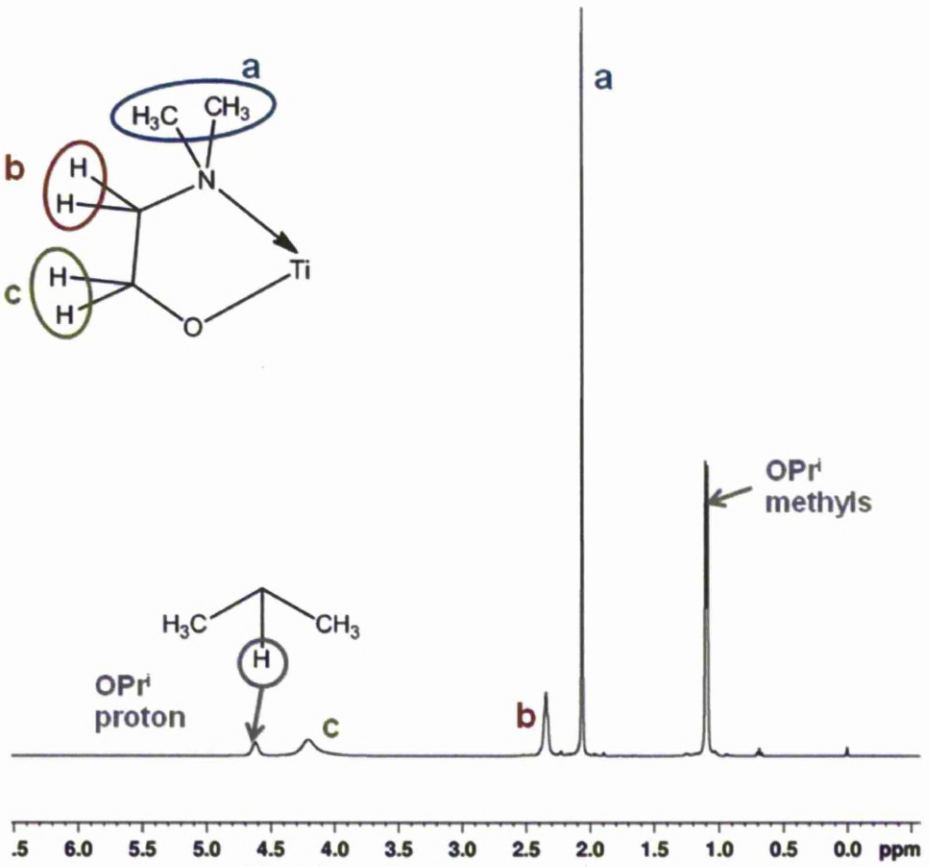

Figure 4. 8: ^{1}H NMR spectrum (C_7D_8) of [Ti(OPr^i)$_2$(dmae)$_2$].

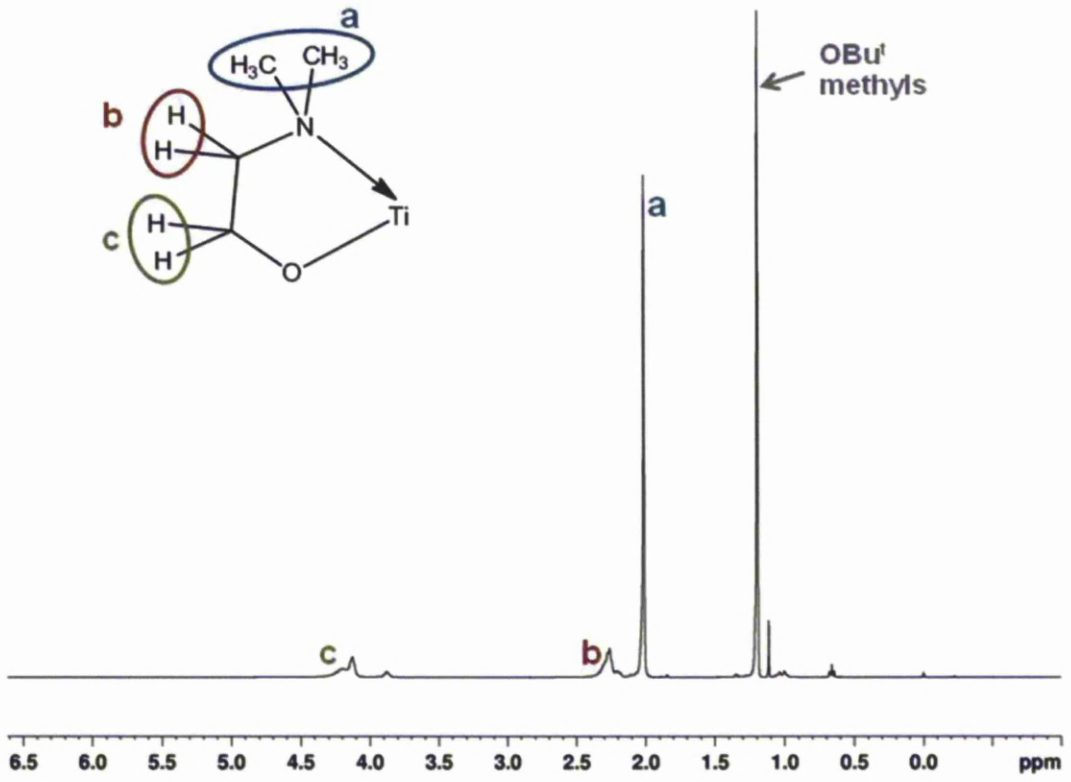

Figure 4. 9: ^{1}H NMR spectrum (C_7D_8) of [Ti(OBu^t)$_2$(dmae)$_2$].

4.2.2. Reaction of [Ti(OPr^i)$_4$] and [Ti(OBu^t)$_4$] with 2 eq. mmpH.

Refluxing [Ti(OPr^i)$_4$] with 2 equivalents of mmpH in hexane for 2 hours yielded [Ti(OPr^i)$_2$(mmp)$_2$] as a colourless oil. CHN analysis was used to confirm the presence of [Ti(OPr^i)$_2$(mmp)$_2$] giving values within 0.1 % of theoretical predictions.

It is difficult to deduce the structure of the complex from the ^{1}H NMR spectrum given in figure 4.10 hence variable temperature ^{1}H NMR was performed. As the temperature decreases (figure 4.11) the broad peak at 4.6 ppm splits into two multiplets indicating two different isopropoxides. At 1.3 ppm the differing isopropoxide methyl groups become two clear doublets. This could be due to the

removal of symmetry of the complex in solution or the occurrence of ligand redistribution reactions.

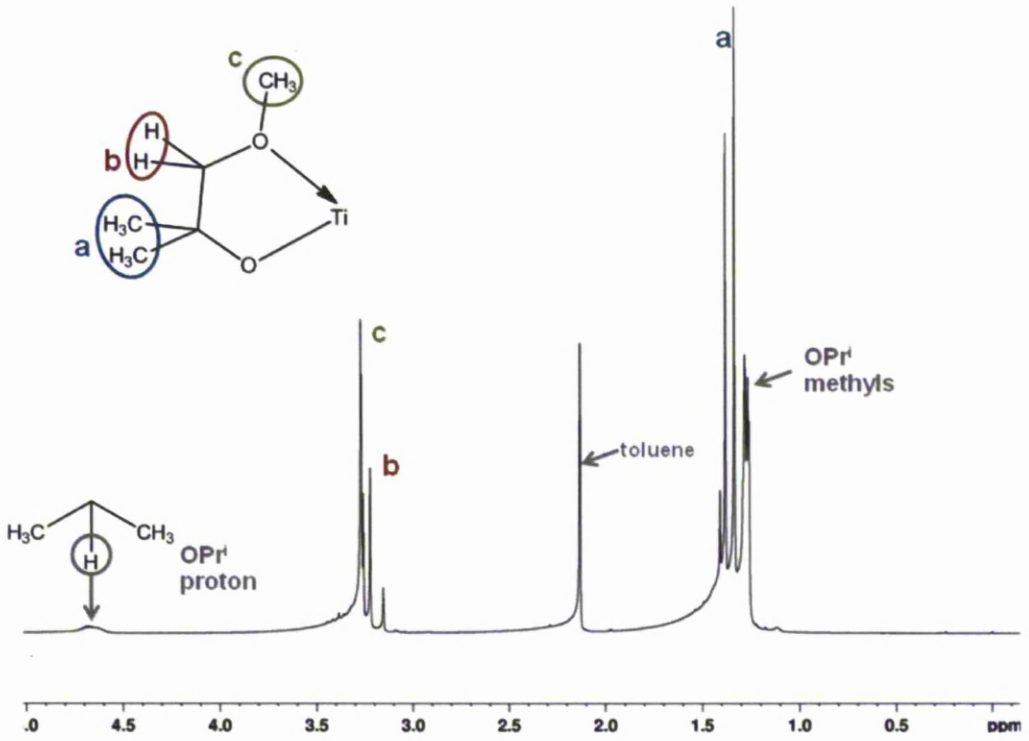

Figure 4. 10: ^{1}H NMR spectrum (C_7D_8) of [Ti(OPr^i)$_2$(mmp)$_2$] at 298 K.

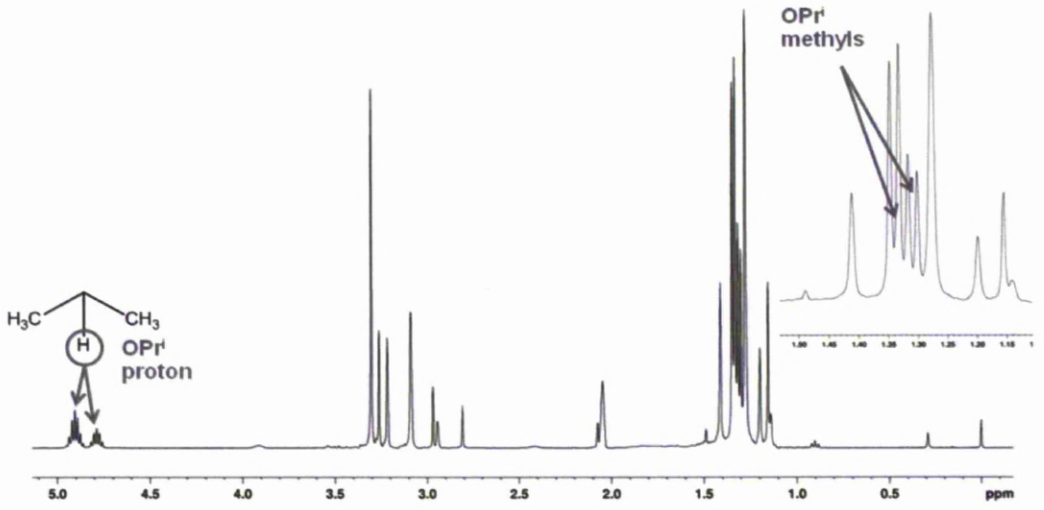

Figure 4. 11: ^{1}H NMR spectrum (C_7D_8) of [Ti(OPr^i)$_2$(mmp)$_2$] at 223 K.

Increasing the temperature to 355 K (figure 4.12) causes the peaks to coalesce. There is now one broad singlet at 6.98 ppm and one doublet at 3.7 ppm for the isopropoxides. The two methyl groups of the mmp ligand are represented by a singlet at 3.65 ppm and the CH_2 and OMe groups merged to form a shoulder peak at 5.67 ppm.

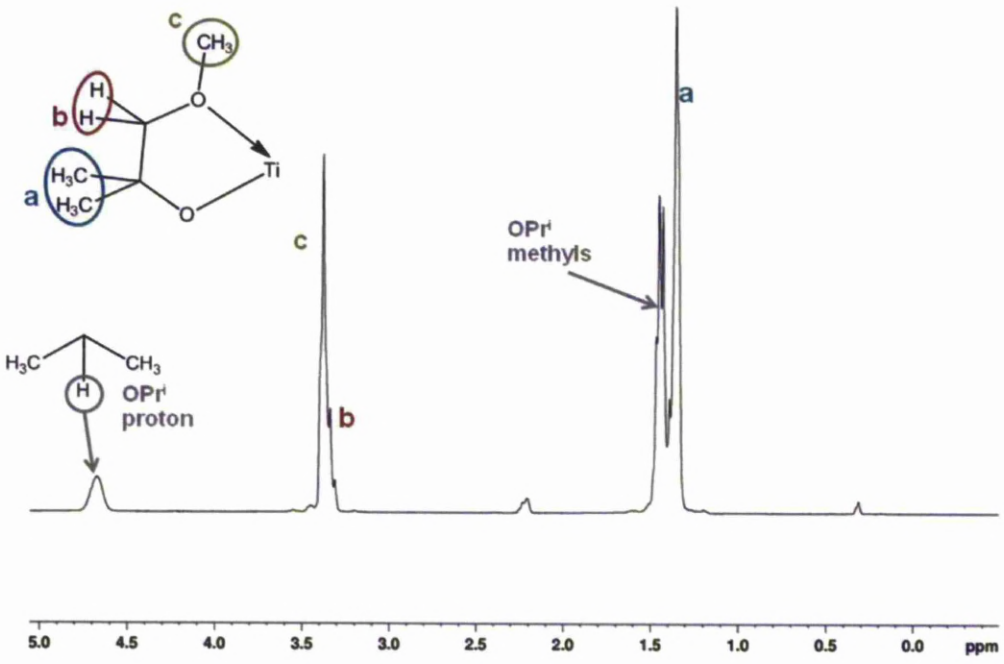

Figure 4. 12: ^{1}H NMR spectrum (C_7D_8) of $[Ti(OPr^i)_2(mmp)_2]$ at 355 K.

The ^{13}C NMR spectrum of $[Ti(OPr^i)_2(mmp)_2]$ also shows more peaks than would be expected possibly due to a reduction in symmetry of the structure. Figure 4.13 shows the NMR spectrum and the likely interpretation of the peaks.

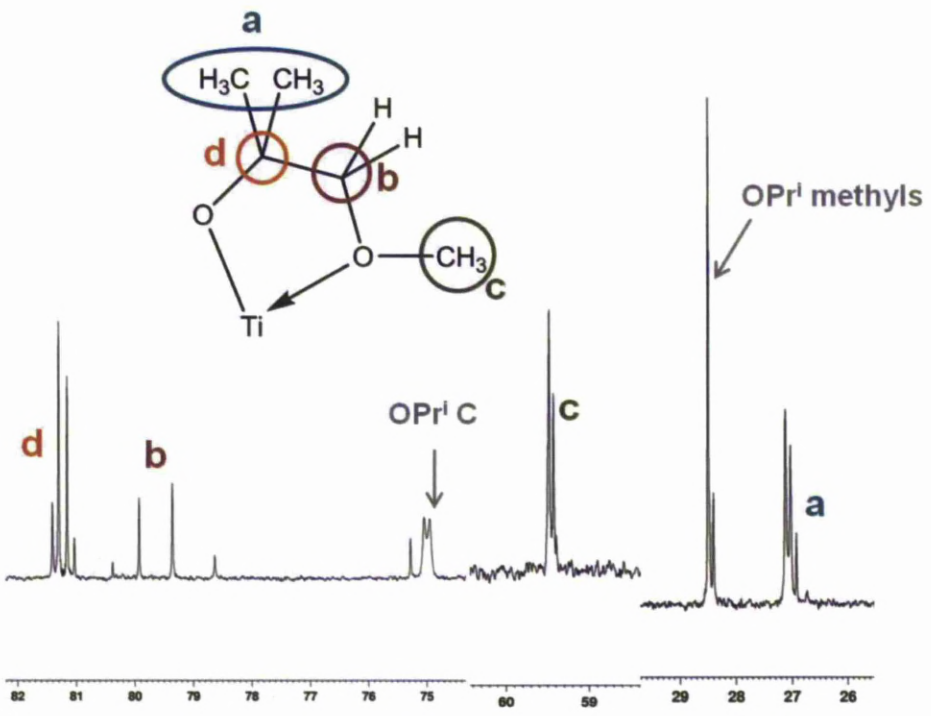

Figure 4. 13: ^{13}C NMR spectrum (C_7D_8) of $[Ti(OPr^i)_2(mmp)_2]$.

$[Ti(OBu^t)_2(mmp)_2]$ was made in the same way as $[Ti(OPr^i)_2(mmp)_2]$ and again the structure of the complex was difficult to determine from the ^1H NMR spectrum. CHN analysis of the resulting colourless oil gave values within 0.16 % of theoretical predictions. The NMR spectrums are more concordant with different species arising from ligand redistributions.

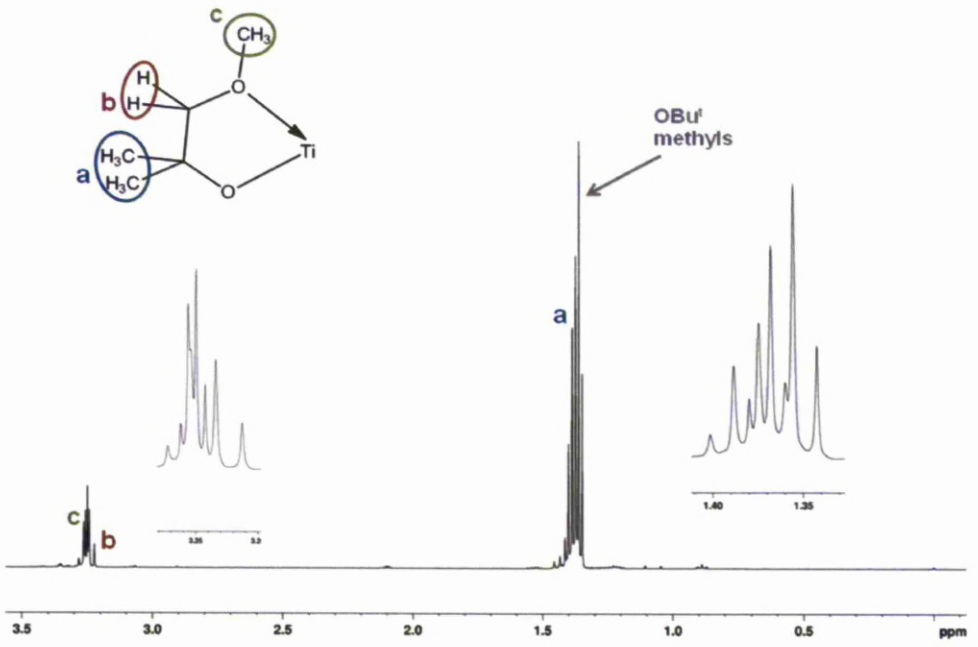

Figure 4. 14: ^{1}H NMR spectrum (C_7D_8) of [Ti(OBu^t)$_2$(mmp)$_2$].

At higher temperature NMR spectroscopy (figure 4.15) the peaks coalesce to form two broad singlets whereas at 193 K (figure 4.16) convergence gives more distinct sets of peaks. There is still some broadening and overlap occurring indicating the ligands are fluxional.

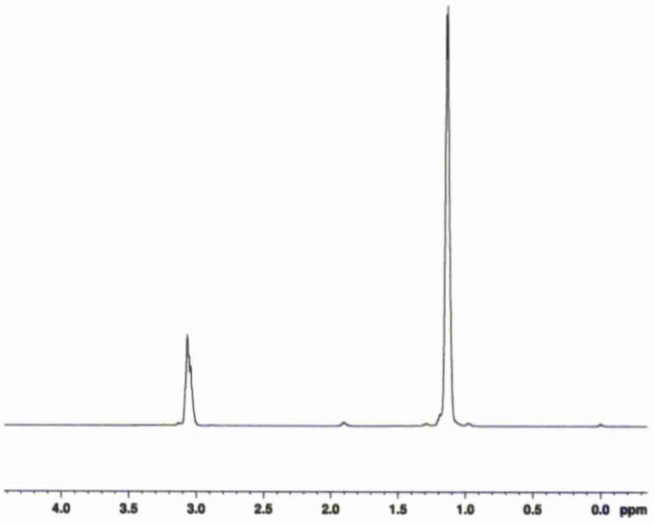

Figure 4. 15: ^{1}H NMR spectrum (C_7D_8) of [Ti(OBu^t)$_2$(mmp)$_2$] at 375 K.

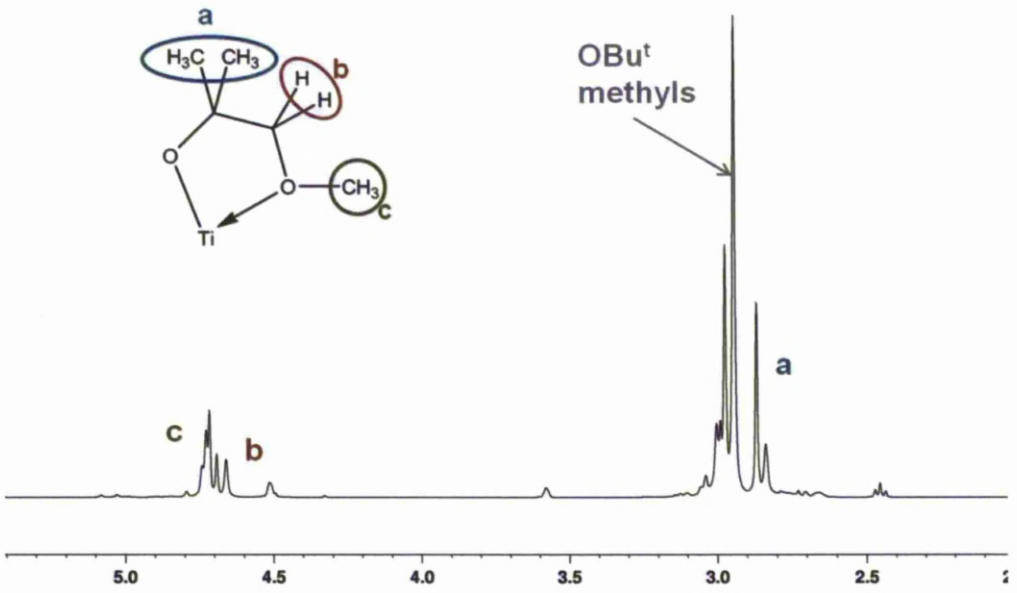

Figure 4. 16: ^{1}H NMR spectrum (C_7D_8) of $[Ti(OBu^t)_2(mmp)_2]$ at 193 K.

Looking at the ^{13}C NMR spectrum (figure 4.17) the peaks are consistent with a statistical mixture of $[Ti(OBu^t)_{4-n}(mmp)_n]$ with n = 0 to 4. The ligand distribution reactions of $[Ti(OR)_2(mmp)_2]$ contrast with the stability of $[M(OBu^t)_2(mmp)_2]$ (M = Zr or Hf) which retain their structures in solution.[112]

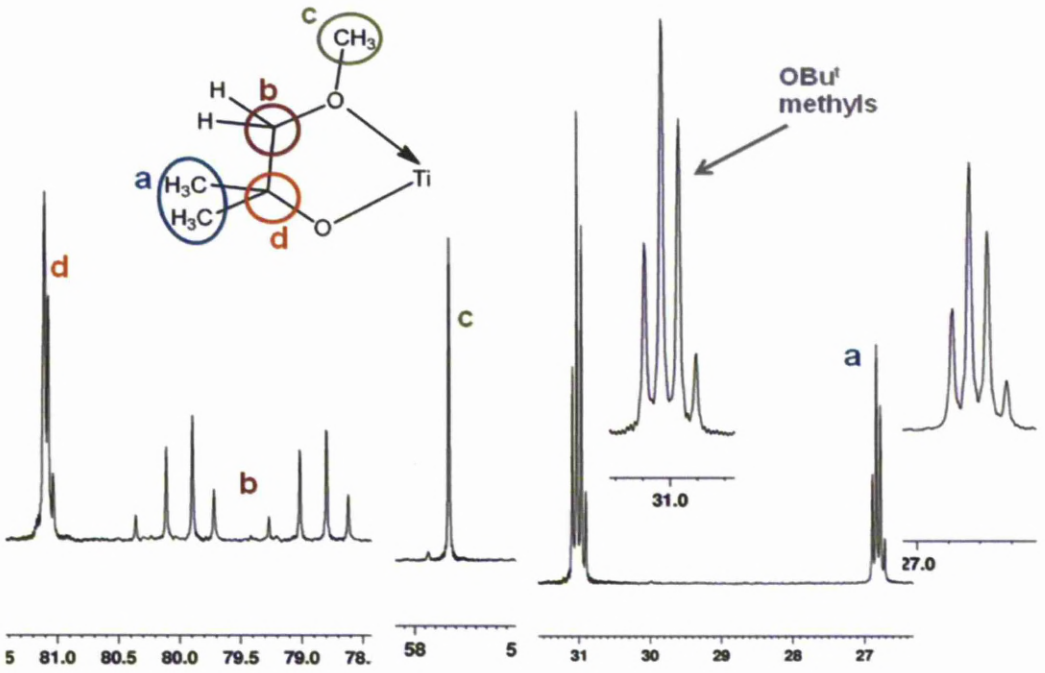

Figure 4. 17: ^{13}C NMR spectrum (C_7D_8) of $[Ti(OBu^t)_2(mmp)_2]$.

4.2.3. Reaction of $[Ti(OPr^i)_4]$ and $[Ti(OBu^t)_4]$with 2 eq. dmopH

$[Ti(OPr^i)_2(dmop)_2]$ was synthesised by refluxing $[Ti(OPr^i)_4]$ in toluene with 2 equivalents of dmopH. After removing the volatiles from the colourless solution a white solid was obtained. This was recrystallised from toluene overnight at -18 °C to give the desired complex as colourless crystals.

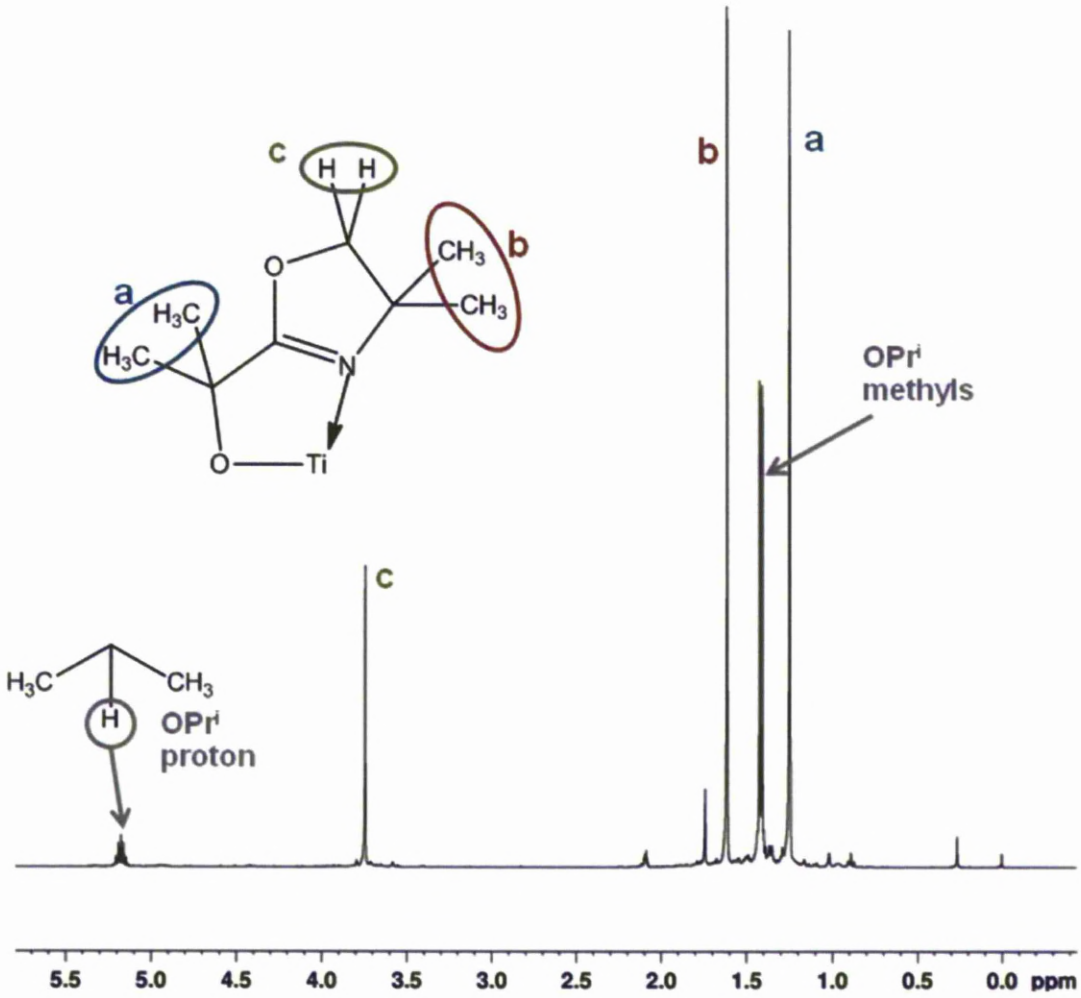

Figure 4. 18: ^{1}H NMR spectrum (C_7D_8) of [Ti(OPr^i)$_2$(dmop)$_2$].

The peaks in the ^{1}H NMR spectrum (figure 4.18) are in the ratio of 6:6:6:2:1 as would be predicted. The complex was also characterised by X-ray crystallography as shown in (figure 4.19). The simplicity of the ^{1}H NMR spectrum and the lack of a plane of symmetry in the dmop ligand of the crystal structure indicate the complex is not fluxional.

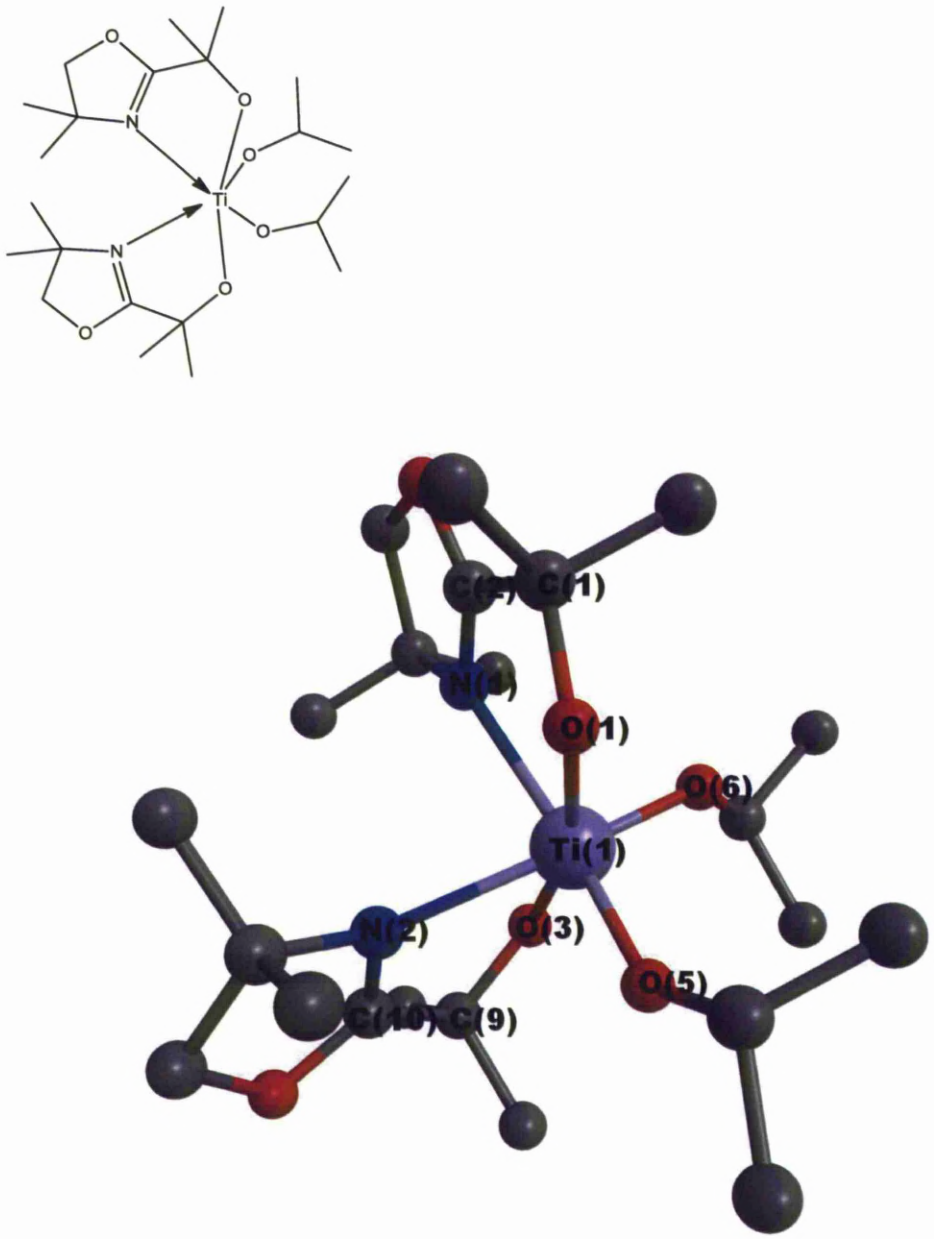

Figure 4. 19: Crystal structure of $[Ti(OPr^{i})_2(dmop)_2]$.

The complex is monoclinic with Ti in a 6-coordinate array with two O (isopropoxide) atoms, two O (alcohol) atoms and two N (imine) atoms. Two types of bonding are present; Ti-O σ bonds and Ti-N dative bonds which sit *cis* to each other. The isopropoxide and dmop ligands are sitting *cis* to each other.

Both of the isopropoxide oxygens (O(5, 6)) have similar bond lengths with Ti of ~ 1.82 Å. These are shorter than the Ti-O bonds from the two dmop alcohols (O(1,3) of ~ 1.93 Å. Unsurprisingly the length of the dative bonds between Ti and the imine nitrogens (N(1,2)) are the longest with 2.259(1) and 2.274(1) Å (table 4.1).

Table 4. 1: Selected bond lengths and angles for the crystal structure of $[Ti(OPr^i)_2(dmop)_2]$.

Atoms	Bond Length (Å)
Ti(1)-N(2)	2.259(1)
Ti(1)-N(1)	2.274(1)
Ti(1)-O(6)	1.824(1)
Ti(1)-O(5)	1.821(1)
Ti(1)-O(3)	1.934(1)
Ti(1)-O(1)	1.930(1)
Atoms	**Bond Angle (°)**
N(1)-Ti(1)-N(2)	83.78(5)
N(2)-Ti(1)-O(6)	163.29(5)
N(2)-Ti(1)-O(5)	87.43(5)
N(2)-Ti(1)-O(3)	74.32(5)
N(2)-Ti(1)-O(1)	93.51(5)
N(1)-Ti(1)-O(6)	89.99(5)
N(1)-Ti(1)-O(5)	161.84(5)
N(1)-Ti(1)-O(3)	92.87(5)
N(1)-Ti(1)-O(1)	74.19(5)
O(6)-Ti(1)-O(5)	102.52(5)
O(6)-Ti(1)-O(3)	90.59(5)
O(6)-Ti(1)-O(1)	99.70(5)
O(5)-Ti(1)-O(3)	100.02(5)
O(5)-Ti(1)-O(1)	90.58(5)
O(3)-Ti(1)-O(1)	163.32(5)

The synthesis of $[Ti(OBu^t)_2(dmop)_2]$ was carried out in the same way refluxing $[Ti(OBu^t)_4]$ and 2 equivalents of in toluene. This gave a colourless solution that became a white solid after removal of the volatiles under *vacuo*. After recrystallising from toluene white, short acicular crystals were obtained. These were

shown by X-ray crystallography to be the trinuclear oxo complex $[Ti_3O_3(dmop)_6]$ (figure 4.20)

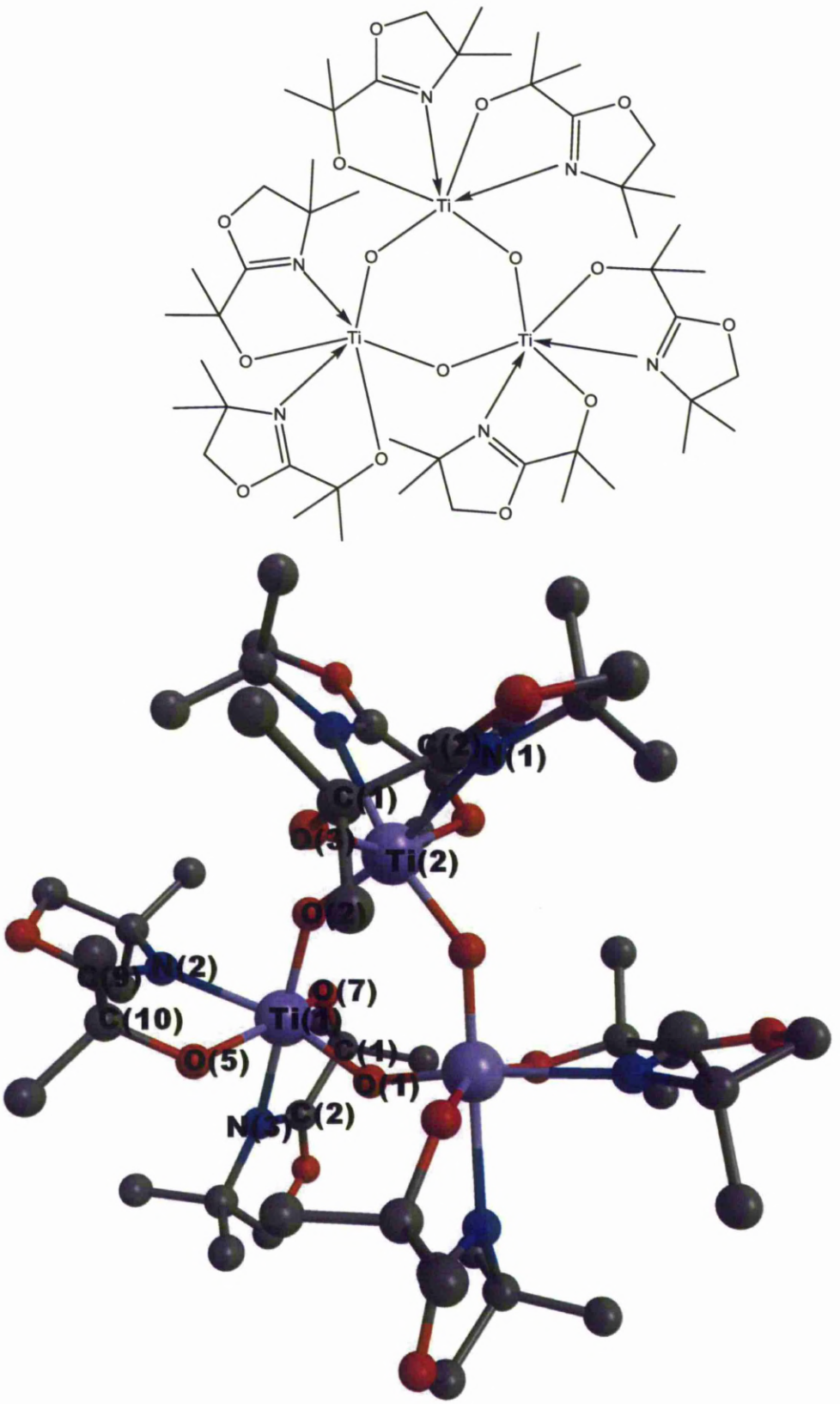

Figure 4. 20: Crystal structure of trimer $[Ti_3O_3(dmop)_6]$.

Table 4. 2: Selected bond lengths for the crystal structure of $[Ti_3O_3(dmop)_6]$.

Bond Atoms	Bond Type	Bond Length (Å)
Ti(1)-O(1)	Bridging	1.823(2)
Ti(1)-O(2)	Bridging	1.808(4)
Ti(2)-O(2)	Bridging	1.835(4)
Ti(1)-O(5)	Terminal	1.927(4)
Ti(1)-O(7)	Terminal	1.921(4)
Ti(1)-N(3)	Terminal	2.301(4)
Ti(1)-N(2)	Terminal	2.275(5)
Ti(2)-O(3)	Terminal	1.922(5)
Ti(2)-N(1)	Terminal	2.302(6)
Ti(2)-O(3)#1	Terminal	1.922(5)
Ti(2)-N(1)#1	Terminal	2.302(6)
Bond Atoms	**Bond Type**	**Bond Angle (°)**
O(1)-Ti(1)-O(2)	Bridging	100.1(2)
O(2)-Ti(2)-O(2)#1	Bridging	99.7(2)
O(5)-Ti(1)-N(2)	Terminal	73.7(2)
O(7)-Ti(1)-O(3)	Terminal	73.5(2)
N(3)-Ti(1)-N(2)	Terminal	87.2(2)
O(3)-Ti(2)-N(1)	Terminal	73.7(2)
O(3)#1-Ti(2)-N(1)#1	Terminal	87.7(2)
N(1)-Ti(2)-N(1)#1	Terminal	89.6(2)
N(3)-C(18)-C(17)-O(7)	Dihedral	-3.2(7)
N(2)-C(9)-C(10)-O(5)	Dihedral	-6.0(7)
N(1)-C(2)-C(1)-O(3)	Dihedral	-7(1)

Each Ti atom has two Ti-O oxo-bridged bonds binding that atom to another Ti and two chelating dmop ligands making the Ti atoms 6 coordinate. The Ti-O (O(1, 2,)) oxo-bridge bond lengths are ~ 1.82 Å, smaller than the 1.92 Å of the dmop alcohol oxygen bond. The Ti-N bond lengths are longer at ~2.30 Å.

The reaction was carried out again adding the dmopH ligand in toluene at 0 °C and stirring for 2 hours. A colourless solution was obtained followed by a white solid after removing the volatiles. This was recrystallised in toluene to give

colourless crystals which were characterised as the desired monomer $[Ti(OBu^t)_2(dmop)_2]$ (figure 4.21)

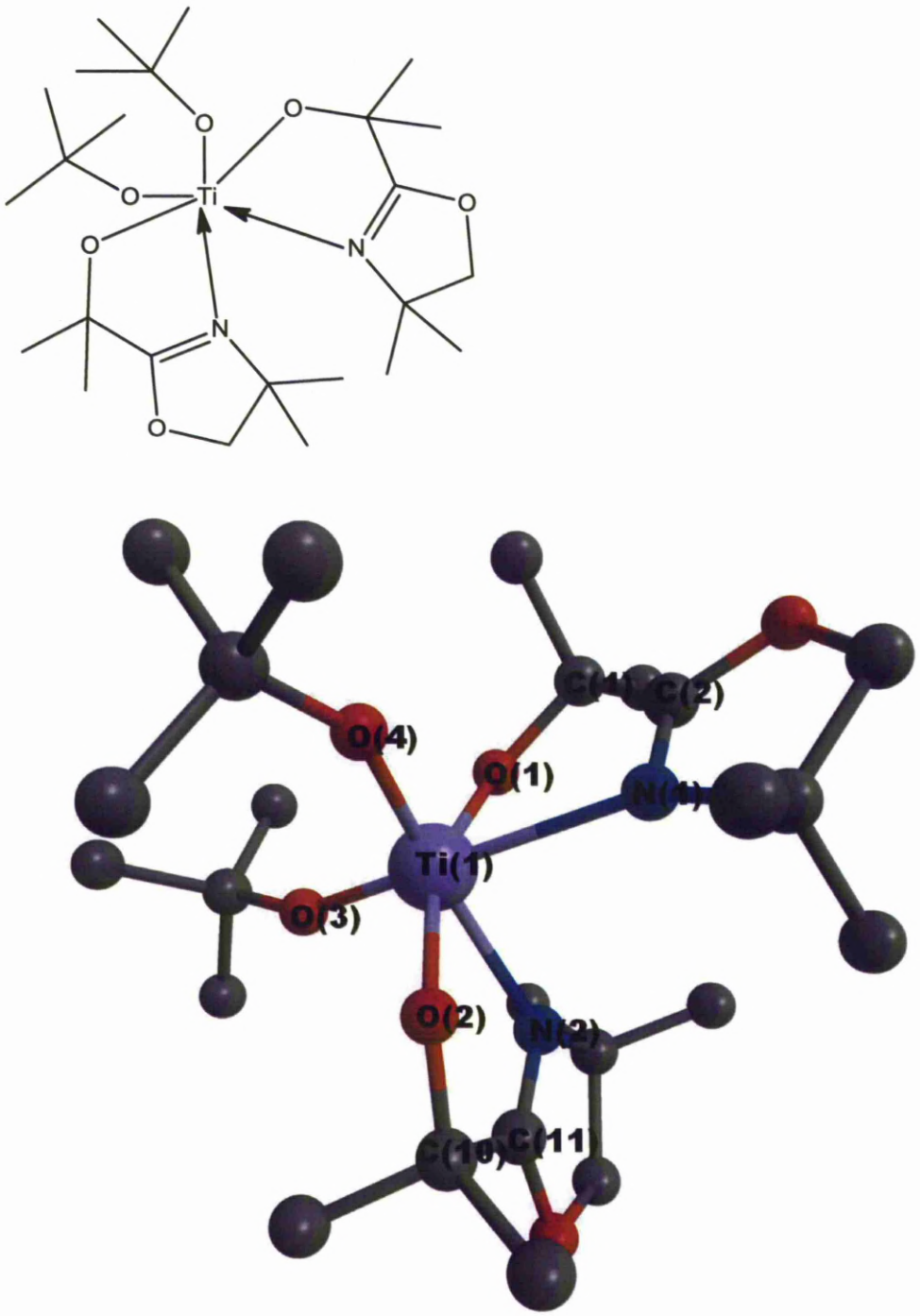

Figure 4. 21: Crystal structure of $[Ti(OBu^t)_2(dmop)_2]$.

Ti is 6 coordinated in an octahedral geometry bonded to the oxygen of each OBu^t group and the bidentally coordinated dmop ligands. The dmop ligands are *cis* to each other in this complex.

Table 4. 3: Selected bond lengths and angles of $[Ti(OBu^t)_2(dmop)_2]$ crystal structures.

Bond Atoms	Bond Length (Å)	Bond Atom	Bond Length (Å)
Ti(1)-O(1)	1.923(3)	Ti(2)-O(8)#1	1.937(3)
Ti(1)-O(2)	1.930(2)	Ti(2)-O(8)	1.937(3)
Ti(1)-O(3)	1.798(2)	Ti(2)-O(9)#1	1.810(3)
Ti(1)-O(4)	1.806(3)	Ti(2)-O(9)	1.810(3)
Ti(1)-N(1)	2.316(3)	Ti(2)-N(3)#1	2.288(4)
Ti(1)-N(2)	2.329(3)	Ti(2)-N(3)	2.288(4)
Bond Atoms	**Angle (°)**	**Bond Angle**	**Angle (°)**
N(2)-Ti(1)-N(1)	85.3(1)	N(3)-Ti(2)-N(3)#1	85.33(13)
N(2)-Ti(1)-O(4)	163.5(1)	O(9)#1-Ti(2)-N(3)#1	163.22(12)
N(2)-Ti(1)-O(3)	88.6(1)	O(9)-Ti(2)-N(3)#1	89.01(13)
N(2)-Ti(1)-O(2)	73.5(1)	O(8)#1-Ti(2)-N(3)#1	73.99(12)
N(2)-Ti(1)-O(1)	89.5(1)	O(8)-Ti(2)-N(3)#1	91.63(13)
N(1)-Ti(1)-O(3)	165.6(1)	O(9)#1-Ti(2)-N(3)	89.01(13)
N(1)-Ti(1)-O(4)	85.7(1)	O(9)-Ti(2)-N(3)	163.22(12)
N(1)-Ti(1)-O(2)	90.9(1)	O(8)#1-Ti(2)-N(3)	91.63(13)
N(1)-Ti(1)-O(1)	73.5(1)	O(8)-Ti(2)-N(3)	73.99(12)
O(2)-Ti(1)-O(1)	158.1(1)	O(8)-Ti(2)-O(8)#1	160.62(11)
O(3)-Ti(1)-O(2)	99.9(1)	O(8)-Ti(2)-O(9)#1	101.99(14)
O(4)-Ti(1)-O(2)	92.9(1)	O(8)#1-Ti(2)-O(9)	101.99(14)
O(4)-Ti(1)-O(1)	101.1(1)	O(8)#1-Ti(2)-O(9)#1	90.43(13)
O(3)-Ti(1)-O(1)	93.4(1)	O(8)-Ti(2)-O(9)	90.43(13)
O(4)-Ti(1)-O(3)	103.1(1)	O(9)-Ti(2)-O(9)#1	100.53(13)
O(1)-C(1)-C(2)-N(1)	-7.7(4)	O(8)#1-C(27)#1-C(28)#1-N(3)#1	9.0(5)
O(3)-C(10)-C(11)-N(2)	-6.5(4)	O(8)-C(27)-C(28)-N(3)	9.0(5)

There are two different complexes in the asymmetric unit. The bond lengths between Ti and the *tert*-butoxide oxygens (O(3, 4, 9, 9#1)) average ~1.80 Å. The Ti bonds with dmop oxygens (O(1, 2, 8, 8#1)) are ~ 1.93 Å and the imine nitrogens (N (1, 2, 3, 3#1)) around 2.30 Å. This is very similar to the lengths recorded for $[Ti(OPr^i)_2(dmop)_2]$ and $[Ti_3O_3(dmop)_6]$. The bond angle between the dmop nitrogen, Ti and dmop oxygen (example N(2)-Ti(1)-O(2)) is also similar throughout the three crystal structures containing dmop at ~ 74.00 °.

The two $[Ti(OBu^t)_2(dmop)_2]$ complexes are bound by intermolecular bonding between a methyl hydrogen and a dmop oxygen with a bond length of 3.538(6) Å (figure 4.22). The complexes differ in their symmetry as the Ti (1) structure exhibits general symmetry whereas the Ti (2) complex has a C_2 symmetry axis. There is also discrepancy when comparing the dihedral angles of the dmop ligands which describes the twist of the ligands compared to each other. The angle is measured from the alcohol oxygen, two carbons connecting the alcohol to the ring and the imine nitrogen, e.g. O(1)-C(1)-C(2)-N(1). Both dihedral angles for the Ti(2) structure have the same angle of 9.0(5) ° allowing for its C_2 symmetry. For the Ti(1) complex the angles are -6.5(4) and -7.7(4) ° further showing the difference in geometry of the two structures.

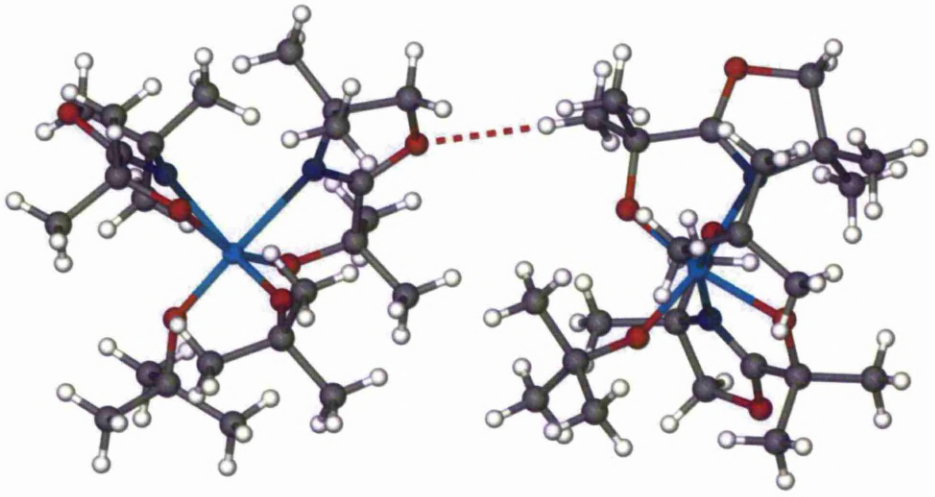

Figure 4. 22: Diagram showing the hydrogen bonding between two complexes of $[Ti(OBu^t)_2(dmop)_2]$.

CHN analysis of the complexes gave values concordant with the material $[Ti(OBu^t)_2(dmop)_2]$ and not the trimer $[Ti_3O_3(dmop)_6]$. This shows that the crystal found in figure 4.20 is not representative of the bulk of the sample but suggests the possibility of decomposition of the heteroleptic complex to the trimer.

Table 4. 4: Elemental Microanalysis for synthesised crystals (actual) and theoretical complexes of Ti with OBu^t and dmop ligands (theo).

	C %	H %	N %
$[Ti(OBu^t)_2(dmop)_2]$ (theo)	56.91	9.15	5.53
$[Ti_3O_3(dmop)_6]$ (theo)	51.07	7.50	7.45
Actual	56.78	8.99	5.41

The ^1H NMR spectrum of the $[Ti(OBu^t)_2(dmop)_2]$ is quite complicated (figure 4.23). Reducing the temperature to 223 K (figure 4.24) causes some of the

peaks to merge. This allows clearer identification of the methyl groups in the complex. There are three distinct peaks where we would expect to see the *tert*-butoxide group methyls and the two different sets of methyls in positions 1 and 3 of the dmop ligand at 1.30, 1.64 and 1.75 ppm respectively.

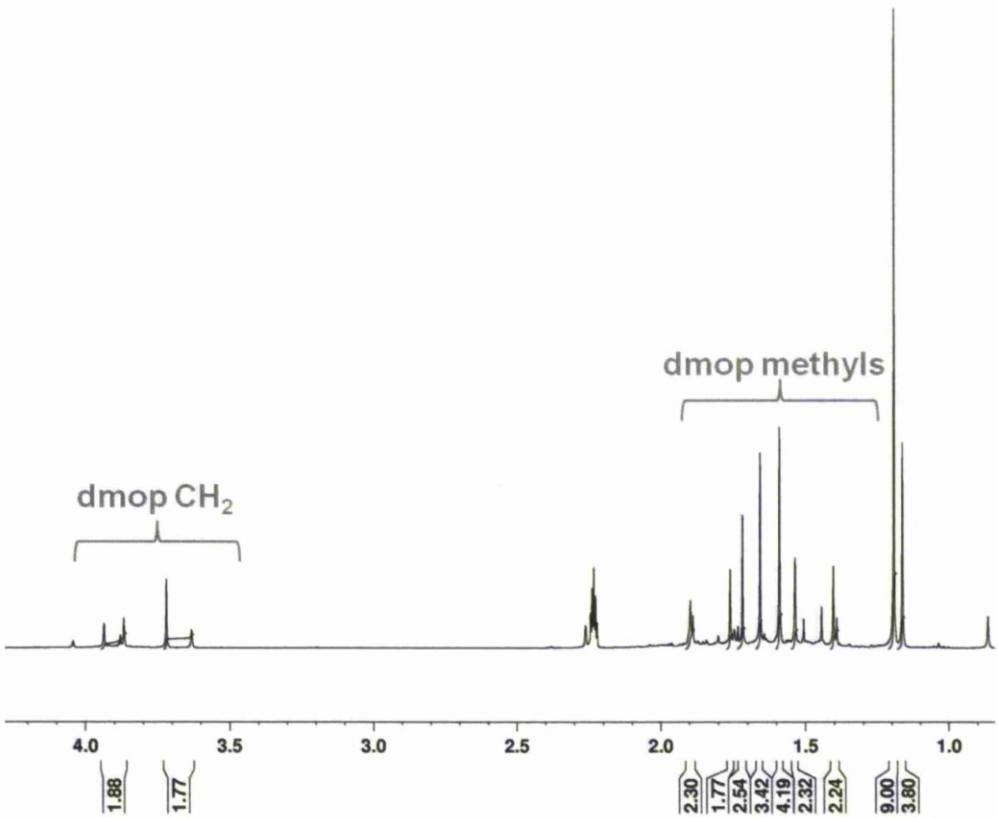

Figure 4. 23: ^{1}H NMR spectrum (C_7D_8) of [Ti(OBu^t)$_2$(dmop)$_2$] at room temperature.

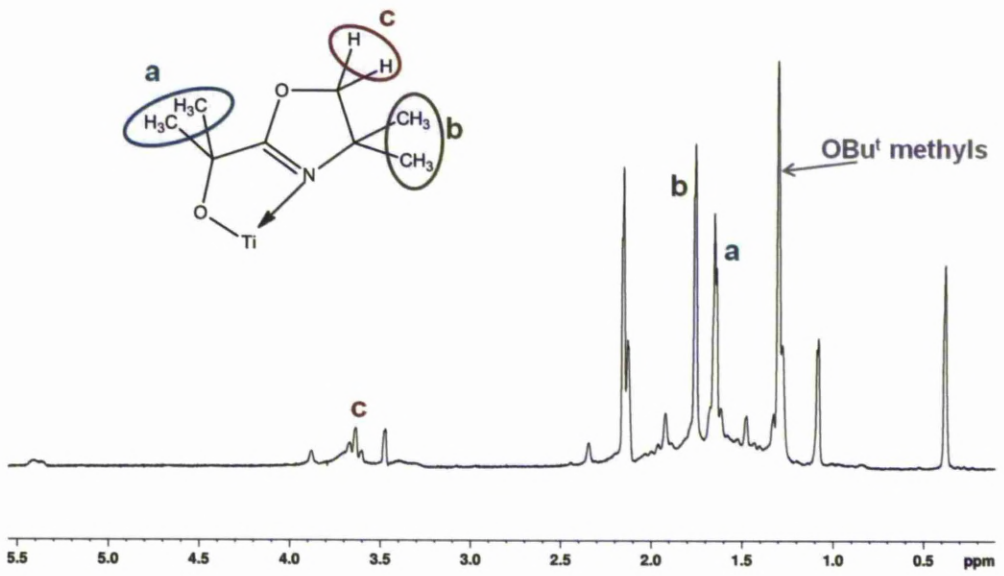

Figure 4. 24: ^{1}H NMR spectrum (C_7D_8) of $[Ti(OBu^t)_2(dmop)_2]$ at 223 K.

4.2.4. Reaction of $[Ti(OPr^i)_4]$ and $[Ti(OBu^t)_4]$ with 2 eq. dmomH.

$[Ti(OPr^i)_2(dmom)_2]$ was synthesised *via* refluxing $[Ti(OPr^i)_4]$ with 2 equivalents of dmomH in toluene for 2 hours. The solution was seen to go from colourless to a light orange. On removal of the volatiles a low-melting point orange solid was formed which solidified around 5 °C. Attempts to crystallise the complex were performed in toluene though no crystal for x-ray characterisation was obtained. The ^{1}H NMR spectrum of the complex (figure 4.25) shows 5 sets of peaks in the ratio 6:6:2:2:1as would be expected for a non-fluxional complex.

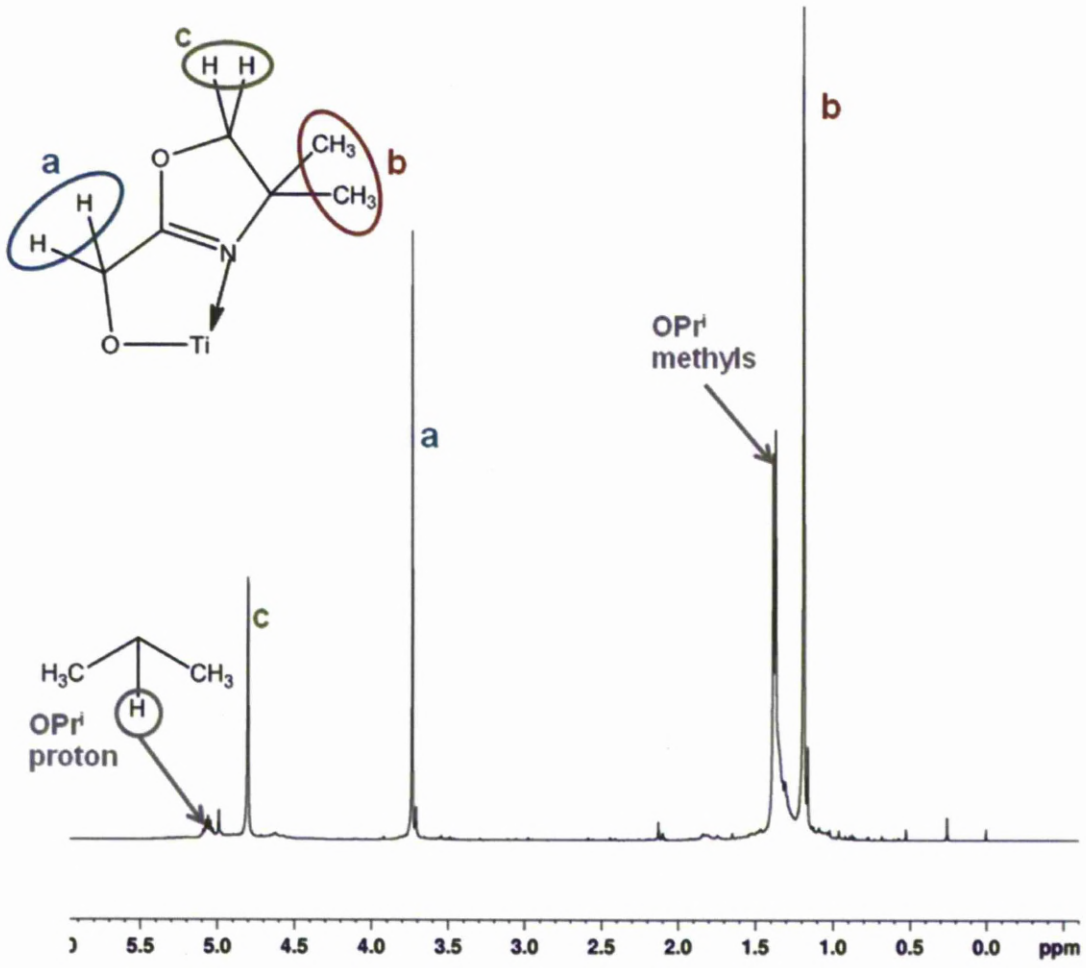

Figure 4. 25:^{1}H NMR spectrum (C_7D_8) of [Ti(OPr^{i})$_2$(dmom)$_2$].

Refluxing 2 equivalents of dmomH with [Ti(OBu^{t})$_4$] in toluene for 2 hours lead to the formation of an orangey oil. The ^{1}H NMR spectrum of the material is shown in figure 4.26.

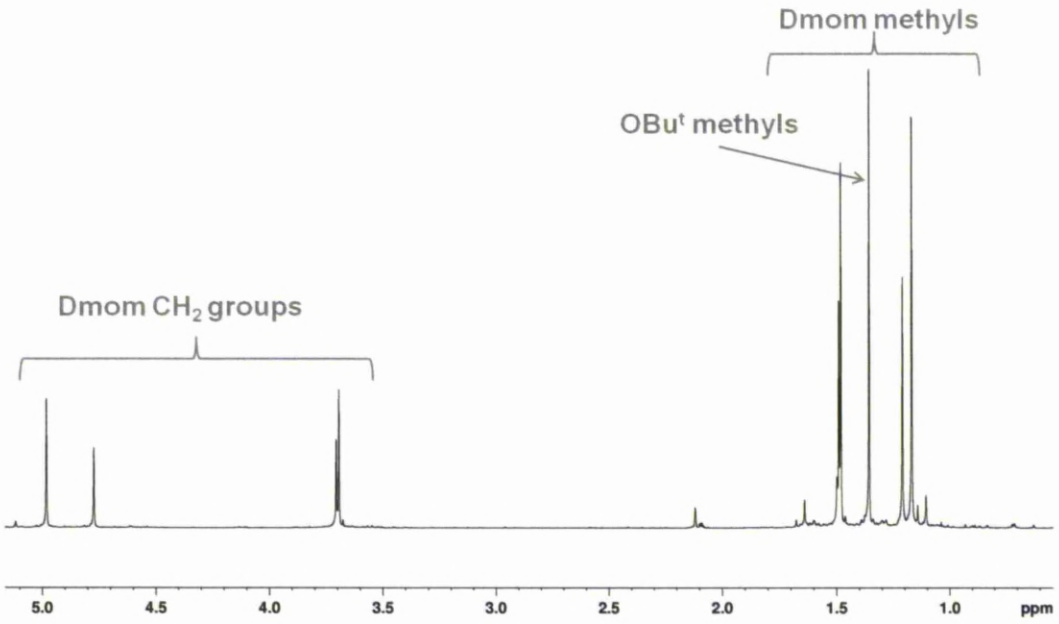

Figure 4. 26: ^{1}H NMR spectrum (C_7D_8) of [Ti(OBu^t)$_2$(dmom)$_2$].

Four peaks would be expected in the ^{1}H NMR spectrum of the monomer in ratios of 9:6:2:2 but seven peaks are visible in the spectrum. Low temperature ^{1}H NMR down to 193 K showed no difference to the spectrum other than slight broadening of the peaks. Analysis by mass spectroscopy gave a peak at 451.23 indicating the $[M+H]^+$ ion of the monomer and CHN analysis gives purity of the monomeric complex within 0.13 % of theoretical values.

There are also more peaks than would be expected in the ^{13}C NMR spectrum. In the region of 170 and 180 ppm there are 4 peaks present which would represent the imine carbon of the dmom ligand. This gives the possibility of there being two isomers present and in each isomer the two dmom ligands exist in differing environments.

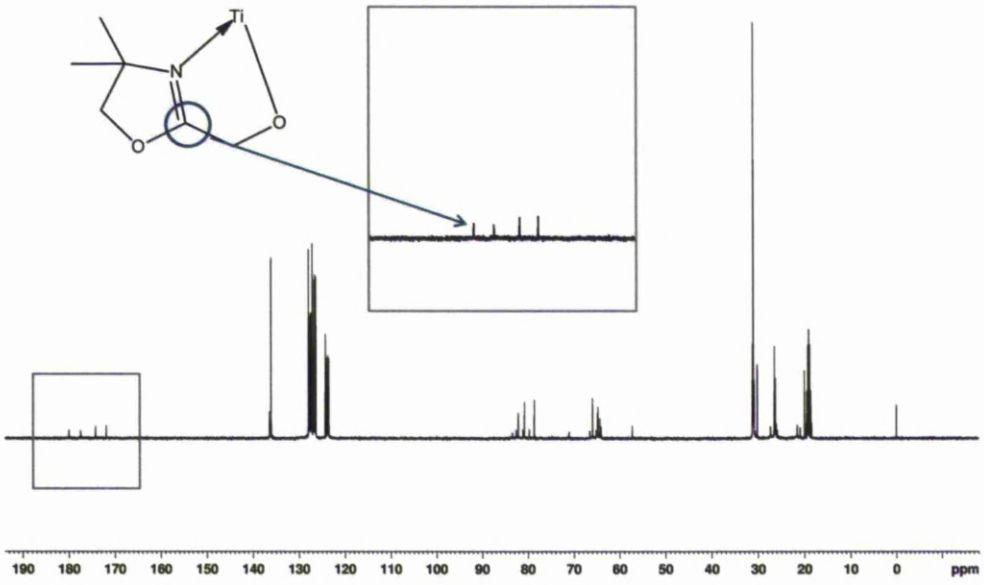

Figure 4. 27: ^{13}C NMR spectrum (C_7D_8) of $[Ti(OBu^t)_2(dmom)_2]$.

4.3. Ti(IV) alkoxides as MOCVD precursors for TiO_2 nanostructures.

(Majority of growth studies performed by Sobia Ashraf,

Department of Engineering Centre for Materials and Structures, University of Liverpool)

4.3.1. Thermogravimetric analysis.

The diagrams in figures 4.28 and 4.29 show the thermogravimetric analysis data for the heteroleptic Ti (IV) complexes and their comparison with $[Ti(OBu^t)_4]$ and $[Ti(OPr^i)_4]$.

4.3.1.1. Complexes containing Isopropoxide.

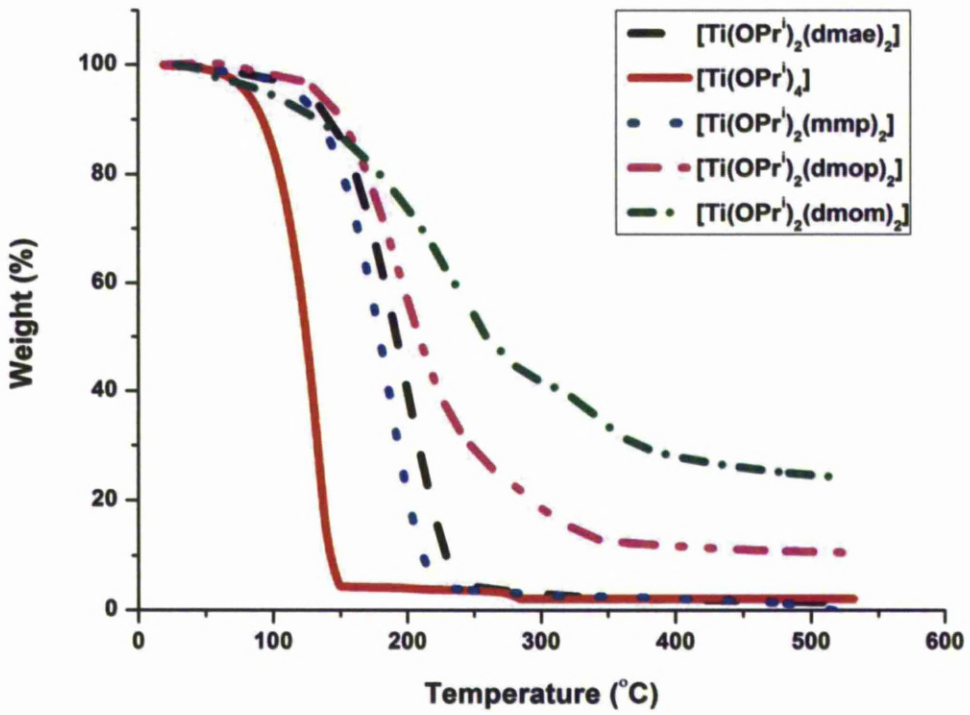

Figure 4. 28: TGA data for the heteroleptic Ti (IV) alkoxide complexes containing the isopropoxide ligand and comparison with the known precursor $[Ti(OPr^i)_4]$. All TGAs were run under the flow of N_2 gas with a heating rate of 10 °C min^{-1}.

$[Ti(OPr^i)_4]$ is clearly the more volatile complex starting to evaporate at ~108 °C its greatest mass loss at ending at ~144 °C leaving behind a 2 % residue. $[Ti(OPr^i)_2(dmae)]_2$ and $[Ti(OPr^i)_2(mmp)_2]$ follow a similar trend though their largest mass loss beings at ~95 °C and finishes at ~230 and 213 °C respectively. Both precursors also result in 0 % residue. $[Ti(OPr^i)_2(dmop)_2]$ shows a more gradual mass loss between temperatures of ~115 °C and 343 °C and leaves a residue of 10.6 % at 530 °C which is equivalent to the mass of Ti. $[Ti(OPr^i)_2(dmom)_2]$ looks to be the worst precursor. It exhibits a gradual mass loss starting from 28 °C up to 260 °C. This is approximately a 50 % weight loss which is then continued slightly more gradually until the endpoint at 531 °C where it leaves a residue of 24.12 %. This is greater than the relative TiO_2 mass percentage (18.91 %)

4.3.1.2. Complexes containing tert-Butoxide.

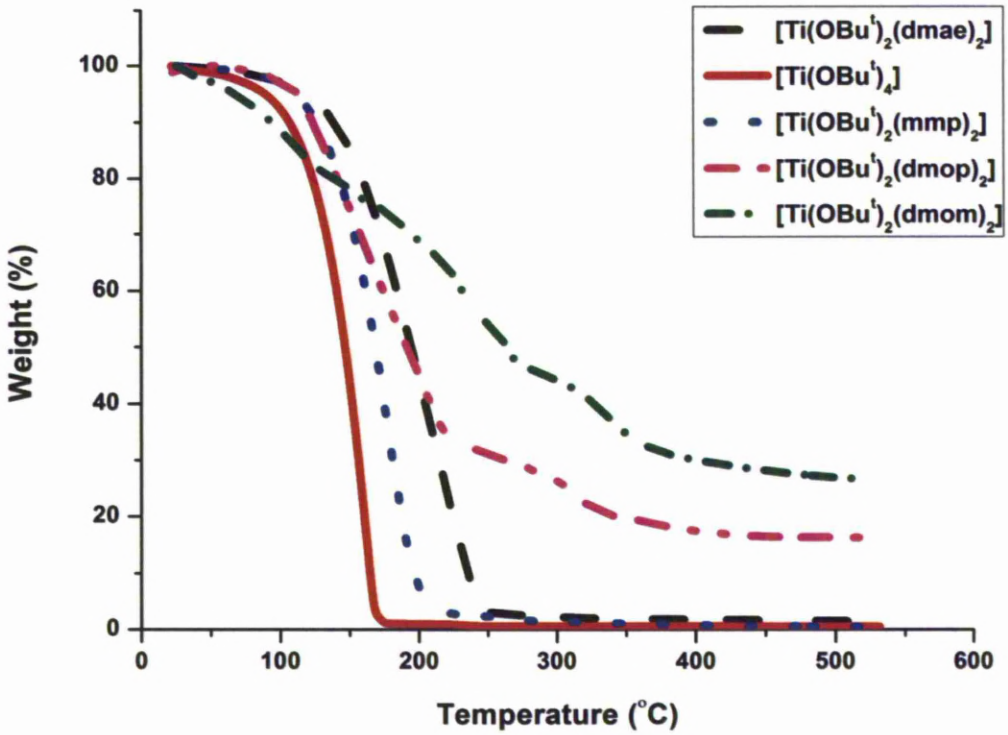

Figure 4. 29: TGA data for the heteroleptic Ti (IV) alkoxide complexes containing the *tert*-butoxide ligand and comparison with the known precursor [Ti(OBu^t)$_4$]. All TGAs were run under the flow of N_2 gas with a heating rate of 10 °C min^{-1}.

The complexes containing the *tert*-butoxide ligand show similar trends in TGA as the complexes with isopropoxide. [Ti(OBu^t)$_4$] achieves its greatest mass loss at 167 °C and leaves behind no residue. [Ti(OBu^t)$_2$(dmae)$_2$] and [Ti(OBu^t)$_2$(mmp)$_2$] exhibit their greatest mass losses at ~ 240 and 200 °C residue respectively and both also leave a 0 % residue. [Ti(OBu^t)$_2$(dmop)$_2$] decomposes gradually across the temperature range leaving a residue of 16.44 % which is equivalent to the mass of TiO_2. The largest mass loss corresponds with the weight of

two dmop ligands. The next two stages are relative to the decomposition of the isopropoxide ligands, first with a mass of ~ 71.0 ($C(CH_3)_3CH_3$) and secondly ~30.4 ($2CH_3$) to leave the resulting TiO_2. $[Ti(OBu^t)_2(dmom)_2]$ results with a residue of 26.52 % which is again greater than the relative TiO_2 mass percentage (17.73 %). Its decomposition is very gradual and similar to that of $[Ti(OPr^i)_2(dmom)_2]$.

4.3.2. Growth Curves.

4.3.2.1. Complexes containing the Isopropoxide Ligand.

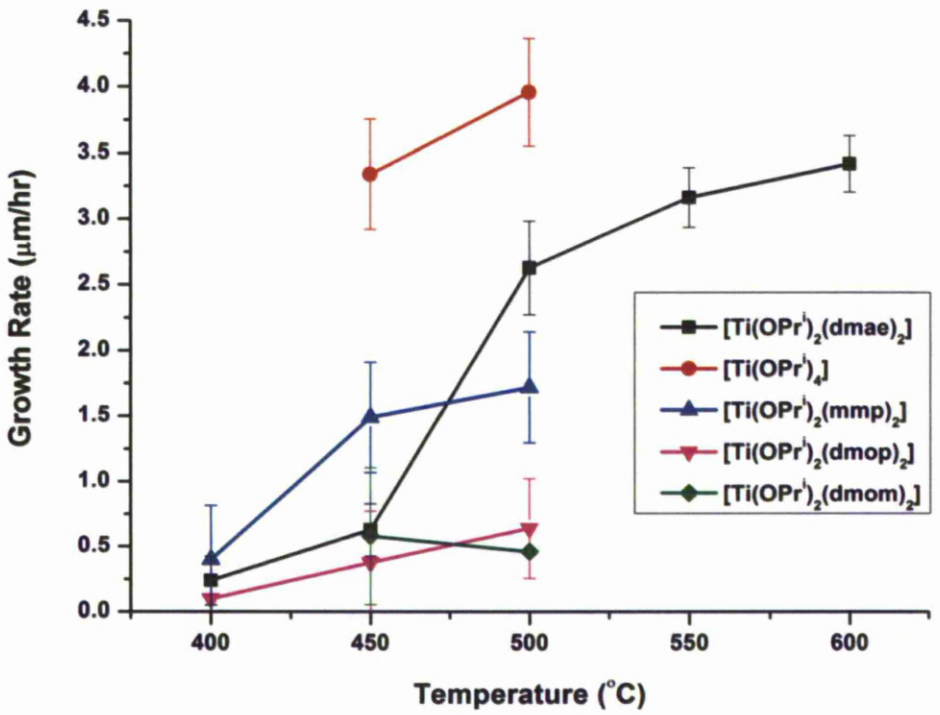

Figure 4. 30: Growth curves for the MOCVD of Ti (IV) alkoxide complexes containing the isopropoxide ligand.

The kinetic region for $[Ti(OPr^i)_4]$ lies at 450-500 °C and exhibits a greater growth rate than the heteroleptic complexes. $[Ti(OPr^i)_2(dmae)_2]$ has a kinetic region from 400-550 °C were it begins to grow films via diffusion control of a fully decomposed precursor. $[Ti(OPr^i)_2(mmp)_2]$ starts diffusion controlled growth at 450 °C with a lower growth rate. $[Ti(OPr^i)_2(dmop)_2]$ shows a poor kinetic region suggesting the complex breaks down very quickly in the reaction chamber causing a small growth rate. There is no difference in growth rate between 450 and 500 °C for $[Ti(OPr^i)_2(dmom)_2]$. This also indicates fast decomposition of the complex possibly before the chamber is reached.

4.3.2.2. Complexes containing tert-Butoxide Ligand.

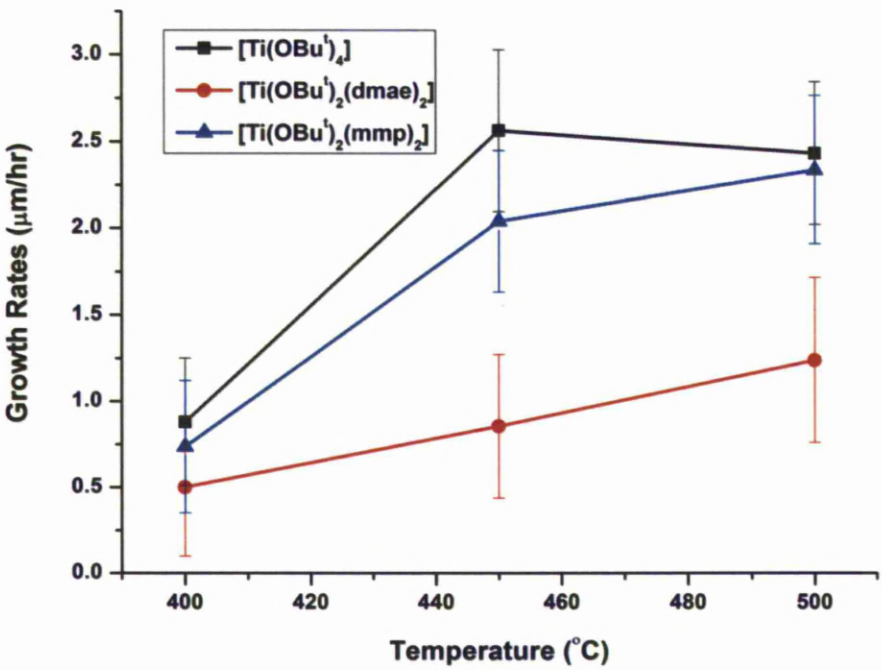

Figure 4. 31: Growth curves for MOCVD of Ti(IV) alkoxide complexes containing the *tert*-butoxide ligand.

$[Ti(OBu^t)_4]$ exhibits a kinetically controlled growth from 400-450 °C. Above 450 °C it begins diffusion controlled growth. $[Ti(OBu^t)_2(dmae)_2]$ and $[Ti(OBu^t)_2(mmp)_2]$ show a similar trend but with a lower growth rate. The complexes $[Ti(OBu^t)_2(dmop)_2]$ and $[Ti(OBu^t)_2(dmom)_2]$ were not used for deposition after seeing the results in the growth curves for $[Ti(OPr^i)_2(dmop)_2]$ and $[Ti(OPr^i)_2(dmom)_2]$.

4.3.3. Growth of TiO_2 Nanostructures.

4.3.3.1. Optimum Parameters.

The purpose of this study was to determine a set of parameters for growing nanostructures of anatase TiO_2 over the substrates of Si(100) and F-doped SnO_2 surfaces via liquid-injection MOCVD. Growth of thin films and structures depends on many differing factors and so three main parameters were looked at: type of precursor, temperature and length of deposition. Table 4.5 shows the general conditions used throughout the study. The precursors were used as single source as growth with O_2 resulted in the deposition of continuous films.

Table 4. 5: Table showing general MOCVD growth conditions.

General MOCVD Growth Conditions	
Solvent	Toluene
Precursor Conc.	0.05 M
Evaporator Temperature	100 °C
Reactor Pressure	1 mbar
Argon Flow Rate	200 cm^3 min^{-1}

The optimum conditions on both substrates were determined by the uniformity and surface coverage of grown nanostructures as well as their resulting phase. These conditions are summarised in table 4.6. $[Ti(OPr^i)_2(dmae)_2]$ gave nanostructures with greater uniformity and coverage compared with any other precursor. The presence of an OPr^i or OBu^t ligand in a precursor had a greater effect on the phase and morphology of the nanostructures grown than the choice of donor-functionalised ligand. Precursors containing a OBu^t ligand grew poor nanostructures and sometimes gave rutile phases whereas those with OPr^i gave exclusively anatase and nanostructures under the majority of conditions.

Table 4. 6: Optimum conditions for the growth of TiO_2 nanostructures on Si(100) and F-doped SnO_2.

Optimum nanostructure growth conditions	
Precursor	$[Ti(OPr^i)_2(dmae)_2]$
Substrate Temperature	450 °C
Length of Deposition	180 mins
Phase obtained	Anatase

A substrate temperature of 450 °C using $[Ti(OPr^i)_2(dmae)_2]$ allows growth in the slower part of the kinetic region (growth curve figure 4.30) with a growth rate of

0.627 μm/hr. The longer deposition time of 180 minutes creates more nucleation sites on the substrate surface resulting in full coverage. These images are shown in figure 4.32.

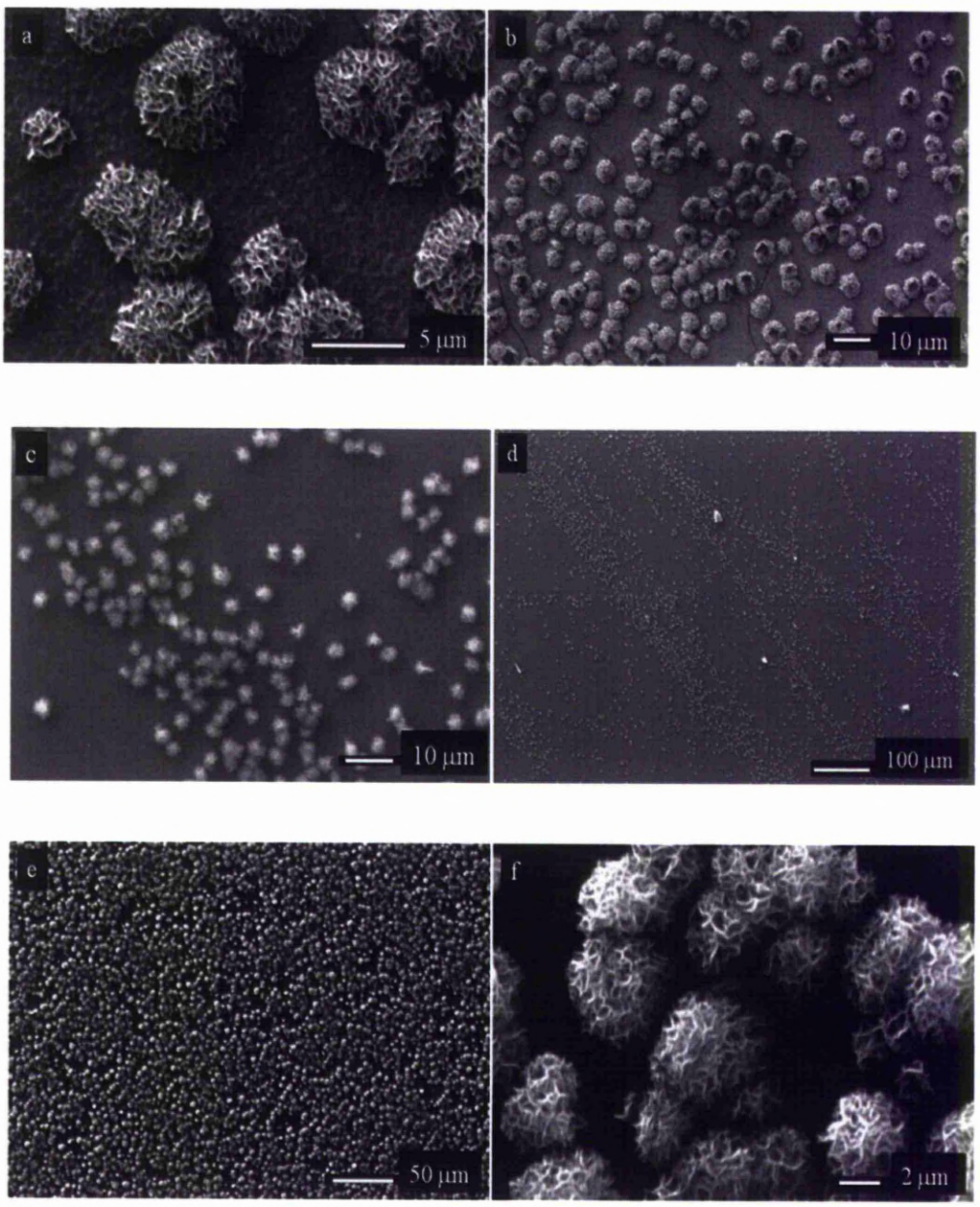

Figure 4. 32: SEM images of growth using 0.05 M $[Ti(OPr^i)_2(dmae)_2]$ in toluene at 450 °C on Si(100) a) and b) 180mins and on F-doped SnO_2 for c) and d) 120 mins, e) and f) 180 mins.

4.3.3.2. Growth of nanostructures with other precursors

As shown by table 4.7 $[Ti(OPr^i)_4]$, $[Ti(OBu^t)_4]$ and six of the heteroleptic Ti(IV) alkoxides were used to grow nanostructures of TiO_2 on F-doped SnO_2 and Si(100). All compounds showed some nanostructure growth under different parameters apart from $[Ti(OBu^t)_2(mmp)_2]$ which only grew continuous films. There are fewer instances of nanostructure growth on Si(100) compared to F-doped SnO_2 and compounds containing the OBu^t grew more continuous films.

Table 4. 7: Experiments tried for anatase TiO_2 nanostructure growth on F-doped SnO_2 and Si(100) surfaces. A = anatase, R = rutile, M = mixed.

Precursor	Temperature (°C)	Time (mins)	Nanostructure Growth		Phase
			SnO_2	Si(100)	
$[Ti(OPr^i)_4]$	500	35	-	-	A
		60	Yes	Yes	A
		90	-	-	A
		180	-	-	A
	450	35	Yes	-	A
$[Ti(OBu^t)_4]$	500	35	-	-	R
	450	35	-	-	R
	400	35	Yes	-	A
		90	Yes	Yes	A
$[Ti(OPr^i)_2(dmae)_2]$	500	35	Yes	-	A
	450	35	Yes	-	A
		120	Yes	-	A
		180	Yes	Yes	A
$[Ti(OBu^t)_2(dmae)_2]$	500	35	-	-	R
	450	35	-	-	R
	400	70	Yes	Yes	A
	350	35	-	-	A
		70	-	-	A
$[Ti(OPr^i)_2(mmp)_2]$	600	35	-	-	A
	550	35	-	-	A
	500	35	Yes	-	A
		120	Yes	-	A
		180	Yes	-	A
		240	-	-	A
	450	35	-	-	A
$[Ti(OBu^t)_2(mmp)_2]$	500	35	-	-	R
	450	35	-	-	M
	400	70	-	-	M
$[Ti(OPr^i)_2(dmop)_2]$	500	35	Yes	Yes	A
	450	35	-	-	A
	400	35	-	-	A
$[Ti(OPr^i)_2(dmom)_2]$	500	35	Yes	-	A
		180	-	-	A
	450	70	-	-	A

4.3.3.2.1. Precursors containing the Isopropoxide Ligand.

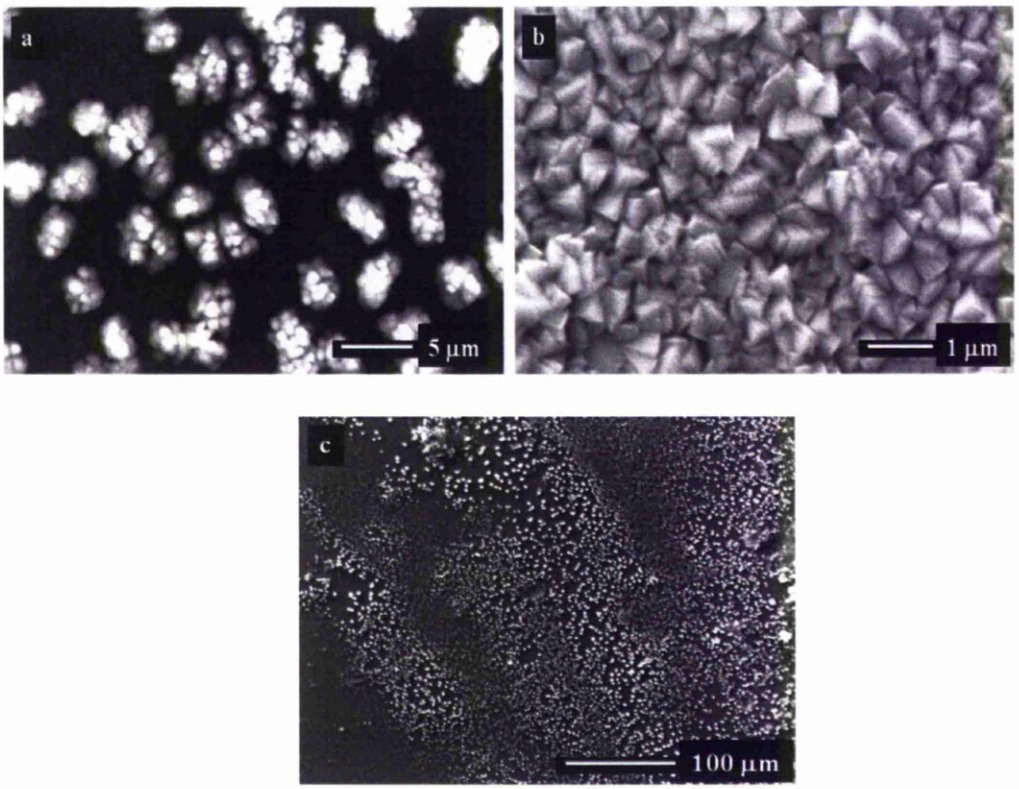

Figure 4. 33: SEM images of TiO_2 nanostructures grown using 0.05 M [$Ti(OPr^i)_4$] in toluene at 500 °C for a) 60 mins and b) 90 mins on F-doped SnO_2 and c) 60 mins on Si(100).

[$Ti(OPr^i)_4$] grew globular structures on F-doped SnO_2 at 500 °C for 60 minutes). Increasing to 90 minutes caused the structures to coalesce forming a film of rigid structures. This is most likely due to its high growth rate at this temperature (4 μm/hr) when compared to [$Ti(OPr^i)_2(dmae)_2$] at 500 °C = 2.6 μm/hr) where nanostructures still grew but in less abundance than at 450 °C. [$Ti(OPr^i)_4$] showed potential for growth on Si(100) surface but only produced structures at the edge of the substrate at 500 °C for 60 minutes.

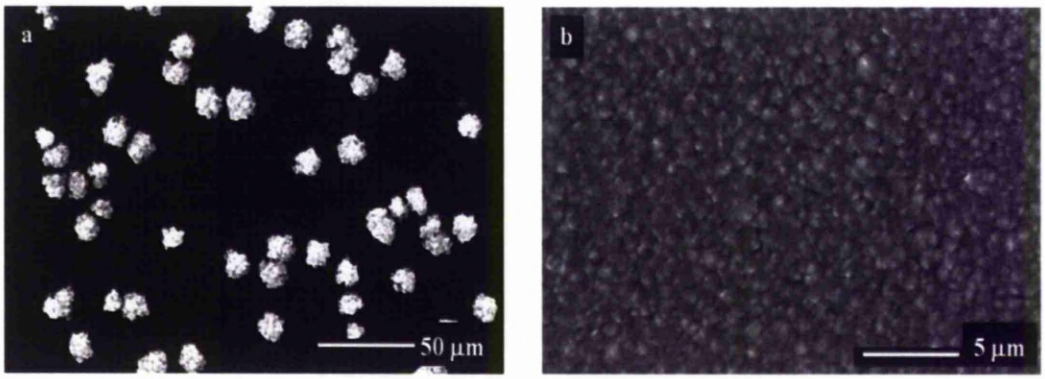

Figure 4. 34: SEM images of TiO_2 films using 0.05 M $[Ti(OPr^i)_2(mmp)_2]$ in toluene for 35 mins at 500 °C b) 180mins, c) 240 mins on F-doped SnO_2

$[Ti(OPr^i)_2(mmp)_2]$ also demonstrated nanostructure growth at 500 °C though it required longer deposition times of 180 minutes and the coverage was not as uniform as for $[Ti(OPr^i)_2(dmae)_2]$. In an attempt to increase their coverage the deposition length was increased to 240 minutes though this resulted in a thin film (figure 4.34b).

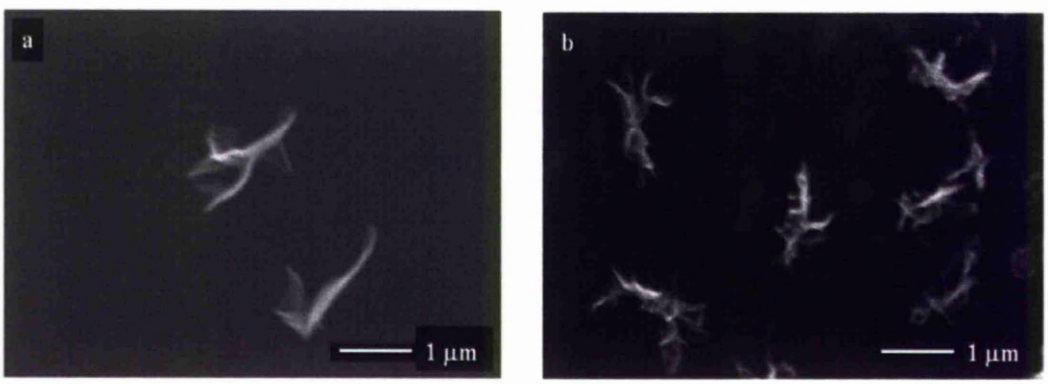

Figure 4. 35: SEM images of nanostructures grown at 500 °C for 35 mins using 0.05 M solution in toluene of a) $[Ti(OPr^i)_2(dmop)_2]$ and b) $[Ti(OPr^i)_2(dmom)_2]$ on F-doped SnO_2.

$[Ti(OPr^i)_2(dmop)_2]$ and $[Ti(OPr^i)_2(dmom)_2]$ both grew thin films of TiO_2 under most conditions only producing poor structures at 500 °C for 35 minutes. At this temperature the growth are similar to that of $[Ti(OPr^i)_2(dmae)_2]$ at its optimum nanostructure growth (0.64 and 0.46 μm/hr respectively). The dmop and dmom ligands therefore decompose by a mechanism that hinders nanostructure growth.

4.3.3.2.2. Precursors with tert-butoxide ligands

$[Ti(OBu^t)_4]$, much like $[Ti(OPr^i)_4]$, created more globular nanostructures on both substrates though these were smaller and with less defined structures. The precursor was more successful with growth on the Si(100) substrate than F-doped SnO_2.

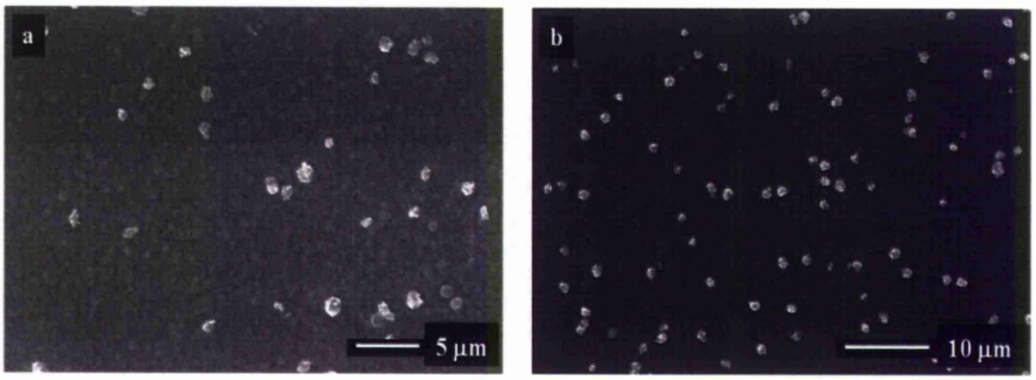

Figure 4. 36: SEM images of TiO_2 nanostructures grown using 0.05 M $[Ti(OBu^t)_4]$ in toluene at 400 °C for 90 mins on a) F-doped SnO_2 and b) Si(100)

$[Ti(OBu^t)_2(dmae)_2]$ grew nanostructures at 400 °C, again towards the slower kinetic region with a growth rate similar to those grown with $[Ti(OPr^i)_2(dmae)_2]$ at

450 °C. [Ti(OBu^t)$_2$(dmae)$_2$] grew less defined structures on both substrates though covered the surface as seen in figure 4.37d.

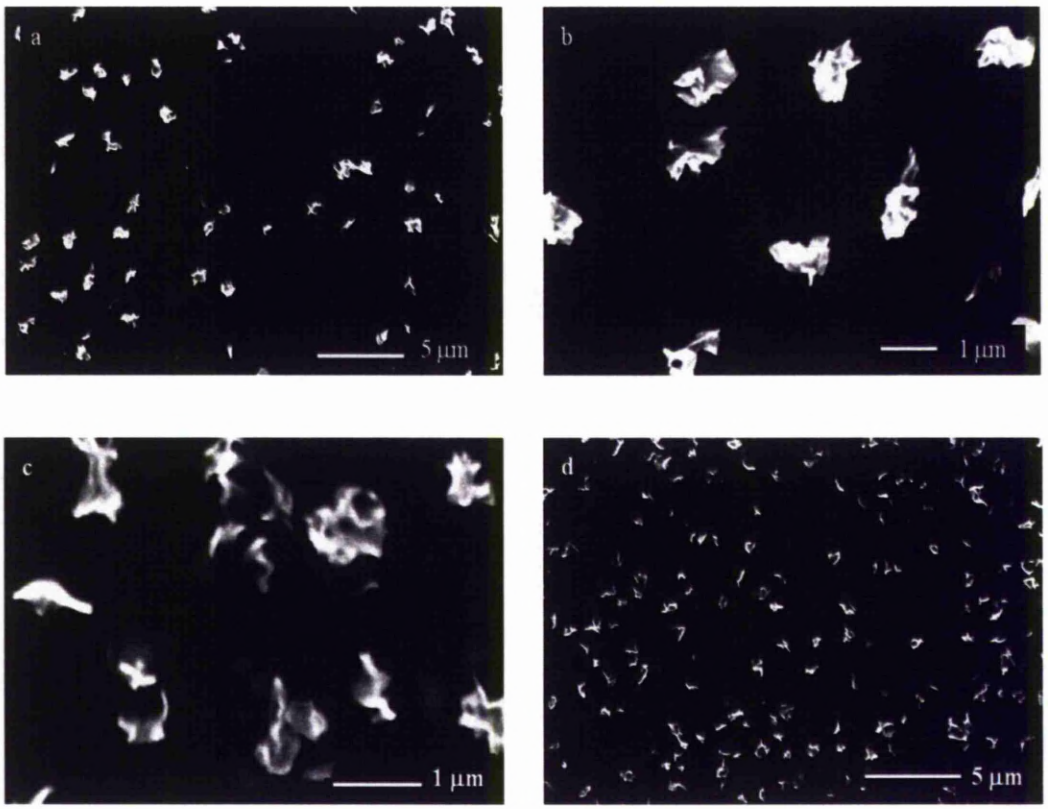

Figure 4. 37: SEM images of TiO_2 nanostructures grown using 0.05 M [Ti(OBu^t)$_2$(dmae)$_2$] in toluene at 400 °C for 70 mins on a),b) Si(100) and c),d) F-doped SnO_2.

4.3.3.3. Nanorod growth with [Ti(OPr^i)$_2$(dmae)$_2$].

Anatase and rutile nanorods of TiO_2 have been grown previously using MOCVD and generally have coarser surfaces than those shown here. All appear to grow at higher temperatures of deposition using precursors such as titanium acetylacetonate on glass at 560 °C (anatase) and 630 °C (anatase and rutile).[70] Most TiO_2 nanorods have been grown by methods like sol-gel processes.[113,114] Structures

like these have attracted great interest in superhydrophobicity studies.[115] With further investigation, deposition with $[Ti(OPr^i)_2(dmae)_2]$ at higher temperatures could be tuned to create more uniform nanorods on different substrates.

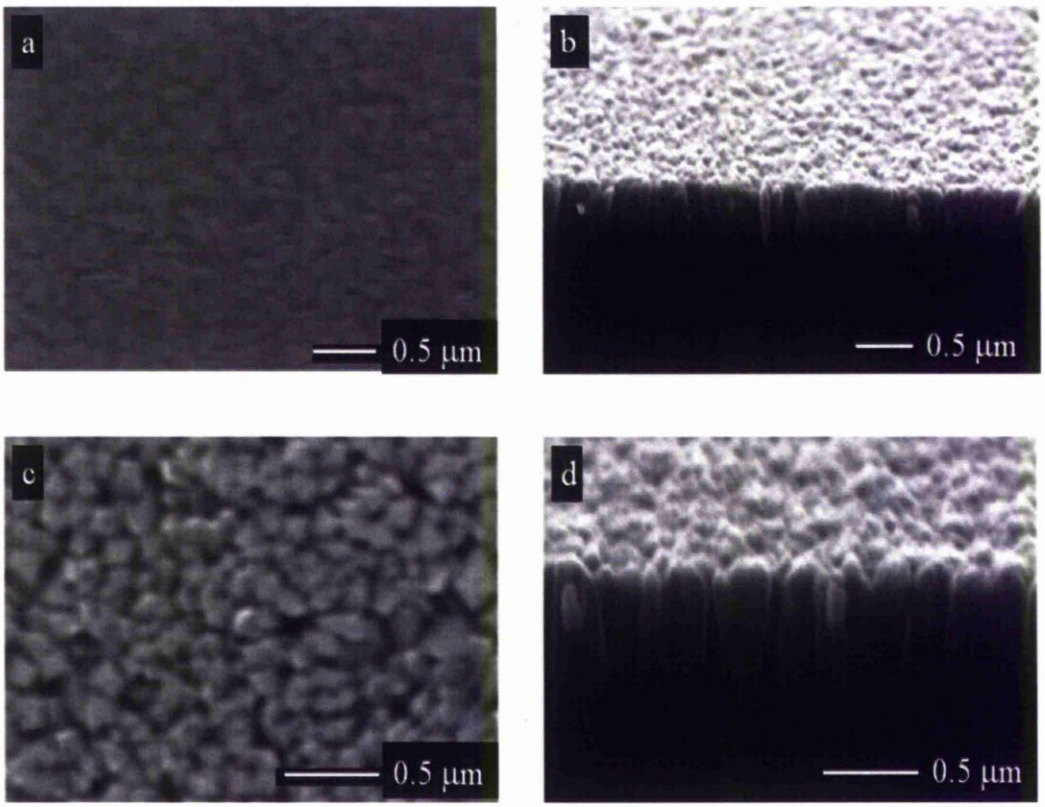

Figure 4. 38: SEM images of growth using 0.05M $[Ti(OPr^i)_2(dmae)_2]$ in toluene for 35 mins on Si(100) a) 550 °C, b) 550 °C cross section, c) 600 °C, d) 600 °C cross section

4.3.3.4. Film Phases.

The phases of the films were determined by Raman spectroscopy. All precursors gave the same phases on both substrates. As recorded in table 4.7 the majority of films are anatase (figure 4.39). The only cases of rutile present were observed when using a precursor containing the *tert*-butoxide ligand at temperatures

above 450 °C (figure 4.40). Thus it can be deduced that the phase obtained has a first-order dependence on the type of precursor used and second-order dependence on the temperature.

The determining ligands in phase formation are the mondentate isopropoxide and *tert*-butoxide. Evans et al[93] attributed the film growth rate to be the critical factor in determining the phase of TiO_2 formed. Precursors like $[Ti(OPr^i)_4]$ that have fast growth rates favour the formation of anatase phases whereas slower growth precursors, such as $TiCl_4$ and ethyl acetate, deposit rutile. Whilst this observation held for the homoleptic complexes studied here, the heteroleptic complexes studied all had lower growth rates than the rutile forming $[Ti(OBu^t)_4]$ yet still formed anatase phases. Thus the monodentate ligand is the determining factor for phase formation since only $[Ti(OBu^t)_4]$, $[Ti(OBu^t)_2(dmae)_2]$ and $[Ti(OBu^t)_2(mmp)_2]$ gave rutile or mixed phase TiO_2 films.

All nanostructures grown had the anatase phase which is concordant with the majority of reports detailing these types of structure. It has been reported that the rate of anatase to rutile phase transformation is dependent on the initial anatase crystal size.[84,87] The smaller the crystals of anatase, the more resistant to conversion to rutile they are. At very small particle sizes (< 14 nm) anatase may be considered thermodynamically stable.[86,116] The different precursors in this study may produce varying crystallite sizes which would hence determine the TiO_2 phase.

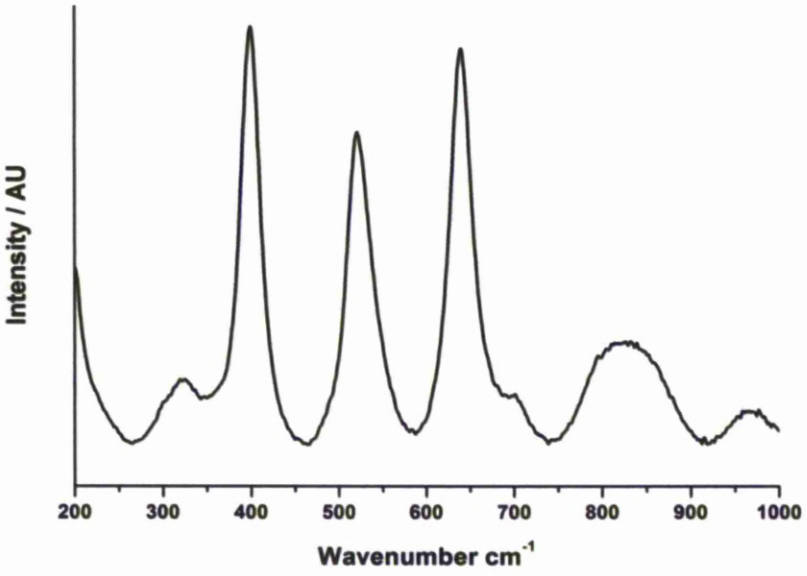

Figure 4. 39: Example of Raman data for anatase phase TiO_2 films (spectrum of film grown at 550 °C using $[Ti(OPr^i)_2(dmae)_2]$).

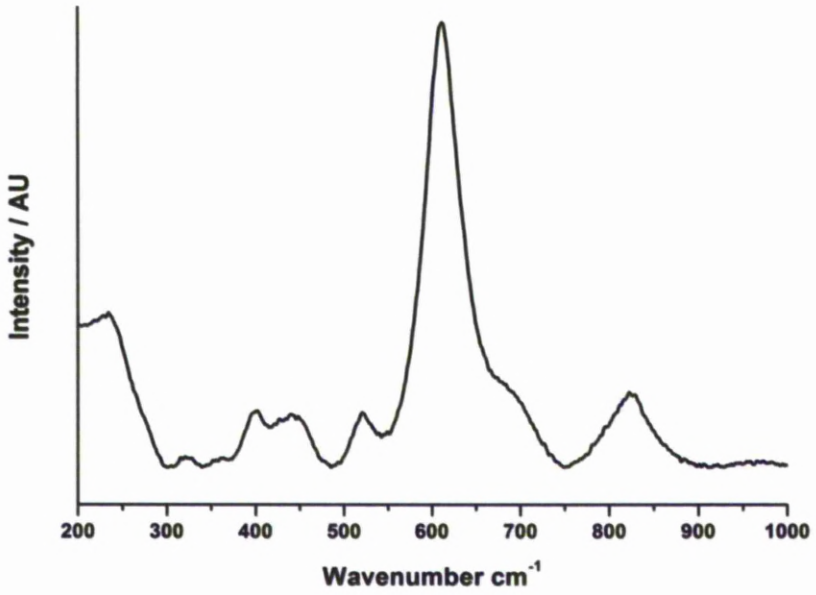

Figure 4. 40: Example of Raman data for rutile phase TiO_2 films (spectrum of film grown at 500 °C using $[Ti(OBu^t)_2(dmae)_2]$).

4.4. Conclusion.

A series of Ti(IV) alkoxide complexes with the monodentate ligands OBu^t and OPr^i and the bidentate ligands dmae, mmp, dmop and dmom have been synthesised. $[Ti(OPr^i)_2(dmop)_2]$ and $[Ti(OBu^t)_2(dmop)_2]$ were characterised crystallography.

These complexes were tested for their use as precursors for the growth of TiO_2 nanostructures on Si(100) and F-doped SnO_2 substrates. $[Ti(OPri)_2(dmae)_2]$ was found to be the best precursor for the growth of uniform films of TiO_2 nanostructures on both substrates at 450 °C. The discovery of nanorods using this precursor at 600 °C on Si(100) should be investigated further.

Chapter 5. Experimental.

5.1. General Experimental Procedures.

$[Ti(OPr^i)_4]$, $[Ti(OBu^t)_4]$, mmpH and dmaeH were provided by SAFC Hitech and used without further purification. All manipulations of air and moisture sensitive compounds were carried out under a dry, oxygen free atmosphere of dinitrogen using standard Schlenk techniques. Toluene, DME, THF and diethyl ether were distilled from sodium benzophenone ketyl. Hexane, petroleum ether and isopropanol were distilled over calcium hydride. All deuterated solvents were distilled under reduced pressure from calcium hydride. All solvents were stored under dinitrogen over 4 Å molecular sieves.

MmpH, dmaeH, dmompH, dmapH and Nujol were degassed three times using the freeze/pump/thaw method and then stored under nitrogen over 4 Å molecular sieves.

Solutions of dmopH and dmomH in toluene were dried over activated sieves.

NMR Spectroscopy

All room temperature NMR spectra were recorded on a Bruker Avance 400. Variable Temperature NMR experiments were ran on a Bruker DPX400 spectrometer. Samples were prepared under nitrogen in dry deuterated solvent. NMR samples were prepared in either a nitrogen filled dry box with a tube cap sealed in

parafilm or an NMR tube fitted with a Young's tap. The tube was flame sealed before analysis. All chemical shifts are reported in p.p.m relative to tetramethylsilane as an internal standard.

Elemental Analysis

Elemental Analysis was carried out by Mr S. Apter and Mr G. Miller of the University of Liverpool. Analysis of moisture sensitive complexes was carried out by Mr S. Boyer of the London Metropolitan University. Compounds were flame sealed in ampoules for delivery.

Mass Spectrometry

Mass Spectrometry on air stable samples was carried out by Miss M. McCarron and Mrs J. Ellis using a Micromass LCT Mass Spectrometer or a Trio 1000 Spectrometer. Mass Spectrometry on air sensitive samples was carried out via the EPSRC Mass Spectrometry service in Swansea.

X-Ray Crystallography

Crystallographic data was collected by mounting a crystal in nujol on a glass fibre and placing in a cold stream at 100K. Single crystal X-ray data were collected on a Bruker APEX diffractometer, with 1.5 kW graphite monochromated Mo radiation.

Scanning Electron Microscopy (SEM)

SEM images were acquired on a JEOL 6619 instrument at an acceleration voltage of 30 kV.

Raman Spectroscopy

Raman spectra were acquired using a Jobin-Yvon LabRam HR consisting of a confocal microscope coupled to a single grating spectrometer equipped with a notch filter and a CCD camera detector.

5.2. Crystal Structure Data.

Table 5. 1: Table showing crystallography data for the complexes $[Ce(mmp)_4]$, $[Ce(dmap)_4]$, $[Ce(dmop)_4].C_7H_8$ and $[Ce_2(mmp)_2(dmop)_4O].C_7H_8$.

	$[Ce(mmp)_4]$	$[Ce(dmap)_4]$	$[Ce(dmop)_4].C_7H_8$	$[Ce_2(mmp)_2(dmop)_4O].C_7H_8$
Habit	prism	prism	prism	
Size/mm	0.20 x 0.20 x 0.10	0.15 x 0.14 x 0.13	0.4 x 0.3 x 0.2	0.4 x 0.3 x 0.2
Formula	$C_{20}H_{44}CeO_8$	$C_{20}H_{48}CeN_4O_4$	$C_{39}H_{64}CeN_4O_8$	$C_{49}H_{86}Ce_2N_4O_{13}$
Formula weight	552.67	548.74	857.06	1219.46
Space group	P2/c	$P6_122$	$P2_1/c$	$P2_1$
a, Å	15.489(3)	9.8993(3)	11.514(5)	10.791(3)
b, Å	9.3685(15)	9.8993(3)	12.546(6)	18.425(5)
c, Å	20.001(3)	46.8411(16)	29.583(13)	14.533(4)
a, deg	90	90	90	90
b, deg	120.906(10)	90	96.245(8)	99.530(4)
g, deg	90	120	90	90
Volume, Å^3	2490.22	3975.3(2)	4248(3)	2849.6(14)
Z	4	6	4	2
r_{calc}, **g cm^{-3}**	1.474	1.375	1.34	1.421
F_{000}	1144	1716	1792	1256
R, %	5.13	2.4	2.15	3.24
Goodness of fit	0.966	1.335	1.069	1.057

Table 5. 2: Table showing crystallography data for the complexes $[Ce_3(OBu^t)(ONep)_9O]$, $[Ti(OPr^i)_2(dmop)_2]$ and $[Ti(OBu^t)_2(dmop)_2]$.

	$[Ce_3(OBu^t)(ONep)_9O]$	$[Ti(OPr^i)_2(dmop)_2]$	$[Ti(OBu^t)_2(dmop)_2]$
Habit		Prism	Prism
Size/mm	0.12 x 0.05 x 0.04	0.22 x 0.21 x 0.08	0.30 x 0.26 x 0.14
Formula	$C_{73}H_{152}Ce_3O_{11}$	$C_{22}H_{42}TiN_2O_6$	$C_{24}H_{46}TiN_2O_6$
Formula weight	1626.31	478.48	506.53
Space group	P-3c1	$P2_1/n$	C2/c
a, Å	19.0918(17)	8.7584(12)	31.322(4)
b, Å	19.0918(17)	16.645(2)	16.424(2)
c, Å	23.342(2)	17.695(2)	19.594(2)
a, deg	90	90	90
b, deg	90	95.853(2)	123.598(2)
g, deg	120	90	90
Volume, Å^3	7368.2(11)	2566.2(10)	8395.9(17)
Z	4	4	12
r_{calc}, g cm^{-3}	1.466	1.238	1.202
F_{000}	3408	1032	3288
R, %	4.74	3.61	6.54
Goodness of fit	0.969	1.038	1.032

5.3. Organic Ligand Preparation

Preparation of 2-(4,4-dimethyl-4,5-dihydro-oxazol-2-yl)-propan-2-ol (dmopH).[45]

2-amino-2-methyl-1-propanol (17.12 g, 0.192 mol) was added to a mixture of hydroxyisobutyric acid (20g, 0.192 mol) in toluene (200 ml). The flask was fitted with a Dean Stark trap and the reaction mixture heated to reflux for 96 hours. 6.5 ml of H_2O was produced and 100 ml toluene was distilled off from the reaction mixture. Xylene (50 ml) was added and heating to reflux was continued for a further 2 days producing another 3 ml of H_2O. The xylene was distilled through a column packed

with glass sieves to give a yellow oil. DmopH was obtained as white acicular crystals by Kugelrohr distillation at 100 °C (6.0 torr) (6.3 g, 20.8 % yield).

^{1}H NMR ($CDCl_3$): δ(ppm): 1.29 [s, 6H, $(C\boldsymbol{H}_3)_2CN$)], 1.45 [s, 6H, $OC(C\boldsymbol{H}_3)_2CO$], 4.03 [s, 2H, $OC\boldsymbol{H}_2C(CH_3)_2$]

Mass Spectrometry CI: Mass Found [M+H] 158.2; Theoretical Mass [$C_8H_{15}NO_2$ + H] 158.12

Preparation of 2-(4,4-dimethyl-4,5-dihydro-oxazol-2-yl)-methanol (dmomH).

2-amino-2-methyl-1-propanol (23.4 g, 0.263 mol) was added to a mixture of glycolic acid (20g, 0.263 mol) in toluene (200 ml). The flask was fitted with a Dean Stark trap and the reaction mixture heated to reflux for 96 hours. 6.5 ml of H_2O was produced and 100 ml toluene was distilled off from the reaction mixture. Xylene (50 ml) was added and heating to reflux was continued for a further 2 days producing another 3 ml of H_2O. The xylene was distilled through a column packed with glass sieves to give a dark yellow oil. DmomH was obtained as a low melting solid by Kugelrohr distillation at 120 °C (6.0 torr), (10.5 g, 30.8 % yield).

^{1}H NMR ($CDCl_3$): δ(ppm): 1.30 [s, 6H, $(C\boldsymbol{H}_3)_2CN$)], 4.02 [s, 2H, $(OC\boldsymbol{H}_2CO)$], 4.23 [s, 2H, $OC\boldsymbol{H}_2C(CH_3)_2$]

Mass Spectrometry CI: Mass Found [M+H] 130.2; Theoretical Mass [$C_6H_{11}NO_2$ + H] 130.08

Preparation of 2-methyl-6-(4-methyl-4,5-dihydrooxazol-2-yl)phenol (dmompH).[51]

$ZnCl_2$ (256 mg, 1.88 mmol) was heated under vacuum for 20 mins. Chlorobenzene (100 ml) was added under N_2 with stirring. 2-hydroxy-3-methylbenzonitrile (5 g, 37.55 mmol) was added followed by 2-amino-2-methyl-1-propanol (5.02 g, 56.33 mmol). The mixture was heated to reflux for 24 hours followed by the removal of volatiles *in vacuo*. The residue was dissolved in DCM and the organic layer washed with water (3 x 100 ml). The water layers were extracted with DCM (50 ml) and the organic phase dried over $MgSO_4$. The solvent was removed *in vacuo* and the resulting brown oil purified by flash chromatography using an eluent of DCM:MeOH (10:1). This gave dmompH as a yellow oil (3.2 g, 36.4 % yield).

^{1}H NMR ($CDCl_3$): δ(ppm): 1.38 [s, 6H, $(C\boldsymbol{H}_3)_2CN$], 2.33 [s, 3H, $C\boldsymbol{H}_3C_6H_3OH$], 4.07 [s, 2H, $OC\boldsymbol{H}_2C(CH_3)_2$], 6.68 [d, 1H, $C_6\boldsymbol{H}_3$], 6.81 [s, 1H, $C_6\boldsymbol{H}_3$]. 7.50 [d, 1H, $C_6\boldsymbol{H}_3$]

Mass Spectrometry CI: Mass Found [M+H] 206.1; Theoretical Mass [$C_{12}H_{15}NO_2$ + H] 206.11

5.4. Ce(IV) Homoleptic Complexes.

Preparation of [Ce(mmp)$_4$].

A solution of $[NH_4]_2[Ce(NO_3)_6]$ (10 g, 18.24 mmol) in dimethoxyethane (DME) (77 mL) was added at room temperature to a stirred solution of $NaOBu^t$ (10.52 g, 109.45 mmol) in DME. After removal of the $NaNO_3$ precipitate, the filtrate was stirred at 0 °C and mmpH (8.52 mL, 72.96 mol) was added. The reaction mixture was heated under reflux for 1 hour, and then left to cool to room temperature. Volatiles were removed *in vacuo*, and the resulting yellow oil was extracted with hexane (3 x 100 mL), which was then concentrated to give the product as yellow crystals on cooling to -18 °C. (5.24 g, 52 % yield). Melting Point: 105–106 °C (0.8 Torr).

^{1}H NMR (C_7D_8): δ(ppm): 1.27 [s, 6H, $OC(C\boldsymbol{H}_3)_2CH_2OCH_3$], 3.60 [s, 2H, $OC(CH_3)_2C\boldsymbol{H}_2OCH_3$], 3.49 [s, 3H, $OC(CH_3)_2CH_2O\boldsymbol{C}H_3$].

^{13}C NMR (C_7D_8): δ(ppm): 26.9 [$OC(\boldsymbol{C}H_3)_2CH_2OCH_3$], 58.2 [$OC(CH_3)_2CH_2O\boldsymbol{C}H_3$], 75.0 [$O\boldsymbol{C}(CH_3)_2CH_2OCH_3$], 84.1 [$OC(CH_3)_2\boldsymbol{C}H_2OCH_3$].

Elemental Microanalysis: calcd. for $CeC_{20}H_{44}O_8$: C, 43.46 ; H, 8.02 %; found: C, 42.58; H, 7.88 %.

Synthesis of [Ce(mmp)$_4$] via [Ce$_2$(OPr^i)$_8$(HOPr^i)$_2$].

2-propanol (0.84 ml, 10.94 mmol) was added to a stirred suspension of NaH (262 mg, 10.94 mmol) in DME (30 ml) at room temperature and the mixture stirred for 1 hour until the effervescence has stopped. A solution of $[NH_4]_2[Ce(NO_3)_6]$ (1 g, 1.82 mmol) in DME (20 ml) and 2-propanol (2 ml) was added *via* cannula and the reaction stirred at room temperature for 2 hours. The $NaNO_3$ precipitate was filtered off and mmpH (0.85 ml, 7.28 mmol) was added with stirring. The yellow mixture was refluxed for 2 hours and left to stir overnight at room temperature. The volatiles were removed *in vacuo* and the crude mixture dissolved in toluene and left at -18 °C to yield [Ce(mmp)$_4$] as yellow crystals (230 mg, 22.9 % yield).

Preparation of [Ce(thd)$_4$].[52]

Schlenk techniques were not required for this preparation. thdH (29ml, 138mmol) was mixed in a 95% ethanol: water solution (150ml) with 4M NaOH (35ml). This was added dropwise to a stirring solution of $CeCl_3.7H_2O$ (14.8g, 39.74mmol) in 1:1 ethanol: water solution (150ml). There was an immediate colour change from colourless to red on the addition of the thdH mixture. After all ligand was added a solution containing a dark red precipitate was formed and left to stir covered at room temperature overnight. The solution was filtered under suction to give a pale red/brown powder. This was dissolved in DCM and the solution was filtered. Volatiles were removed from the filtrate to give [Ce(thd)$_4$] (24.32g 79% yield).

Elemental Microanalysis: calcd. for $CeC_{44}H_{76}O_8$: C 60.52, H 8.79 % ; found C 60.02; H 6.90 %

Preparation of [Ce(dmae)$_4$].

[Ce(dmae)$_4$] was synthesised following the route used for [Ce(mmp)$_4$] using CAN (1g, 1.824 mmol), NaOBu^t (1.05 g, 96.10 mmol) and dmaeH (0.75 ml, 7.30 mmol). The reaction mixture was refluxed for 2 hours and volatiles removed *in vacuo* to give a yellow oil (350 mg, 38.95 % yield).

Elemental Microanalysis: calcd. for $CeC_{16}H_{40}O_4N_4$: C 39.01; H 8.18, N 11.37 %; found: C, 38.88, H 8.08, N 11.19 %

Preparation [Ce(dmap)$_4$].

[Ce(dmap)$_4$] was synthesised following the route used for [Ce(mmp)$_4$] using CAN (7 g, 12.77 mmol), NaOBu^t (7.36 g, 76.61 mmol) and dmapH (6.3 ml, 51.08 mmol). Recyrstallisation from toluene gave the complex as yellow crystals (3.10 g, 44 % yield).

^{1}H NMR ($CDCl_3$): δ(ppm): 1.12 [d, 3H, J=6.13, $OCH(C\boldsymbol{H}_3)CH_2N(CH_3)_2$], 2.13 [m, 2H, $OCH(CH_3)C\boldsymbol{H}_2N(CH_3)_2$], 2.27 [s, 6H, $OCH(CH_3)CH_2N(C\boldsymbol{H}_3)_2$], 3.78 [br m, 1H, $OC\boldsymbol{H}(CH_3)CH_2N(CH_3)_2$]

^{13}C NMR ($CDCl_3$): δ(ppm): 24.6 [$OCH(CH_3)CH_2N(C\boldsymbol{H}_3)_2$], 46.1 [$OCH(\boldsymbol{C}H_3)CH_2N(CH_3)_2$], 70.3 [$OCH(CH_3)\boldsymbol{C}H_2N(CH_3)_2$]

Elemental Microanalysis: calcd for $C_{20}H_{48}CeN_4O_4$: C 43.78, H 8.82, N 10.21 %; found: C 43.96, H 8.76, N 10.07 %

Preparation of [Ce(dmop)$_4$].

A solution of $[NH_4]_2[Ce(NO_3)_6]$ (1g, 1.82 mmol) in DME (20 ml) was added at room temperature to a stirred solution of [NaOBu^t] (1.05 g, 10.95 mmol) in DME. After removal of the $NaNO_3$ precipitate, the filtrate was stirred at 0 °C and a solution of dmopH (1.13g, 7.3 mmol) in DME (10ml) was added. The reaction mixture was allowed to warm to room temperature and stirred overnight. Volatiles were removed *in vacuo*, and the yellow solid residue was extracted with toluene (3 x 50 mL), which was then concentrated to give the product as yellow crystals on cooling to -18 °C. (437 mg, 31.32 % yield).

^{1}H NMR (C_7D_8): δ(ppm): 1.52 [s, 6H, $NC(CH_3)_2CH_2$], 1.54 [s, 6H, $OC(CH_3)_2C$], 3.82 [s, 2H, $NC(CH_3)_2CH_2$]

^{13}C {^{1}H}(C_7D_8): δ(ppm): 27.92 [$NC(CH_3)_2CH_2$], 28.01 [$OC(CH_3)_2C$], 77.04 [$NC(CH_3)_2CH_2$], 78.36 [$OC(CH_3)_2C$], 80.65 [$NC(CH_3)_2CH_2$]

Elemental Microanalysis: calcd. For $CeC_{32}H_{56}N_4O_8$: C 50.25, H 7.38, N 7.32 %; found C 50.07, H 7.49, N 7.19 %.

Characterisation of [Ce$_2$(dmop)$_6$O].

[$Ce_2(dmop)_6O$] was found as the residue after the sublimation of dmopH from [$Ce(dmop)_4$].

^{1}H NMR (C_7D_8): δ(ppm): 1.02 [s], 1.16 [d, J = 3.2811 Hz], 1.44 [b.r s], 1.52 [br. m], 1.53 [br. s], 1.65 [s], 1.74 [s], 1.78 [s], 1.84 [s], 2.08 [br. m], 3.47 [s], 3.57 [s], 3.64 [d, J = 3.2811 Hz], 3.79 [br. s], 3.82 [br. s], 3.90 [br. s], 3.92 [br. s]

^{13}C $\{^1H\}(C_7D_8)$: δ(ppm): 27.62, 29.97, 28.20, 28.36, 28.57, 28.73, 28.80 [NC(C***H***$_3)_2CH_2$], 30.13, 30.39, 30.39, 30.82, 31.22, 32.11, 32.16 [OC(***C***$H_3)_2$C], 66.74, 66.89, 67.30 [N***C***$(CH_3)_2CH_2$], 77.07, 78.40, 79.40 [O***C***$(CH_3)_2$C], 80.67, 81.80, 82.50, 82.73 [NC$(CH_3)_2$***C***H_2], 171.43 [OC$(CH_3)_2$***C***]

Elemental Microanalysis: calc. For $Ce_2C_{48}H_{84}N_6O_{13}$: C 46.74; H 6.86; N 6.81 %; found C 46.89; H 6.92; N 6.85 %

Preparation of [Ce(dmomp)$_4$].

Reaction was performed in the same way as the synthesis of [Ce(mmp)$_4$] using 532 mg (0.97 mmol) CAN and 562 mg (5.85 mmol) NaOBu^t. Following the preparation of [Ce(OBu^t)$_4$] dmompH (800 mg, 3.9 mmol) in DME (10 ml) was added to the yellow solution with stirring at room temperature. A colour change to deep red was seen and after 2 hours the volatiles were removed *in vacuo* to give a dusty red solid (328 mg, 35 % yield).

^1H NMR ($CDCl_3$): δ(ppm): 0.95 [s, 3H, NC(C***H***$_3)_2CH_2$], 1.21 [s, 3H, NC(C***H***$_3)_2CH_2$], 2.04 [s, 3H, C***H***$_3(C_6H_3O)$], 3.87 [d, J = 7.90 Hz, 1H, NC$(CH_3)_2$C***H***$_2$], 3.97 [d, J = 7.85 Hz, 1H, NC$(CH_3)_2$C***H***$_2$], 6.54 [t, 1H, C_6***H***$_3$], 7.23 [s, 1H, C_6***H***$_3$], 7.71 [d of d, 1H,. C_6***H***$_3$]

^{13}C NMR ($CDCl_3$): δ(ppm): 15.24 [***C***$H_3(C_6H_3O)$], 24.59 [NC(***C***$H_3)_2CH_2$], 27.47 [NC(***C***$H_3)_2CH_2$], 68.7 [N***C***$(CH_3)_2CH_2$], 77.58 [NC$(CH_3)_2$***C***H_2], 115.97 [Ar], 116.44 [Ar], 123.91 [Ar], 126.65 [Ar], 132.97 [Ar], 161.84 [$CH_2(C_5H_3$***C***O)], 165.48 [$CH_3(C_6H_3O)$***C***N]

Mass Spectroscopy EI: Mass Found [M+] 956.3; Theoretical Mass [$C_{48}H_{56}CeN_4O_8$] 956.3

ASAP: Mass Found $[M+H]^+$ 958.3; Theroetical Mass $[C_{48}H_{56}CeN_4O_8 + H]^+$ 958.3

5.5. Ce(IV) Heteroleptic Complexes.

Preparation of [Ce(mmp)$_2$(dbm)$_2$].

A solution of dbmH (800 mg, 3.6 mmol) in toluene (20 ml) was added dropwise via canula to a stirred solution of [Ce(mmp)$_4$] (1g, 1.8 mmol) in toluene (20 ml) at 0 °C. After full addition the reaction was stirred for 1 hour at 0 °C and allowed to warm to room temperature for a further 1 hour. The volatiles from the deep orange solution were removed *in vacuo* and the crude oil recrystallised in toluene to give a low melting point solid at -18 °C (447 mg, 31.2 % yield).

^{1}H NMR ($(C_4D_8)O$): δ(ppm): 1.06 [s, 6H, $OC(C\boldsymbol{H}_3)_2CH_2OCH_3$], 3.08 [s, 2H, $OC(CH_3)_2C\boldsymbol{H}_2OCH_3$], 3.28 [s, 3H, $OC(CH_3)_2CH_2O\boldsymbol{C}H_3$], 6.85 [s, $(C_6H_5CO)_2C\boldsymbol{H}$], 7.27 [m, Ar], 7.38 [m, Ar], 8.10 [m, Ar].

^{13}C NMR ($(C_4D_8)O$): δ(ppm): 26.84 [$OC(\boldsymbol{C}H_3)_2CH_2OCH_3$], 59.22 [$OC(CH_3)_2CH_2O\boldsymbol{C}H_3$],], 69.56 [$O\boldsymbol{C}(CH_3)_2CH_2OCH_3$], 82.72 [$OC(CH_3)_2\boldsymbol{C}H_2OCH_3$], 98.28 [$(C_6H_5CO)_2\boldsymbol{C}H$], 128.82 [Ar], 129.57 [Ar], 130.49 [Ar]. 130.63 [Ar], 131.16 [Ar], 131.89 [Ar], 139.76 [Ar], 184.97 [$(C_6H_5\boldsymbol{C}O)_2CH$],

Elemental Microanalysis: calcd. for $CeC_{40}H_{44}O_8$: C 60.59; H 5.59 %; found: C, 60.68, H 5.40 %

Mass Spectrometry ASAP: Mass Found $[M+H]^+$ 793.22; Theoretical Mass $[CeC_{40}H_{44}O_8+H]$ 793.22; $[Ce(mmp)(dbm)_2]^+$ 689; $[Ce(mmp)_2(dbm)]^+$ 569; $[(Ce(mmp)(dbm))_2]$-H 931

Preparation of [Ce(dmap)$_2$(dbm)$_2$].

A solution of dbmH (433 mg, 1.93 mmol) in toluene (4 ml) was added dropwise *via* canula to a stirred solution of $[Ce(mmp)_4]$ (530g, 0.97 mmol) in toluene (20 ml) at 0 °C and the reaction stirred for two hours. Volatiles were removed under vacuo to give the compound as an orangey/red oil (613 mg, 79.9 % yield).

^{1}H NMR (C_7D_8): δ(ppm): 1.08 [d, J = 5.76 Hz, 3H, $OCH(C\boldsymbol{H}_3)CH_2N(CH_3)_2$], 2.25 [s, 6H, $OCH(CH_3)CH_2N(C\boldsymbol{H}_3)_2$], 2.44 [d, J = 9.84 Hz, 1H, $OCH(CH_3)C\boldsymbol{H}_2N(CH_3)_2$], 3.41 [t, J = 11.36 Hz, 1H, $OCH(CH_3)C\boldsymbol{H}_2N(CH_3)_2$], 5.23 [br. m, 1H, $OC\boldsymbol{H}(CH_3)CH_2N(CH_3)_2$], 6.43 [s, 1H, $(C_6H_5CO)_2CH$], 7.07 [t, J = 7.50 Hz, 6H, Ar], 7.17 [d, J = 7.12, 5H, Ar], 7.17 [d, J = 8.04, 2H, Ar], 7.26 [t, J = 7.12, 3H, Ar], 7.78 [d, J = 7.52, 3H, Ar].

^{13}C NMR ($CDCl_3$): δ(ppm): 20.3 $[OCH(\boldsymbol{C}H_3)CH_2N(CH_3)_2]$, 46.2 $[OCH(CH_3)CH_2N(\boldsymbol{C}H_3)_2]$, 71.3 $[OCH(CH_3)\boldsymbol{C}H_2N(CH_3)_2]$, 95.7 $[(C_6H_5)_2(CO)_2\boldsymbol{C}H]$, 124.2 [Ar], 126.5 [Ar], 126.8 [Ar], 127.1 [Ar], 127.9 [Ar], 129.3 [Ar], 136.6 [Ar], 139.1 [Ar], 182.9 $[(C_6H_5)_2(\boldsymbol{C}O)_2CH]$

Elemental Microanalysis: calcd for $C_{40}H_{46}CeN_2O6$: C 60.74, H 5.86, N 3.54 %; found: C 60.64, H 6.03, N 3.46 %

Preparation of [Ce(mmp)$_2$(dmomp)$_2$].

A solution of dmompH (179 mg, 0.87 mmol) in toluene (10 ml) was added dropwise *via* canula to a stirred solution of [Ce(mmp)$_4$] (241g, 0.87 mmol) in toluene (10 ml) at -83 °C (liquid N_2 and ethylacetate). On addition of the ligand a colour change from yellow to orange was seen. After stirring for 1 hour the volatiles were removed *in vacuo* to give an orange oil (185 mg, 56.2 % yield).

^{1}H NMR (C_7D_8): δ(ppm): 1.14 [br, s, 3H, NC(C***H***$_3$)$_2$CH$_2$], 1.31 [s, 6H, OC(C***H***$_3$)$_2$CH$_2$OCH$_3$], 1.66 [br s, 3H, NC(C***H***$_3$)$_2$CH$_2$], 2.49 [s, 3H, C***H***$_3$(C$_6$H$_3$O)], 3.19 [s, 2H, OC(CH$_3$)$_2$C***H***$_2$OCH$_3$], 3.22 [s, 3H, OC(CH$_3$)$_2$CH$_2$OC***H***$_3$], 3.56 [s, 2H, NC(CH$_3$)$_2$C***H***$_2$], 6.56 [t, J = 7.3 Hz, 1H, CH$_3$(C$_6$***H***$_3$O)], 7.22 [d, J = 7.2 Hz, 1H, CH$_3$(C$_6$***H***$_3$O)], 7.86 [d, J = 8.0 Hz, 1H, CH$_3$(C$_6$***H***$_3$O)]

^{13}C {^{1}H}(C_7D_8): δ(ppm): 16.96 [***C***H$_3$(C$_6$H$_3$O)], 28.32 [OC(***C***H$_3$)$_2$CH$_2$OCH$_3$], 29.39 [NC(***C***H$_3$)$_2$CH$_2$], 59.23 [OC(CH$_3$)$_2$CH$_2$O***C***H$_3$], 68.62 [O***C***(CH$_3$)$_2$CH$_2$OCH$_3$], 78.86 [N***C***(CH$_3$)$_2$CH$_2$], 84.46 [OC(CH$_3$)$_2$***C***H$_2$OCH$_3$], 115.59 [NC(CH$_3$)$_2$***C***H$_2$], 117.04 [CH$_3$(***C***$_6$H$_3$O)], 127.00 [CH$_3$(***C***$_6$H$_3$O)], 128.51 [CH$_3$(***C***$_6$H$_3$O)], 129.32 [CH$_3$(***C***$_6$H$_3$O)], 134.93 [CH$_3$(***C***$_6$H$_3$O)], 166.04 [CH$_3$(***C***$_6$H$_3$O)], 167.08 [(C$_6$H$_3$O)***C***NC(CH$_3$)$_2$]

Elemental Microanalysis: calcd. for $CeC_{34}H_{50}CeN_2O_8$: C 54.10, H 6.68, N 3.7 %: found C 53.86, H 6.45, N 3.56 %

Mass Spectrometry EI: Mass Found [M-2H] 752.3; Theroetical Mass [$CeC_{34}H_{50}CeN_2O_8$ – 2H] 752.87. CI: Mass Found [M-H] 753.3; Theoretical Mass [$CeC_{34}H_{50}CeN_2O_8$ – H] 753.88

Reaction of [Ce(mmp)$_4$] with 2 equivalents of dmopH.

A solution of dmopH (499 mg, 3.17 mmol) in toluene (10 ml) was added dropwise *via* canula to a stirred solution of [Ce(mmp)$_4$] (877g, 1.59 mmol) in toluene (20 ml) at 0 °C and the reaction stirred for 2 hours. The volatiles were removed *in vacuo* and the crude materials recrsytallised in toluene to give [$Ce_2(mmp)_2(dmop)_4O$] as yellow crystals (253 mg, 19.3 % yield).

^{1}H NMR (C_7D_8): δ(ppm): 1.42 [s, 6H], 1.48 [m, 24H], 1.57 [s, 6H], 1.65 [s, 6H], 1.74 [s, 6H], 1.79 [s, 6H], 1.96 [s, 6H], 3.30 [s, 6H $OC(CH_3)_2CH_2OC\boldsymbol{H}_3$], 3.34 [d, 2H, J = 2.24 Hz], 3.38 [d, 2H, J = 2.24 Hz], 3.74 [d, 2H, J = 8.09 Hz], 3.76 [d, 2H, J = 8.09 Hz], 3.78 [d, 2H, J = 8.09 Hz], 3.91 [d, 2H, J = 8.09 Hz]

Elemental Microanalysis: calcd. for $Ce_2C_{42}H_{78}O_{13}N_4$: C 44.75; H 6.97, N 4.97 %; found: C 44.60, H 6.84, N 4.90 %

Preparation of [Ce(mmp)$_2$(dmom)$_2$].

A solution of dmomH (406 mg, 3.14 mmol) in toluene (10 ml) was added dropwise *via* canula to a stirred solution of [Ce(mmp)$_4$] (869g, 1.57 mmol) in toluene (20 ml)

at 0 °C and the reaction stirred for 2 hours. The volatiles were removed *in vacuo* to give an oily yellow solid (707 mg, 74.7 % yield).

^{1}H NMR (C_7D_8): δ(ppm): 1.08 [s, 6H, $OC(C\boldsymbol{H}_3)_2CH_2OCH_3$], 1.24 [s], 1.54 [br m], 2.87 [s], 3.02 [s, 2H, $OC(CH_3)_2C\boldsymbol{H}_2OCH_3$], 3.30 [s, 3H, $OC(CH_3)_2CH_2OC\boldsymbol{H}_3$], 3.53 [br, m], 5.26 [d, J = 18.40 Hz], 5.48 [s], 6.02 [d, J = 18.16 Hz]

^{13}C NMR (C_7D_8): δ(ppm): 28.5 [$OC(\boldsymbol{C}H_3)_2CH_2OCH_3$], 29.8 [$NC(\boldsymbol{C}H_3)_2CH_2$], 59.0 [$N\boldsymbol{C}(CH_3)_2CH_2$], 59.4 [$OC(CH_3)_2CH_2O\boldsymbol{C}H_3$], 67.5 [$O\boldsymbol{C}(CH_3)_2CH_2OCH_3$], 82.0 [$NC(CH_3)_2\boldsymbol{C}H_2$], 84.9 [$OC(CH_3)_2\boldsymbol{C}H_2OCH_3$]

Elemental Microanalysis: calcd. For $C_{22}H_{42}CeN_2O_8$: C 43.84, H 7.02, N 4.65; found C 43.68, H 6.93, N 4.85 %.

5.6. Ti(IV) Alkoxide Complexes.

Preparation of [Ti(OPr^i)$_2$(dmae)$_2$].

DmaeH (4.39 g, 49.26 mmol) was added *via* canula to a stirred solution of [Ti(OPr^i)$_4$] (7 g, 24.63 mmol) in dry hexane (50 ml) and the colourless mixture heated to reflux for 1.5 hours then allowed to cool. The volatiles were removed *in vacuo* and the crude product purified by vacuum distillation (85 °C/0.8 Torr) to give [Ti(OPr^i)$_2$(dmae)$_2$] as a colourless oil (5.66 g, 67.1 % yield).

^{1}H NMR (C_7D_8): δ(ppm): 1.1 [d, 12H, $OCH(C\boldsymbol{H}_3)_2$], 2.1 [s, 12H, $OCH_2CH_2N(C\boldsymbol{H}_3)_2$], 2.4 [t, 4H, $OCH_2C\boldsymbol{H}_2N(CH_3)_2$], 4.2 [s, 4H, $OC\boldsymbol{H}_2CH_2N(CH_3)_2$], 4.6 [broad m, 2H, $OC\boldsymbol{H}(CH_3)_2$].

^{13}C {^{1}H}(C_7D_8): δ(ppm): 25.3 [$OCH(\boldsymbol{C}H_3)_2$], 45.2 [$OCH_2CH_2N(\boldsymbol{C}H_3)_2$], 61.7 [$OCH_2\boldsymbol{C}H_2N(CH_3)_2$], 69.8 [$O\boldsymbol{C}H_2CH_2N(CH_3)_2$], 74.8 [$O\boldsymbol{C}H(CH_3)_2$].

Elemental Microanalysis: calcd. for $C_{14}H_{34}N_2O_4Ti$: C 49.12; H 10.01; N 8.18 %; found: C 48.99; H 10.05; N 8.03 %.

Preparation of [Ti(OBu^t)$_2$(dmae)$_2$].

DmaeH (3.67 g, 41.14 mmol) was added *via* canula to a stirred solution of [Ti(OBu^t)$_4$] (7 g, 20.57 mmol) in hexane and the the mixture heated to reflux for 1.5 hours. After cooling the volatiles were removed *in vacuo* and the resulting oil purified by vacuum distillation (105 °C/0.8 Torr) to give [Ti(OBu^t)$_2$(dmae)$_2$] (7.34 g, 96.4 %).

^{1}H NMR (C_7D_8): δ(ppm): 1.2 [s, 18H, $OC(C\boldsymbol{H}_3)_3$], 2.0 [s, 12H, $OCH_2CH_2N(C\boldsymbol{H}_3)_2$], 2.3 [broad t, 4H, $OCH_2C\boldsymbol{H}_2N(CH_3)_2$], 4.1 [broad t, 4H, $OC\boldsymbol{H}_2CH_2N(CH_3)_2$].

^{13}C {^{1}H}(C_7D_8): δ 31.0 [$OC(\boldsymbol{C}H_3)_3$], 44.9 [$OCH_2CH_2N(\boldsymbol{C}H_3)_2$], 61.4 [$OCH_2\boldsymbol{C}H_2N(CH_3)_2$], 70.1 [$O\boldsymbol{C}H_2CH_2N(CH_3)_2$], 78.1 [$O\boldsymbol{C}(CH_3)_3$].

Elemental Microanalysis: calcd. for $C_{16}H_{38}N_2O_4Ti$: C 51.89; H 10.34; N 7.56 %; found: C 51.79; H 10.21; N 7.40 %.

Preparation of [Ti(OPr^i)$_2$(dmop)$_2$].

A solution of dmopH (2.33 g, 14.82 mmol) in toluene (20 ml) was added *via* canula to a stirred solution of [Ti(OPr^i)$_4$] (2.11 g, 7.41 mmol) in toluene (20 ml) and the reaction mixture heated to reflux for 1.5 hours. After cooling to room temperature the volatiles were removed *in vacuo* to give a white solid that was purified via recrystallisation from toluene at -18 °C to give [Ti(OPr^i)$_2$(dmop)$_2$] (2.54 g, 71.6 % yield).

^{1}H NMR (C_7D_8): δ(ppm): 1.2 [s, 12H, NC(C***H***$_3$)$_2$CH$_2$], 1.4 [d, 12H, OCH(C***H***$_3$)$_2$], 1.6 [s, 12H, OC(C***H***$_3$)$_2$C], 3.7 [s, 4H, NC(CH$_3$)$_2$C***H***$_2$], 5.2 [m, 2H, OC***H***(CH$_3$)$_2$].

^{13}C {^{1}H}(C_7D_8): δ(ppm): 24.8 [NC(***C***H$_3$)$_2$CH$_2$], 26.0 [OCH(***C***H$_3$)$_2$], 26.5 [OC(***C***H$_3$)$_2$C], 64.2 [O***C***H(CH$_3$)$_2$], 74.1 [N***C***(CH$_3$)$_2$CH$_2$], 74.9 [O***C***(CH$_3$)$_2$C], 82.9 [NC(CH$_3$)$_2$***C***H$_2$], 179.9 [OC(CH$_3$)$_2$***C***].

Elemental Microanalysis: calcd. for $C_{22}H_{34}N_2O_6Ti$: C 55.23; H 8.85; N 5.86 %; found: C 55.08; H 8.95; N 5.71 %.

Mass Spectrometry +ve CI: [dmopH$^+$] 158.0, [M-(OPr^i+dmop+3H)]$^+$ 260.2, [M-OPri]$^+$ 419.2, [M- CH$_3$]$^+$ 463.2

Preparation of [Ti(OPr^i)$_2$(dmom)$_2$].

A solution of dmomH (2.32 g, 17.95 mmol) in toluene (20 ml) was added *via* canula to a stirred solution of [Ti(OPr^i)$_4$] (2.6 g, 8.97 mmol), in toluene (20 ml) and the reaction mixture heated to reflux for 1.5 hours. After cooling to room temperature

the volatiles were removed *in vacuo* to give an oily orange solid that was purified via recrystallisation from toluene at -18 °C to give $[Ti(OPr^i)_2(dmom)_2]$ (2.9 g, 76.6 % yield).

^1H NMR (C_7D_8): δ(ppm): 1.2 [s, 12H, $NC(CH_3)_2CH_2$], 1.4 [d, 12H, $OCH(CH_3)_2$], 3.7 [s, 4H, $NC(CH_3)_2CH_2$], 4.8 [s, 4H, OCH_2C], 5.1 [m, 2H, $OCH(CH_3)_2$].

^{13}C $\{^1H\}$(C_7D_8): δ(ppm): 26.9 [$NC(CH_3)_2CH_2$], 27.9 [$OCH(CH_3)_2$], 66.0 [$OCH(CH_3)_2$], 66.6 [$NC(CH_3)_2CH_2$], 76.6 [OCH_2C], 84.2 [$NC(CH_3)_2CH_2$], 177.3 [OCH_2C].

Elemental Microanalysis: calcd. for $C_{18}H_{34}N_2O_6Ti$: C 51.19; H 8.11, N 6.63 %; found: C 51.16; H 8.17, N 6.56 %.

Preparation of $[Ti(OBu^t)_2(dmom)_2]$.

A solution of dmomH (3.27 g, 25.32 mmol) in toluene (20 ml) was added *via* canula to a stirred solution of $[Ti(OBu^t)_4]$ (4.3 g, 12.66 mmol) in toluene (20 ml) and the reaction mixture heated to reflux for 1.5 hours. Removal of the volatiles *in vacuo* gave a sticky orange oil (5.32 g, 93.3 % yield).

^1H NMR (C_7D_8): δ(ppm): 1.18 [s, 3H, $NC(CH_3)_2CH_2$], 1.22 [s, 3H, $NC(CH_3)_2CH_2$], 1.35 [s, 9 H $OC(CH_3)_3$], 1.46 [s 6H], 3.76 [d, 2H, $NC(CH_3)_2CH_2$], 4.75 [s, 1H, OCH_2C], 4.95 [s, 1H, OCH_2C]

^{13}C $\{^1H\}(C_7D_8)$: δ(ppm): 26.3, 26.5 [NC(***C***$H_3)_2CH_2$], 30.9 [NC(***C***$H_3)_2CH_2$], 31.1 [OC(***C***$H_3)_3$], 31.2 [NC(***C***$H_3)_2CH_2$], 64.4, 64.8 [N***C***$(CH_3)_2CH_2$], 65.9 [O***C***$(CH_3)_3$], 78.6, 79.6 [O***C***H_2C], 80.8, 82.2 [NC$(CH_3)_2$***C***H_2], 171.9, 174.3 [OCH_2***C***].

Elemental Microanalysis: calcd. for $C_{22}H_{42}N_2O_4Ti$: C 59.19; H 9.48, N 6.27 %; found: C 59.06; H 9.39, N 6.22 %.

Preparation of [Ti(OPr^i)$_2$(mmp)$_2$].

MmpH (4.11 ml, 35.18 mmol) was added *via* canula to a stirred solution of [Ti(OPr^i)$_4$] (5 g, 17.59 mmol) in hexane (30 ml) and the mixture heated to reflux for 1.5 hours. Volatiles were removed *in vacuo* to give a colourless oil which was purified *via* distillation (85 °C/0.8 Torr) to give [Ti(OPr^i)$_2$(mmp)$_2$] (5.5 g, 84.0 % yield).

^1H NMR (C_7D_8): δ(ppm): 1.27 [br. m], 1.35 [s], 1.39 [br. s], 3.23 [br. s], 3.27 [br. s], 4.67 [br. m]

^{13}C $\{^1H\}$ (C_7D_8): δ(ppm): 25.3 [OC(***C***$H_3)_2CH_2OCH_3$], 26.7 [OCH(***C***$H_3)_2$], 57.7 [OC$(CH_3)_2CH_2$O***C***H_3], 75.0 [O***C***H$(CH_3)_2$], 79.4 [O***C***$(CH_3)_2CH_2OCH_3$], 81.3 [OC$(CH_3)_2$***C***H_2OCH_3]

Elemental Microanalysis: calcd. for $C_{16}H_{36}O_6Ti$: C 51.61; H 9.75 %; found: C 51.74; H 9.66 %.

Mass Spectrometry +ve CI: [M-OPr^i]$^+$ 313.1, [M-CH_3] 357.1, [M+H]$^+$ 373.2

Preparation of [Ti(OBu^t)$_2$(mmp)$_2$].

MmpH (3.43 ml, 29.38 mmol) was added *via* canula to a stirred solution of [Ti(OBu^t)$_4$] (5 g, 14.69 mmol) in hexane (30 ml) and the mixture heated to reflux for 1.5 hours. Volatiles were removed under *vacuo* to give a colourless oil which was purified *via* distillation to give [Ti(OBu^t)$_2$(mmp)$_2$] (5.5g, 93.5 % yield).

^{1}H NMR (C_7D_8): δ(ppm): 1.34 [s], 1.36 [s], 1.37 [s], 1.38 [s], 1.39 [s], 3.21 [s], 3.23 [s], 3.25 [s], 3.26 [br. s], 3.27 [br. m]

^{13}C {^{1}H} (C_7D_8): δ(ppm): 26.8 [OC(***C***H$_3$)$_2$CH$_2$OCH$_3$], 31.0 [OC(***C***H$_3$)$_3$], 57.7 [OC(CH$_3$)$_2$CH$_2$O***C***H$_3$], 78.8 [O***C***(CH$_3$)$_2$CH$_2$OCH$_3$], 79.9 [O***C***(CH$_3$)$_3$], 81.1 [OC(CH$_3$)$_2$***C***H$_2$OCH$_3$]

Elemental Microanalysis: calcd. for $C_{18}H_{40}O_6Ti$: C 54.00; H 10.07 %; found: C 53.84; H 9.90 %.

Mass Spectrometry +ve EI: [M-OBu^t]$^+$ 327.1, [M-mmp]$^+$ 297.1

Preparation of [Ti(OBu^t)$_2$(dmop)$_2$].

A solution of dmopH (924 mg, 5.88 mmol) in toluene (10 ml) was added *via* canula to a stirred solution of [Ti(OBu^t)$_4$] (1, 2.9 mmol) in toluene (20 ml) at 0 °C and the reaction mixture stirred for 2 hours. After removing the volatiles *in vacuo* the crude white solid was recrystallised to give the complex as white crystals (420 mg, 28.6 % yield)

^{1}H NMR (C_7D_8): δ(ppm): 1.19 [d, J = 11.7 Hz], 1.40 [d, J = 4.8 Hz], 1.44 [s], 1.54 [s], 1.59 [s], 1.66 [s], 1.72 [s], 1.76 [s], 1.89 [s], 1.90 [s], 3.63 [s], 3.72 [s], 3.88 [d, J = 4.8 Hz], 3.94 [s], 4.03 [s], 4.04 [s].

^{13}C {^{1}H} (C_7D_8): δ(ppm): 27.7, 28.1, 28.14 , 28.2 [NC($\boldsymbol{C}$H$_3$)$_2$CH$_2$], 28.3, 28.4, 31.3, 32.3 [OCH($\boldsymbol{C}$H$_3$)$_2$], 32.4 [OC($\boldsymbol{C}$H$_3$)$_3$], 65.7, 66.9 [N$\boldsymbol{C}$(CH$_3$)$_2$CH$_2$], 68.1, 68.4 [O$\boldsymbol{C}$H$_2$C], 83.2, 84.0 [NC(CH$_3$)$_2$$\boldsymbol{C}H_2$].

Elemental Microanalysis: calcd. For $C_{24}H_{46}N_2O_6Ti$: C 56.91; H 9.15; N 5.53 %; found C 56.78; H 8.99; N 5.41 %

Mass Spectrometry ASAP: [Ti(dmop)$_3$]H$^+$ 516, [Ti$_2$(dmop)$_4$O$_2$]H$^+$ 753, [M-OBu^t]$^+$ 433

Chapter 6. References

(1) Baklanov, M.; Green, M.; Maex, K. *Dielectric Films for Advanced Microelectronics Wiley*, 2007.

(2) Waser, R. *Nanoelectronics and Information Technology: Advanced Electronic Materials and Novel Devices*; Wiley-VCH, 2003.

(3) Taylor, S.; Williams, P. A.; Roberts, J. L.; Jones, A. C.; Chalker, P. R. *Electronics Letters* **2002**, 38, 1285.

(4) Jones, A. C.; Aspinall, H. C.; Chalker, P. R.; Potter, R. J.; Manning, T. D.; Loo, Y. F.; O'Kane, R.; Gaskell, J. M.; Smith, L. M. *Chemical Vapor Deposition* **2006**, 12, 83.

(5) Krupanidhi, S. B.; Maffei, N.; Sayer, M.; Elassal, K. *Journal of Applied Physics* **1983**, 54, 6601.

(6) Sreenivas, K.; Sayer, M.; Baar, D. J.; Nishioka, M. *Applied Physics Letters* **1988**, 52, 709.

(7) Ramesh, R.; Inam, A.; Chan, W. K.; Tillerot, F.; Wilkens, B.; Chang, C. C.; Sands, T.; Tarascon, J. M.; Keramidas, V. G. *Applied Physics Letters* **1991**, 59, 3542.

(8) Jones, A. C. *Journal of Materials Chemistry* **2002**, 12, 2576.

(9) Watson, I. M. *Chemical Vapor Deposition* **1997**, 3, 9.

(10) Fahlman, B. D.; Barron, A. R. *Advanced Materials for Optics and Electronics* **2000**, 10, 223.

(11) Malandrino, G.; Lo Nigro, R.; Fragala, I. L.; Benelli, C. *European Journal of Inorganic Chemistry* **2004**, 500.

(12) Gulino, A.; Fragala, I. *Inorganica Chimica Acta* **2005**, 358, 4466.

(13) Jones, A. C.; Aspinall, H. C.; Chalker, P. R. *Surface & Coatings Technology* **2007**, 201, 9046.

(14) Williams, P. A.; Roberts, J. L.; Jones, A. C.; Chalker, P. R.; Tobin, N. L.; Bickley, J. F.; Davies, H. O.; Smith, L. M.; Leedham, T. J. *Chemical Vapor Deposition* **2002**, 8, 163.

(15) Fleeting, K. A.; O'Brien, P.; Jones, A. C.; Otway, D. J.; Andrew, A. J. P.; Williams, D. J. *Journal of the Chemical Society-Dalton Transactions* **1999**, 2853.

(16) Matero, R.; Ritala, M.; Leskela, M.; Jones, A. C.; Williams, P. A.; Bickley, J. F.; Steiner, A.; Leedham, T. J.; Davies, H. O. *Journal of Non-Crystalline Solids* **2002**, 303, 24.

(17) Manning, T. D.; Loo, Y. F.; Jones, A. C.; Aspinall, H. C.; Chalker, P. R.; Bickley, J. F.; Smith, L. M.; Critchlow, G. W. *Journal of Materials Chemistry* **2005**, 15, 3384.

(18) Fix, R. M.; Gordon, R. G.; Hoffman, D. M. *Chemistry of Materials* **1990**, 2, 235.

(19) Ohshita, Y.; Ogura, A.; Hoshino, A.; Hiiro, S.; Suzuki, T.; Machida, H. *Thin Solid Films* **2002**, 406, 215.

(20) de Rouffignac, P.; Park, J. S.; Gordon, R. G. *Chemistry of Materials* **2005**, 17, 4808.

(21) de Rouffignac, P.; Gordon, R. G. *Chemical Vapor Deposition* **2006**, 12, 152.

(22) Mine, N.; Fujiwara, Y.; Taniguchi, H. *Chemistry Letters* **1986**, 357.

(23) Johnson, C. R.; Tait, B. D. *Journal of Organic Chemistry* **1987**, 52, 281.

(24) Hitchcock, P. B.; Lappert, M. F.; Protchenko, A. V. *Chemical Communications* **2006**, 3546.

(25) Droese, P.; Crozier, A. R.; Lashkari, S.; Gottfriedsen, J.; Blaurock, S.; Hrib, C. G.; Maichle-Moessmer, C.; Schaedle, C.; Anwander, R.; Edelmann, F. T. *Journal of the American Chemical Society* **2010**, 132, 14046.

(26) Aspinall, H. C. *Chemistry of the f-Block Elements*; Gordon and Breach Science Publishers, 2001.

(27) Cotton, S. *Lanthanides and Actinides*; Macmillan Education, 1991.

(28) Malandrino, G.; Lo Nigro, R.; Benelli, C.; Castelli, F.; Fragala, I. L. *Chemical Vapor Deposition* **2000**, 6, 233.

(29) Bradley, D. C.; Chatterjee, A. K.; Wardlaw, W. *Journal of the Chemical Society* **1957**, 2600.

(30) Evans, W. J.; Deming, T. J.; Olofson, J. M.; Ziller, J. W. *Inorganic Chemistry* **1989**, 28, 4027.

(31) Cotton, F. A.; Marler, D. O.; Schwotzer, W. *Inorganica Chimica Acta-Articles and Letters* **1984**, 85, L31.

(32) Arnold, P. L.; Casely, I. J.; Zlatogorsky, S.; Wilson, C. *Helvetica Chimica Acta* **2009**, 92, 2291.

(33) Gradeff, P. S.; Schreiber, F. G.; Mauermann, H. *Journal of the Less-Common Metals* **1986**, 126, 335.

(34) Vaarstra, B. A.; Huffman, J. C.; Gradeff, P. S.; Hubertpfalzgraf, L. G.; Daran, J. C.; Parraud, S.; Yunlu, K.; Caulton, K. G. *Inorganic Chemistry* **1990**, 29, 3126.

(35) Yunlu, K.; Gradeff, P. S.; Edelstein, N.; Kot, W.; Shalimoff, G.; Streib, W. E.; Vaartstra, B. A.; Caulton, K. G. *Inorganic Chemistry* **1991**, 30, 2317.

(36) Suh, S.; Guan, J.; Miinea, L. A.; Lehn, J. S. M.; Hoffman, D. M. *Chemistry of Materials* **2004**, 16, 1667.

(37) Hitchcock, P. B.; Hulkes, A. G.; Lappert, M. F. *Inorganic Chemistry* **2004**, 43, 1031.

(38) Morton, C.; Alcock, N. W.; Lees, M. R.; Munslow, I. J.; Sanders, C. J.; Scott, P. *Journal of the American Chemical Society* **1999**, 121, 11255.

(39) Droese, P.; Gottfriedsen, J. *Zeitschrift Fur Anorganische Und Allgemeine Chemie* **2008**, 634, 87.

(40) Ribot, F.; Toledano, P.; Sanchez, C. *Chemistry of Materials* **1991**, 3, 759.

(41) Paivasaari, J.; Putkonen, M.; Niinisto, L. *Journal of Materials Chemistry* **2002**, 12, 1828.

(42) Carter, W. B.; Book, G. W.; Polley, T. A.; Stollberg, D. W.; Hampikian, J. M. *Thin Solid Films* **1999**, 347, 25.

(43) Guillon, H.; Daniele, S.; Hubert-Pfalzgraf, L. G.; Letoffe, J. M. *Polyhedron* **2004**, 23, 1467.

(44) Loo, Y. F.; O'Kane, R.; Jones, A. C.; Aspinall, H. C.; Potter, R. J.; Chalker, P. R.; Bickley, J. F.; Taylor, S.; Smith, L. M. *Journal of Materials Chemistry* **2005**, 15, 1896.

(45) Loo, Y. F.; O'Kane, R.; Jones, A. C.; Aspinall, H. C.; Potter, R. J.; Chalker, P. R.; Bickley, J. F.; Taylor, S.; Smith, L. M. *Chemical Vapor Deposition* **2005**, 11, 299.

(46) Sarazin, Y. S.; Chenal, T.; Mortreux, A.; Vezin, H.; Carpentier, J. F. *Journal of Molecular Catalysis a-Chemical* **2005**, 238, 207.

(47) Sen, A.; Stecher, H. A.; Rheingold, A. L. *Inorganic Chemistry* **1992**, 31, 473.

(48) Abrutis, A.; Hubert-Pfalzgraf, L. G.; Pasko, S. V.; Bartasyte, A.; Weiss, F.; Janickis, V. *Journal of Crystal Growth* **2004**, 267, 529.

(49) Gant, T. G.; Meyers, A. I. *Tetrahedron* **1994**, 50, 2297.

(50) Frump, J. A. *Chemical Reviews* **1971**, 71, 483.

(51) Bolm, C.; Weickhardt, K.; Zehnder, M.; Ranff, T. *Chemische Berichte* **1991**, 124, 1173.

(52) Song, H. Z.; Wang, H. B.; Zhang, J.; Peng, D. K.; Meng, G. Y. *Materials Research Bulletin* **2002**, 37, 1487.

(53) Song, H. Z.; Jiang, Y. Z.; Xia, C. R.; Meng, G. Y.; Peng, D. K. *Journal of Crystal Growth* **2003**, 250, 423.

(54) Jiang, Y.; Liu, M.; Wang, Y.; Song, H.; Gao, J.; Meng, G. *Journal of Physical Chemistry A* **2006**, 110, 13479.

(55) Blank, J. H.; Beckers, J.; Collignon, P. F.; Rothenberg, G. *Chemphyschem* **2007**, 8, 2490.

(56) Dimoulas, A.; Panayiotatos, Y.; Sotiropoulos, A.; Tsipas, P.; Brunco, D. P.; Nicholas, G.; Van Steenbergen, J.; Bellenger, F.; Houssa, M.; Caymax, M.; Meuris, M. *Solid-State Electronics* **2007**, 51, 1508.

(57) Shiohara, Y.; Yoshizumi, M.; Izumi, T.; Yamada, Y. *Physica C-Superconductivity and Its Applications* **2007**, 463, 1.

(58) Trovarelli, A. *Catalysis by Ceria and Related Materials*; Imperial College Press, 2002.

(59) Pollard, K. D.; Jenkins, H. A.; Puddephatt, R. J. *Chemistry of Materials* **2000**, 12, 701.

(60) Leskela, M.; Sillanpaa, R.; Niinisto, L.; Tiitta, M. *Acta Chemica Scandinavica* **1991**, 45, 1006.

(61) Becht, M.; Gerfin, T.; Dahmen, K. H. *Chemistry of Materials* **1993**, 5, 137.

(62) Becht, M.; Morishita, T. *Chemical Vapor Deposition* **1996**, 2, 191.

(63) Bradley, D. C.; Chatterjee, A. K.; Wardlaw, W. *Journal of the Chemical Society* **1956**, 3469.

(64) Aspinall, H. C.; Gaskell, J.; Williams, P. A.; Jones, A. C.; Chalker, P. R.; Marshall, P. A.; Smith, L. M.; Critchlow, G. W. *Chemical Vapor Deposition* **2004**, 10, 13.

(65) Aspinall, H. C.; Gaskell, J. M.; Loo, Y. F.; Jones, A. C.; Chalker, P. R.; Potter, R. J.; Smith, L. M.; Critchlow, G. W. *Chemical Vapor Deposition* **2004**, 10, 301.

(66) Oregan, B.; Gratzel, M. *Nature* **1991**, 353, 737.

(67) Takahashi, Y.; Tsuda, K.; Sugiyama, K.; Minoura, H.; Makino, D.; Tsuiki, M. *Journal of the Chemical Society-Faraday Transactions I* **1981**, 77, 1051.

(68) Takahashi, Y.; Ogiso, A.; Tomoda, R.; Sugiyama, K.; Minoura, H.; Tsuiki, M. *Journal of the Chemical Society-Faraday Transactions I* **1982**, 78, 2563.

(69) Lee, J.-C.; Park, K.-S.; Kim, T.-G.; Choi, H.-J.; Sung, Y.-M. *Nanotechnology* **2006**, 17, 4317.

(70) Wu, J. J.; Yu, C. C. *Journal of Physical Chemistry B* **2004**, 108, 3377.

(71) Palgrave, R. G.; Parkin, I. P. *Chemistry of Materials* **2007**, 19, 4639.

(72) Ni, M.; Leung, M. K. H.; Leung, D. Y. C.; Sumathy, K. *Renewable & Sustainable Energy Reviews* **2007**, 11, 401.

(73) Mills, A.; LeHunte, S. *Journal of Photochemistry and Photobiology a-Chemistry* **1997**, 108, 1.

(74) Sopyan, I.; Watanabe, M.; Murasawa, S.; Hashimoto, K.; Fujishima, A. *Journal of Photochemistry and Photobiology a-Chemistry* **1996**, 98, 79.

(75) Zheng, Z.; Teo, J.; Chen, X.; Liu, H.; Yuan, Y.; Waclawik, E. R.; Zhong, Z.; Zhu, H. *Chemistry-a European Journal* **2010**, 16, 1202.

(76) Sunada, K.; Kikuchi, Y.; Hashimoto, K.; Fujishima, A. *Environmental Science & Technology* **1998**, 32, 726.

(77) Kamat, P. V. *Journal of Physical Chemistry C* **2007**, 111, 2834.

(78) Min, Y. S.; Cho, Y. J.; Asanov, I. P.; Han, J. H.; Kim, W. D.; Hwang, C. S. *Chemical Vapor Deposition* **2005**, 11, 38.

(79) Harada, Y.; Ogawa, K.; Irie, Y.; Endo, H.; Feril, L. B., Jr.; Uemura, T.; Tachibana, K. *Journal of Controlled Release* **2011**, 149, 190.

(80) Mills, A.; Hill, G.; Bhopal, S.; Parkin, I. P.; O'Neill, S. A. *Journal of Photochemistry and Photobiology a-Chemistry* **2003**, 160, 185.

(81) Watanabe, T.; Nakajima, A.; Wang, R.; Minabe, M.; Koizumi, S.; Fujishima, A.; Hashimoto, K. *Thin Solid Films* **1999**, 351, 260.

(82) Hurum, D. C.; Agrios, A. G.; Gray, K. A.; Rajh, T.; Thurnauer, M. C. *Journal of Physical Chemistry B* **2003**, 107, 4545.

(83) Diebold, U. *Surface Science Reports* **2003**, 48, 53.

(84) Penn, R. L.; Banfield, J. F. *American Mineralogist* **1999**, 84, 871.

(85) Tang, H.; Prasad, K.; Sanjines, R.; Schmid, P. E.; Levy, F. *Journal of Applied Physics* **1994**, 75, 2042.

(86) Zhang, H. Z.; Banfield, J. F. *Journal of Physical Chemistry B* **2000**, 104, 3481.

(87) Gribb, A. A.; Banfield, J. F. *American Mineralogist* **1997**, 82, 717.

(88) Czanderna, A. W.; Rao, C. N. R.; Honig, J. M. *Transactions of the Faraday Society* **1958**, 54, 1069.

(89) Taylor, C. J.; Gilmer, D. C.; Colombo, D. G.; Wilk, G. D.; Campbell, S. A.; Roberts, J.; Gladfelter, W. L. *Journal of the American Chemical Society* **1999**, 121, 5220.

(90) Kim, J. W.; Kim, D. O.; Hahn, Y. B. *Korean Journal of Chemical Engineering* **1998**, 15, 217.

(91) Kim, T. W.; Jung, M.; Kim, H. J.; Park, T. H.; Yoon, Y. S.; Kang, W. N.; Yom, S. S.; Na, H. K. *Applied Physics Letters* **1994**, 64, 1407.

(92) Lu, J. P.; Wang, J. D.; Raj, R. *Thin Solid Films* **1991**, 204, L13.

(93) Evans, P.; Pemble, M. E.; Sheel, D. W. *Chemistry of Materials* **2006**, 18, 5750.

(94) Peng, X. S.; Chen, A. C. *Journal of Materials Chemistry* **2004**, 14, 2542.

(95) Battiston, S.; Minella, M.; Gerbasi, R.; Visentin, F.; Guerriero, P.; Leto, A.; Pezzotti, G.; Miorin, E.; Fabrizio, M.; Pagura, C. *Carbon* **2010**, 48, 2470.

(96) Lazar, A. M.; Chaumont, D.; Lacroute, Y.; Gomez, M. E.; Caicedo, J. C.; Zambrano, G.; Sacilotti, M. *Physica Status Solidi a-Applications and Materials Science* **2008**, 205, 289.

(97) Chen, C. A.; Chen, Y. M.; Korotcov, A.; Huang, Y. S.; Tsai, D. S.; Tiong, K. K. *Nanotechnology* **2008**, 19.

(98) Nakaso, K.; Okuyama, K.; Shimada, M.; Pratsinis, S. E. *Chemical Engineering Science* **2003**, 58, 3327.

(99) Tarselli, M. A.; Micalizio, G. C. *Organic Letters* **2009**, 11, 4596.

(100) Funakubo, H.; Nagai, A.; Asano, G.; Koo, J.-M.; Shin, S.-M.; Park, Y. *Surface & Coatings Technology* **2007**, 201, 9279.

(101) Parthangal, P. M.; Zachariah, M. R. *Chemistry of Materials* **2005**, 17, 3830.

(102) Lee, J.-C.; Kim, T. G.; Lee, W.; Han, S.-H.; Sung, Y.-M. *Crystal Growth & Design* **2009**, 9, 4519.

(103) Chen, I. S.; Hendrix, B. C.; Bilodeau, S. M.; Wang, Z. Y.; Xu, C. Y.; Johnston, S.; Van Buskirk, P. C.; Baum, T. H.; Roeder, J. F. *Japanese Journal of Applied Physics Part 1-Regular Papers Short Notes & Review Papers* **2002**, 41, 6695.

(104) Thomas, R.; Bhakta, R.; Ehrhart, P.; Fischer, R. A.; Waser, R.; Devi, A. *Surface & Coatings Technology* **2007**, 201, 9135.

(105) Baunemann, A.; Hellwig, M.; Varade, A.; Bhakta, R. K.; Winter, M.; Shivashankar, S. A.; Fischer, R. A.; Devi, A. *Dalton Transactions* **2006**, 3485.

(106) Hollingsworth, N.; Kanna, M.; Kociok-Koehn, G.; Molloy, K. C.; Wongnawa, S. *Dalton Transactions* **2008**, 631.

(107) Jones, A. C.; Williams, P. A.; Bickley, J. F.; Steiner, A.; Davies, H. O.; Leedham, T. J.; Awaluddin, A.; Pemble, M. E.; Critchlow, G. W. *Journal of Materials Chemistry* **2001**, 11, 1428.

(108) Jones, A. C.; Leedham, T. J.; Wright, P. J.; Crosbie, M. J.; Fleeting, K. A.; Otway, D. J.; O'Brien, P.; Pemble, M. E. *Journal of Materials Chemistry* **1998**, 8, 1773.

(109) Lee, J. P.; Park, M. H.; Chung, T. M.; Kim, Y.; Sung, M. M. *Bulletin of the Korean Chemical Society* **2004**, 25, 475.

(110) Davis, A. V.; Firman, T. K.; Hay, B. P.; Raymond, K. N. *Journal of the American Chemical Society* **2006**, 128, 9484.

(111) Rzepa, H. S.; Cass, M. E. *Inorganic Chemistry* **2007**, 46, 8024.

(112) Williams, P. A.; Roberts, J. L.; Jones, A. C.; Chalker, P. R.; Bickley, J. F.; Steiner, A.; Davies, H. O.; Leedham, T. J. *Journal of Materials Chemistry* **2002**, 12, 165.

(113) Miao, L.; Tanemura, S.; Toh, S.; Kaneko, K.; Tanemura, M. *Journal of Crystal Growth* **2004**, 264, 246.

(114) Cozzoli, P. D.; Kornowski, A.; Weller, H. *Journal of the American Chemical Society* **2003**, 125, 14539.

(115) Feng, X. J.; Zhai, J.; Jiang, L. *Angewandte Chemie-International Edition* **2005**, 44, 5115.

(116) Zhang, H. Z.; Banfield, J. F. *Journal of Materials Chemistry* **1998**, 8, 2073.